Dissertation

ctDNA as a predictor of treatment response in NSCLC patients treated with immune modulating therapy

submitted by

Sabrina Hammer, BSc MSc MSc

for the Academic Degree of

Doctor of Medical Science (Dr. scient. med.)

at the

Medical University of Graz

Diagnostic & Research Institute of Human Genetics

under the Supervision of

Univ.-Prof.in Dr.in Ellen HEITZER

2025

DECLARATION OF ACADEMIC INTEGRITY

I hereby confirm that the present diploma thesis is the result of my own independent scholarly work. I also confirm that in all cases, where material from the work of others (in books, articles, essays, dissertations, and on the internet) is acknowledged, quotations and paraphrases are clearly indicated. No material other than that cited in the reference list has been used. I have read and understood the Medical University's regulations and procedures concerning plagiarism.

Furthermore, I hereby declare that if artificial intelligence (AI) tools were used for the generation and/or correction of certain text passages in the creation of this work, such employment was conducted in compliance with ethical principles, academic integrity, and the regulations of my university. Additionally, it was ensured that this usage was transparently disclosed and appropriately attributed.

Graz, July 2025 Sabrina HAMMER

DISCLOSURES

Please note that parts of this thesis have already been published in:

Weber S [1,2], Spiegl B[1], Perakis SO[1], Ulz CM[3], Abuja PM [2,3], Kashofer K[3], Leest PV[4], Azpurua MA[4], Tamminga M[4], Brudzewsky D[5], Rothwell DG[6], Mohan S[6], Sartori A[7], Lampignano R[8], Konigshofer Y[5], Sprenger-Haussels M[9], Wikman H[10], Bergheim IR[11], Kloten V[8], Schuuring E[4], Speicher MR[1], Heitzer E[1,2]. Technical Evaluation of Commercial Mutation Analysis Platforms and Reference Materials for Liquid Biopsy Profiling. Cancers (Basel). 2020 Jun 16;12(6):1588. doi: 10.3390/cancers12061588. PMID: 32560092; PMCID: PMC7352370.

and

Weber S[1,2], van der Leest P[4], Donker HC[4], Schlange T[8], Timens W[4], Tamminga M[4], Hasenleithner SO[1], Graf R[1], Moser T[1], Spiegl B[1], Yaspo ML[12], Terstappen LWMM[13], Sidorenkov G[4], Hiltermann TJN[4], Speicher MR[1], Schuuring E[4], Heitzer E[1,2], Groen HJM E[4],. Dynamic Changes of Circulating Tumor DNA Predict Clinical Outcome in Patients With Advanced Non-Small-Cell Lung Cancer Treated With Immune Checkpoint Inhibitors. JCO Precis Oncol. 2021 Nov;5:1540-1553. doi: 10.1200/PO.21.00182. Erratum in: JCO Precis Oncol. 2022 Jan;6:e2100566. PMID: 34994642.

[1] Institute of Human Genetics, Diagnostic & Research Center for Molecular BioMedicine, Medical University of Graz, 8010 Graz, Austria. [2] Christian Doppler Laboratory for Liquid Biopsies for Early Detection of Cancer, Medical University of Graz, 8010 Graz, Austria. [3] Institute of Pathology, Diagnostic & Research Center for Molecular BioMedicine, Medical University of Graz, 8010 Graz, Austria. [4] University of Groningen, University Medical Center of Groningen, 9713 GZ Groningen, The Netherlands. [5] SeraCare Life Sciences, Milford, USA. [6] Cancer Research UK MI, University of Manchester, Manchester M13 9PL, UK. [7] Agena Bioscience GmbH, D-22761 Hamburg, Germany. [8] Bayer AG, Biomarker Research, 42117 Wuppertal, Germany. [9] QIAGEN GmbH, 40724 Hilden, Germany. [10] University Medical Center Hamburg-Eppendorf, 20251 Hamburg, Germany. [11] Department of Cancer Genetics, Institute of Cancer Research, Oslo University Hospital, N-0310 Oslo, Norway. [12] Max Plank Institute for Molecular Genetics, Otto Warburg Laboratory Gene Regulation and Systems Biology of Cancer, Berlin, Germany. [13]Faculty of Science and Technology, University of Twente, Enschede, the Netherlands.

All co-authors have consented to the inclusion of their published data in this dissertation, and the necessary permission to reproduce illustrations and figures from both original and third-party sources have been secured.

ACKNOWLEDGEMENTS

This dissertation marks the end of a long and meaningful journey, and I wish to thank all those who have accompanied, supported and encouraged me along the way.

First and foremost, I would like to express my deepest gratitude to **Prof. Ellen Heitzer** for her mentorship, support and guidance throughout this journey. I am especially thankful for the opportunity to pursue this doctoral program in her research group, and for the chance to combine work and research in such a supportive environment. Her expertise and encouragement have been invaluable to me, both academically and personally.

I would also like to sincerely thank the members of my dissertation committee- **Prof. Michael Speicher**, **Assoc. Prof. Nadia Dandachi** and **Assoc. Prof. Jochen Geigl** – for their time, their thoughtful feedback and for enriching this work with their insights. I also thank our collaboration partners at the UMCG Groningen, **Prof. Ed Schuuring** and **Prof. Harry Groen**, for their productive partnership and shared dedication to our research.

I am incredibly grateful to my former colleagues in the research group, especially **Samantha**, for the scientific discussions, shared laughs, and the sense of belonging that helped me grow. A heartfelt thank you goes to my colleagues in the diagnostic group - especially **Jasmin** - for all the weekends spent side by side with our dissertations – and for being there with empathy, a listening ear, and the occasional after-work drink to keep us going.

From the bottom of my heart, I thank my family - especially **my parents** and my husband **Andi** - for their endless love and unwavering support. Thank you for believing in me, and for your gentle patience when I felt lost or did not know how to go on. Though my **father** left us far too early to see the completion of this journey, his love, strength and belief in me never left my side. I carried him with me every step of the way.

Sabrina Hammer received funding from the Medical University of Graz through the Doctoral School “Molecular Medicine and Inflammation” and has been awarded a dissertation scholarship from the Medical University of Graz. This work was supported by the Austrian Federal Ministry for Digital and Economic Affairs (Christian Doppler Research Fund for Liquid Biopsies for Early Detection of Cancer).

TABLE OF CONTENTS

ABBREVIATIONS VII
LIST OF FIGURES XII
LIST OF TABLES XIV
ZUSAMMENFASSUNG XV
ABSTRACT XVII
1. INTRODUCTION 1
1.1. Lung cancer 1
1.2. Histology 1
1.3. Treatment options and mutational landscape 2
1.3.1. Tyrosine kinase inhibitor therapy 3
1.3.2. Immune checkpoint inhibitors 4
1.4. Tumor-derived ICI-related biomarkers 7
1.4.1. PD-1/PD-L1 expression 7
1.4.2. Tumor mutational burden 8
1.4.3. Other biomarkers 9
1.5. Liquid biopsy 10
1.5.1. Cell-free circulating tumor DNA 11
1.5.2. Challenges of ctDNA analysis 12
1.5.3. Methodological approaches for ctDNA analysis 13
1.5.4. Circulating tumor cells 15
2. AIMS 17
3. MATERIALS AND METHODS 19
3.1. Reference material 19
3.2. Ethics and patient cohort 21
3.3. Evaluation of response to the treatment 22
3.4. Blood sample collection, processing and isolation of cfDNA 23
3.4.1. Plasma extraction 23
3.4.2. cfDNA extraction 23
3.5. Lymphocyte collection from EDTA blood and gDNA isolation 24
3.6. Assay validation and selection 24
3.6.1. QIAseq™ Human Actionable Solid Tumor Assay (QIAGEN) 26

3.6.2. NEBNext Direct™ Cancer HotSpot Panel for Illumina (New England Biolabs) .. 27
3.6.3. AVENIO ctDNA Targeted and Expanded Kit (Roche) 28
3.6.4. AVENIO ctDNA Targeted and Expanded data analysis 30
3.7. Assessment of ctDNA levels and molecular response 32
3.8. Tumor specimen handling and tissue NGS 32
3.9. Statistical analysis 33
4. RESULTS 35
4.1. Assay validation and selection 35
4.1.1. Setup A: Variants with a VAF of 1% were detected across all platforms 35
4.1.2. Setup B: Sensitivity assessment of different mutation assays 38
4.1.3. Setup C: AVENIO kits showed the best performance after assay validation 43
4.2. ctDNA-based response evaluation in NSCLC undergoing ICI therapy 44
4.2.1. Patient characteristics 44
4.2.2. Correlation of ctDNA levels using various metrics while aMM provides the most accurate measurement 48
4.2.3. Prevalence of clonal hematopoiesis-related variants 50
4.2.4. Molecular profiling and ctDNA levels of the cohort 53
4.2.5. Dynamics of ctDNA response patterns and impact of CH-related variants 60
4.2.6. Prognostic value of molecular ctDNA response for survival outcomes 65
4.2.7. Tumor-guided versus *de novo* mutation calling 72
4.2.8. *STK11* and/or *KEAP1* mutations are associated with poor prognosis 74
4.2.9. Multivariate analysis of biomarkers 76
5. DISCUSSION 79
5.1. Analytical performance assessment 80
5.2. ctDNA as a predictor of long-term outcome in NSCLC patients treated with ICI 86
5.2.1. High Sensitivity and Broad Coverage in ctDNA Profiling of NSCLC 87
5.2.2. Predictive value of ctDNA dynamics 88
5.2.3. Prognostic impact of ctDNA dynamics 89
5.2.4. Impact of CH-related variants 91
5.2.5. Strengths and limitations 94
6. CONCLUSION 95
REFERENCES 97

ABBREVIATIONS

°C	Degree Celsius
ACK	Ammonium-chloride-potassium
ALK	Anaplastic lymphoma kinase
aMM	Average mutant molecules per milliliter of plasma
aVAF	Average variant allele frequency
BAM	Binary alignment map
BCT	Blood collection tube
bp	Base pairs
BRAF	B-Raf proto-oncogene, serine/threonine kinase
BRCA2	BRCA2 DNA repair associated
CD74	Cluster of Differentiation 74
cfDNA	Cell-free DNA
cfRNA	Cell-free RNA
CGP	Comprehensive genomic profiling
CH	Clonal hematopoiesis
CHIP	Clonal hematopoiesis of indeterminate potential
CI	Confidence intervals
CNV	Copy number variation
COSMIC	Catalogue of Somatic Mutations in Cancer
CR	Complete response
CRUK	Cancer Research United Kingdom
CSCC	Cutaneous squamous cell carcinoma
CT	Computed tomography
CTC	Circulating tumor cells
ctDNA	Circulating tumor DNA
CTLA-4	Cytotoxic T-Lymphocyte-Associated Protein 4
CV	Coefficients of variation

dbSNP	Single Nucleotide Polymorphism Database (dbSNP)
DCR	Durable clinical responders
ddPCR	Droplet digital Polymerase Chain Reaction
DDR	DNA damage response
dMMR	Deficient mismatch repair
DNA	Deoxyribonucleic Acid
dsDNA	Double-Stranded Deoxyribonucleic acid
EDTA	Ethylenediaminetetraacetid acid
EGFR	EGFR Epidermal Growth Factor Receptor
EML4	Echinoderm Microtubule-Associated Protein-Like 4
ER	Early responders
ESMO	European Society of Medical Oncology
ExAC	Exome Aggregation Consortium
FDA	U.S. Food and Drug Administration
FDG	Fluorodeoxyglucose
FEM	Fragment end motif
FFPE	Formalin-fixed paraffin-embedded
g	Gravitational acceleration
gDNA	Genomic DNA
gnomAD	Genome Aggregation Database
hMM	Highest mutant molecules per milliliter of plasma
HR	Hazard ratio
hVAF	Highest variant allele frequency
ICI	Immune checkpoint inhibitors
iDES	Integrated digital error suppression
IgG4	Immunoglobulin G subclass 4
IGV	Integrative Genomics Viewer
IMI	Innovative Medicines Initiative
Indels	Insertions and deletions
iRECIST	Immune Response Evaluation Criteria in Solid Tumor

KEAP1	Kelch-like ECH-associated Protein 1
KRAS	KRAS proto-oncogene, GTPase
LDT	Laboratory-developed test
LOD	Limits of detection
LoF	Loss-of-Function
mAB	Monoclonal antibody
MEK	Mitogen-activated protein kinase kinase
MET	MET proto-oncogene, receptor tyrosine kinase
ml	Milliliter
MM	Mutant molecules per milliliter of plasma
MSI	Microsatellite instability
MUG	Medical University of Graz
mut/Mb	Mutations per megabase
NCCN	National Comprehensive Cancer Network
NCOA4	Nuclear Receptor Coactivator 4
ND	Not detected
NDR	Non-durable responders
NE	Not evaluable
ng	Nanogram
NGS	Next Generation Sequencing
NR	Non-responders
NSCLC	Non-small cell lung cancer
NTRK	NTRK Neurotrophic receptor tyrosine kinase
OR	Odds ratio
ORR	Objective response rate
OS	Overall survival
PBMCs	Peripheral blood mononuclear cells
PCR	Polymerase Chain Reaction
PD	Progressive disease
PD-1	Programmed Cell Death Protein 1

PD-L1	Programmed Cell Death 1 Ligand 1
PD-L2	Programmed Cell Death 1 Ligand 2
PET	Positron Emission Tomography
PFS	Progression-free survival
PR	Partial tumor response
qPCR	Quantitative Polymerase Chain Reaction
RECIST	Response Evaluation Criteria in Solid Tumors
RET	Ret proto-oncogene
RNA	Ribonucleic Acid
ROS1	ROS proto-oncogene 1, receptor tyrosine kinase
RPM	Revolutions per minute
SCLC	Small cell lung cancer
SCNA	Somatic Copy Number Alteration
SD	Stable disease
SNP	Single nucleotide polymorphism
SNV	Somatic Nucleotide Variant
STK11	Serine/Threonine Kinase 11
TCGA	The Cancer Genome Atlas Program
TKI	Tyrosine kinase inhibitor
TMB	Zumor mutational burden
TP53	Tumor protein p53
TPS	Tumor Proportion Score
UMCG	University Medical Center Groningen
UMI	Unique molecular identifiers
UNIMAN	University Manchester
VAF	Variant allele frequency
VCF	Variant call format
WES	Whole Exome Sequencing
WGS	Whole Genome Sequencing
WHO	World Health Organization

WT	Wild-type
µg	Microgram
µl	Microliter
µM	Micromolar

LIST OF FIGURES

Figure 1: Immune checkpoints regulate different components in the evolution of an immune response……5

Figure 2: Checkpoint proteins……8

Figure 3: Genomic coverage of different ctDNA detection methods……14

Figure 4: Experimental setup to assess Seraseq® reference material……24

Figure 5: Somatic custom filter settings……31

Figure 6: Precision within a single run (intra-run) and reproducibility across three different runs (inter-run) of various assays, showcasing their performance in detecting mutations at a set VAF of 1%……37

Figure 7: Variability assessment of qPCR-based and NGS assays using five clinically relevant mutations……38

Figure 8: Detection performance of five mutation assays (A-F) and concordance of expected versus observed VAFs (G)……40

Figure 9: Accuracy rates of three NGS assays assessed with the Seraseq® ctDNA Reference material (A-D) and of the AVENIO ctDNA Targeted ctDNA assay assessed with the Seraseq® ctDNA Complete™ reference material (E)……42

Figure 10: Evaluation of the AVENIO ctDNA Expanded Assay using SerasSeq ctDNA Complete™ Reference Material……44

Figure 11: Flowchart and study design……46

Figure 12: Survival curves of the lung cancer cohort……47

Figure 13: Correlation of the ctDNA values assessed using various measures……48

Figure 14: CH-related variants are frequently observed in patients with advanced NSCLC……51

Figure 15: Comparison of age, variant allele frequency (VAF), and fragment size distribution between clonal hematopoiesis (CH)-related variants and tumor-specific variants……52

Figure 16: Distribution and clinical impact of CHIP variants in advanced NSCLC patients……53

Figure 17: Molecular profiling of plasma samples and concordance with tissue tissue……55

Figure 18: ctDNA level distribution stratified by treatment response and time point……61

Figure 19: Correlation of dynamic ctDNA changes with response to ICI……63

Figure 20: ctDNA molecular responses differ between responders and non-responders……64

Figure 21: Impact of clonal hematopoiesis (CH)-related variants on interpretation of ctDNA response.....64

Figure 22: Elevated ctDNA is linked to poorer survival outcomes, while low or absent ctDNA correlates with improved prognosis 66

Figure 23: Changes in ctDNA levels during ICI treatment correlate with patient survival.....68

Figure 24: Impact of molecular ctDNA response thresholds on survival outcomes with and without exclusion of CHIP-related variants.....69

Figure 25: On treatment changes are linked to survival outcomes.....71

Figure 26: *De novo* mutation calling from plasma yields comparable results to a tumor-guided strategy.....73

Figure 27: *De novo* variant calling offers comparable patient stratification performance to the tumor-guided approach.....73

Figure 28: Impact of *STK11* and *KEAP1* mutations on survival outcomes.....75

LIST OF TABLES

Table 1: FDA-approved immune checkpoint inhibitors for the treatment of NSCLC with corresponding clinical trials.....6

Table 2: Mutations in the Seraseq® ctDNA reference material v2 covered by the various NGS kits included in the study.....20

Table 3: Mutations in Seraseq® ctDNA Complete™ reference material covered by the AVENIO Targeted and the AVENIO Expanded assay.....21

Table 4: Overview of Cancer-ID partner sites and the mutation analysis assays they conducted 26

Table 5: False positive variant detections across different LOD thresholds.....42

Table 6: Variant allele frequency (VAF) of mutations in Seraseq® ctDNA Complete™ reference material using the AVENIO Expanded assay.....43

Table 7: Baseline patient characteristics.....45

Table 8: Stepwise Cox regression analysis aimed at determining which ctDNA metric (median aMM, hMM, aVAF, hVAF) best discriminates overall survival (OS) at two time points (t_0 and t_1).....49

Table 9: Stepwise Cox regression analysis used to evaluate which ctDNA proxy response (aMM, hMM, aVAF, hVAF) best predicts overall survival (OS), using 50% a cut-off for response.....50

Table 10: Concordance of tissue and plasma molecular profiling.....56-59

Table 11: Multivariate Cox regression analysis of clinical factors associated with survival.....76

Table 12: Impact of dynamic ctDNA response and STK11/KEAP1 mutation status on progression-free survival (PFS), adjusted for clinical parameters, in 152 patients with advanced NSCLC receiving immune checkpoint inhibitors. 77

Table 13: Influence of dynamic ctDNA response and STK11/KEAP1 mutation status on overall survival (OS), adjusted for clinical parameters, in 152 patients with advanced NSCLC undergoing ICI therapy. 77

Table 14: Effect of dynamic ctDNA changes on overall survival (OS), adjusted for clinical parameters, in 110 patients* with advanced NSCLC and available PD-L1 expression data.....78

Table 15: Effect of dynamic ctDNA changes and PD-L1 expression on landmark overall survival (OS), adjusted for clinical variables, in 96 patients*.....78

ZUSAMMENFASSUNG

Trotz erheblicher Fortschritte im Bereich der Krebs-Immuntherapie bleibt die prädiktive Bewertung des Ansprechens auf Immun-Checkpoint-Inhibitoren bei Patient:innen mit fortgeschrittenem nicht-kleinzelligem Lungenkarzinom (NSCLC) eine zentrale Herausforderung. Ziel dieser Arbeit war es, die Dynamik zirkulierender Tumor-DNA (ctDNA) in peripherem Blutplasma als nicht-invasiven Biomarker zur Überwachung des Ansprechens auf Immun-Checkpoint-Inhibitoren zu untersuchen und ihren prädiktiven sowie prognostischen Nutzen zu bewerten.

Zur Auswahl eines geeigneten Analyseverfahrens wurden mehrere kommerzielle ctDNA-Assays hinsichtlich Sensitivität und Spezifität mittels standardisierter Referenzmaterialen geprüft. Der AVENIO ctDNA Expanded Kit zeigte dabei die beste Gesamtperformance und wurde deshalb für die nachfolgende, klinische Studie eingesetzt. In dieser Studie wurden 167 Patient:innen mit fortgeschrittenem NSCLC eingeschlossen, die mit Immun-Checkpoint-Inhibitoren behandelt wurden. Die ctDNA-Analysen mittels NGS erfolgten zu zwei definierten Zeitpunkten: vor Therapiebeginn (t_0) und nach zwei Zyklen mit Immun-Checkpoint-Inhibitoren (t_1). Zusätzlich wurden periphere mononukleäre Blutzellen (PBMCs) sequenziert, um Varianten, die mit klonaler Hämatopoese assoziiert sind (CH), und Keimbahnvarianten auszuschließen.

Die quantitative Auswertung erfolgte über mehrere ctDNA-Parameter (z. B. durchschnittliche Mutantenmoleküle/ml Plasma (aMM), Variant-Allelfrequenz (VAF)). Eine Abnahme der aMM um ≥ 50 % zwischen t_0 und t_1 war signifikant mit verbessertem progressionsfreiem Überleben (Median 10,0 vs. 2,0 Monate) und Gesamtüberleben (Median 18,4 vs. 5,9 Monate) assoziiert. Eine 2-Monats-Landmark-Analyse bestätigte die prognostische Relevanz des molekularen Ansprechens. Darüber hinaus zeigte sich, dass Patient:innen ohne detektierbare ctDNA zu beiden Zeitpunkten eine besonders günstige Prognose aufwiesen. Die prognostische Relevanz der ctDNA-Dynamik blieb auch in multivariaten Modellen unter Berücksichtigung klinischer Parameter bestehen. Aufgrund des Ausschlusses der CH-assoziierten Varianten, die in 45% der Patient:innen nachweisbar waren, konnte die Aussagekraft der molekularen ctDNA-Analyse

gesteigert werden. Ohne Korrektur durch PBMC-Daten wären 20 Patient:innen fälschlich als molekulare Responder oder Non-Responder eingestuft worden. Zudem war das Vorliegen von *STK11*- und/oder *KEAP1*-Mutatonen mit einer ungünstigen Prognose assoziiert, unabhänging von ctDNA-Dynamik oder PD-L1 Expression. Die Tumor-PD-L1-Expression allein (≥50 % vs. <50 %) war kein signifikanter unabhängiger Prädiktor für das Überleben, was den Mehrwert dynamischer ctDNA-Messungen unterstreicht.

Diese Arbeit belegt, dass ctDNA Dynamik, vor allem die frühe Reduktion der aMM, als zuverlässiger, nichtinvasiver Biomarker zur Therapieüberwachung bei NSCLC-Patient:innen unter ICI-Therapie dienen könnte. Die Kombination aus analytisch validierter NGS-Plattform, Ausschluss von biologischen Störfaktoren (CH), umfassender molekularer Charakterisierung und klinischer Korrelation liefert eine robuste Grundlage für den Einsatz von ctDNA als Instrument der personalisierten Onkologie.

ABSTRACT

Non-small cell lung cancer (NSCLC) remains one of the most lethal malignancies worldwide, and while immune checkpoint inhibitors (ICIs) have transformed the treatment landscape for advances stages, reliable biomarkers to predict treatment response and guide clinical decision-making are still lacking. This study investigated the potential of circulating tumor DNA (ctDNA) dynamics as a minimally invasive biomarker to predict and monitor treatment outcomes in NSCLC patients undergoing ICI therapy. The study evaluated both the technical feasibility and clinical relevance of ctDNA profiling, leveraging high- sensitivity next-generation sequencing (NGS) approaches.

To identify the most suitable ctDNA detection method, multiple commercial assays were rigorously validated using standardized reference materials with known variant allele frequencies (VAF). The AVENIO ctDNA Expanded Kit demonstrated the highest sensitivity and specificity, detecting 65% of expected variant even at a 0.1% VAF. Based on this performance, the assay was applied to a cohort of 167 patients with IIIB-IV NSCLC treated with ICIs. ctDNA was extracted from plasma samples at two time points: before treatment start (t_0) and after two cycles (t_1). ctDNA levels were quantified using multiple proxies, including average mutant molecules per milliliter (aMM) and VAF metrics.

Dynamic changes in ctDNA levels, particularly a ≥50% reduction in aMM were strongly correlated with improved progression-free survival (median 10.0 vs. 2.0 months) and overall survival median (18.4 vs. 5.9 months). Furthermore, a landmark analysis at two months confirmed the early predictive value of molecular response, supporting its utility for real-time clinical decision-making.

To ensure specificity of tumor-derived variants, paired sequencing of peripheral blood mononuclear cells (PBMCs) was performed to exclude clonal hematopoiesis (CH)-related mutations, which were found in about 45% of patients. This correction substantially improved response classification and reduced false-positive ctDNA signals. Additionally, patients with *STK11* or *KEAP1* mutations exhibited significantly poorer outcomes.

These findings demonstrate that ctDNA dynamics, when corrected for CH interference and measured using a validated assay, serve as a robust early indicator of therapeutic effectiveness and patient prognosis in advanced NSCLC, offering valuable guidance for personalized treatment strategies.

1. INTRODUCTION

1.1. Lung cancer

Lung cancer is the top cause of cancer-related deaths worldwide, responsible for around 1.8 million deaths annually according to the World Health Organization (WHO) (1, 2) with more cancer deaths in 2020 than breast, prostate, and colorectal cancers together. In the United States 350 individuals per day die of lung cancer (3). Both men and women are affected by lung cancer, but men have a slightly higher incidence rate. Smoking is the primary risk factor, which is responsible for over 80% of all cases (4). As a result, smoking cessation has become a significant focus of public health efforts to reduce the incidence and mortality of lung cancer (5, 6). However, non-smokers can also develop lung cancer, and 12% of patients with lung cancer have never smoked cigarettes (7). Consequently, other risk factors such as passive smoking (8), previous radiation therapy (9), exposure to radon (10), asbestos, and other carcinogens, as well as a family history of lung cancer (11, 12), may contribute to the development of lung cancer, albeit not as strongly as smoking (13, 14).

As symptoms such as cough, thoracic pain, and shortness of breath are very nonspecific and can be misdiagnosed to other health conditions, lung cancer is most frequently diagnosed at a locally advanced stage (stage III) or with synchronous metastases (stage IV) (15-17). Merely, a limited fraction of individuals with non-small cell lung cancer (<20%) receive an early-stage diagnosis. Despite advances in diagnostic tools and treatment options, the prognosis for lung cancer patients remains poor. The 5-year relative survival rate for all stages combined is around 22% (3).

1.2. Histology

The first diagnostic screening tests for people with suspected lung cancer are chest X-ray, Computed tomography (CT) scan and/or Positron Emission Tomography (PET) /CT scan (18). Due to the different treatment options for the various subtypes of lung carcinoma, exact subtyping is crucial and is mostly carried out on tissue samples, which are obtained by bronchoscopy, transbronchial needle aspiration, transthoracic fine needle aspiration, core

biopsy etc. (19). Lung cancer is a heterogeneous disease with two main histologic types including non-small cell lung cancer (NSCLC) and small cell lung cancer (SCLC). SCLC is a highly aggressive subtype of lung cancer characterized by small, round cells, with a higher likelihood of spreading beyond the lungs at the time of diagnosis compared to non-small cell lung cancer (20, 21), making it challenging to treat.

NSCLC accounts for 80-85% of all lung cancer cases (1) and is further subclassified in adenocarcinoma, squamous cell carcinoma, and large cell carcinoma.

Adenocarcinomas are the most prevalent type of NSCLC (40%) (22), with a slight overrepresentation in women compared to men (23, 24). This subtype can be treated more effectively than other types of lung cancer because it often carries actionable mutations that can be targeted with specific treatments (25).

Squamous cell carcinomas account for 25% to 30% of lung cancers and is strongly associated with smoking. It is typically found in the central parts of the lungs, near the bronchial tubes (22).

Large cell carcinoma, a less common and more aggressive subtype, can develop in any part of the lung. It typically grows and spreads faster than the other two subtypes, making it more challenging to treat effectively. The incidence of large cell carcinomas has decreased to 1% due to advanced immunophenotyping methods, which enable more precise classification of poorly differentiated carcinomas (26, 27).

In 2015, the WHO released a revised version on lung cancer classification with adenocarcinoma, squamous cell carcinoma, and neuroendocrine tumors as the main histological types (20). Other defined categories include large cell carcinoma, adenosquamous carcinoma, sarcomatoid carcinoma, and miscellaneous unclassified tumors (23). According to the updated WHO classification guidelines, SCLC is no longer considered a distinct tumor type; instead, it is now categorized as a subtype of neuroendocrine tumors (20).

1.3. Treatment options and mutational landscape

The field of NSCLC is experiencing continuous and dynamic changes, especially with regard to treatment methods. Alongside conventional platinum-based chemotherapy standard

treatments, the biomarker-guided targeted therapies are gaining importance, and the concept of "precision medicine" is assuming a progressively significant role in the field of treatment.

The diverse composition of the mutations landscape and growth patterns of NSCLC pose a major challenge in the treatment of patients with advanced stages of the disease (28, 29). Traditional treatment modalities for NSCLC include surgery, chemotherapy, and radiation therapy, alone or in combination, depending on subtype and tumor stage. Despite their effectiveness in some cases, these conventional treatments have limitations and may not be suitable for patients with advanced-stage NSCLC who are not candidates for surgical resection due to comorbidities or poor overall health status. Additionally, chemotherapy can cause systemic toxicity and adverse side effects (30).

Treatment response is currently monitored mostly by imaging using RECIST (Response Evaluation Criteria in Solid Tumors) or iRECIST (i.e., immune) criteria (31), however this approach may not be the best predictive marker. RECIST primarily evaluates changes in tumor size to assess treatment efficacy. However, many therapies, such as immunotherapy, may not immediately reduce tumor size despite being effective. For instance, immune checkpoint inhibitors can lead to a phenomenon called pseudoprogression, where the tumor initially appears to grow due to immune cell infiltration before shrinking. Moreover, RECIST relies on imaging interpretations that may be influenced by variations in imaging quality, reader expertise, and criteria application, introducing variability and potential biases in evaluation (31).

1.3.1. Tyrosine kinase inhibitor therapy

Tyrosine kinase inhibitors (TKIs) are a class of targeted cancer therapies that block the action of enzymes called tyrosine kinases. These enzymes play a critical role in signaling pathways that regulate cell growth, division, and survival and are frequently mutated in NSCLC. In particular, somatic alterations in genes such as *ALK*, *EGFR*, *BRAF*, *MET*, *NTRK, RET* and *ROS1* play a crucial role in determining the most appropriate therapy for patients who are eligible for TKI therapy. As NSCLC is characterized by various oncogenic driver mutations, such as point mutations, insertions, deletions, and rearrangements (32), proper molecular testing is essential to guide treatment decisions. The European Society of Medical Oncology (ESMO)

recommends in their NSCLC guidelines the molecular testing of *EGFR* and *BRAF* mutations and assessment of *ALK*, *ROS1*, and *NTRK* rearrangements (19). *EGFR* mutations are the most common targets for targeted therapy, as approximately 10-20% of lung adenocarcinoma tumors in Caucasian patients carry an activating mutation in this gene (19, 33), with small deletions in exon 19 and a missense mutation known as L858R in exon 21 being the most prevalent ones. These specific mutations have been linked to a positive response to TKI therapy and guidelines recommend the complete sequencing of exons 18-21 (19, 34-36). However, despite initial responses and prolonged remissions, the development of secondary resistance ultimately results in treatment failure (37).

In the majority of cases, resistance to first- and second-generation *EGFR* tyrosine kinase inhibitors in *EGFR*-driven cancers can be attributed to the occurrence of the *T790M* exon 20 mutation. This genetic alteration blocks the binding of both first-generation and second-generation TKIs to the EGFR protein, thereby impeding their therapeutic efficacy (38). Osimertinib, a third-generation EGFR-TKI, is currently approved as a first-line therapy for patients with NSCLC harboring sensitizing *EGFR* mutations, as a second-line therapy for patients with the resistance-associated T790M mutation following prior EGFR-TKI treatment, and as adjuvant therapy for patients with early-stage resected NSCLC with *EGFR* mutations. Despite durable responses in patients with advanced NSCLC, resistance to osimertinib, like other targeted therapies, inevitably develops (39).

Following the approval of BRAF and MEK inhibitors for *BRAF* V600 mutant NSCLC, numerous countries now mandate *BRAF* mutation testing (19).

1.3.2. Immune checkpoint inhibitors

In NSCLC patients, who do not have oncogenic driver alterations, treatment with immune checkpoint inhibitors (ICI) shows success in terms of therapy response and overall survival (OS) (40-44). ICI therapy has dramatically changed the management of advanced NSCLC by leading to long-term disease control with fewer side effects compared to chemotherapy (40, 45). In contrast to conventional therapies, ICIs exert antitumor effects by activating the host immune system to target and eliminate cancer cells (46-48).

Tumors employ various strategies to evade immune recognition, including impaired antigen presentation, secretion of immunosuppressive factors, recruitment of inhibitory immune cells, down-regulation of natural killer cells, and modulation of immune checkpoint pathways. Immune checkpoint pathways, in particular cytotoxic T-lymphocyte-associated antigen 4 (CTLA-4) and programmed cell death protein 1 (PD-1) with its ligands programmed cell death 1- ligand 1 (PD-L1) and programmed cell death 1 – ligand 2 (PD-L2) play a crucial role in the regulation of lymphocyte activation and are key targets for cancer immunotherapy (45, 46). Only ICIs targeting CTLA-4 and PD-1/PD-L1 have been approved by the U.S. Food and Drug Administration (FDA) and widely used. CTLA-4 regulates T-cell activity at an early stage, whereas PD-1 predominantly regulates later effector T-cell activity within tissues and tumors (extensively reviewed in (45, 47), (Figure 1)).

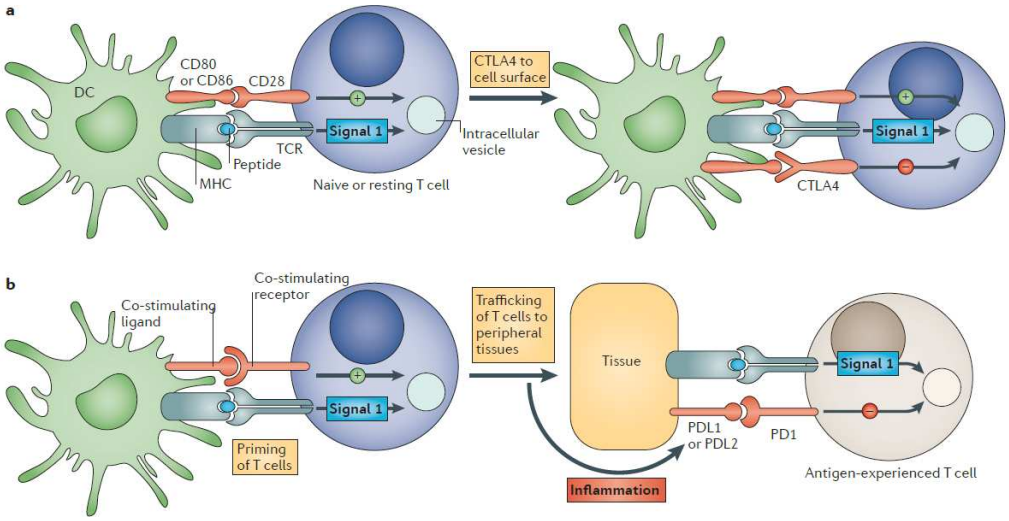

Figure 1: Immune checkpoints regulate different components in the evolution of an immune response.
a | The CTLA4-mediated immune checkpoint is induced in T cells at the time of their initial response to antigen. The level of CTLA4 induction depends on the amplitude of the initial T cell receptor (TCR)-mediated signalling. High-affinity ligands induce higher levels of CTLA4, which dampens the amplitude of the initial response. The key to the regulation of T cell activation levels by the CD28–CTLA4 system is the timing of surface expression. Naive and memory T cells express high levels of cell surface CD28 but do not express CTLA4 on their surface. Instead, CTLA4 is sequestered in intracellular vesicles. After the TCR is triggered by antigen encounter, CTLA4 is transported to the cell surface. The stronger the stimulation through the TCR (and CD28), the greater the amount of CTLA4 that is deposited on the T cell surface. Therefore, CTLA4 functions as a signal dampener to maintain a consistent level of T cell activation in the face of widely varying concentrations and affinities of ligand for the TCR. **b |** By contrast, the major role of the programmed cell death protein 1 (PD1) pathway is not at the initial T cell activation stage but rather to regulate inflammatory responses in tissues by effector T cells recognizing antigen in peripheral tissues. Activated T cells upregulate PD1 and continue to express it in tissues. Inflammatory signals in the tissues induce the expression of PD1 ligands, which downregulate the activity of T cells and thus limit collateral tissue damage in response to a microorganism infection in that tissue. The best characterized signal for PD1 ligand 1 (PDL1; also known as B7-H1) induction is interferon-γ (IFNγ), which is predominantly produced by T helper 1 (TH1) cells, although many of the signals have not yet been defined completely. Excessive induction of PD1 on T cells in the setting of chronic antigen exposure can induce an exhausted or anergic state in T cells. MHC, major histocompatibility complex. [Figure and legend originally published from Pardoll (45), reprinted with permission from Springer Nature BV (license number: 1443241-1)]

The first ICI ipilimumab, a fully human IgG1κ monoclonal antibody (mAb) directed against cytotoxic CTLA4, was FDA-approved in 2011 for the treatment of advanced melanoma and later for metastatic lung cancer (48). In 2015, two ICI targeting PD-1, nivolumab and pembrolizumab, got approval for second line therapy of NSCLC (49). Later, in 2016, atezolizumab (OAK trial) was accepted as second-line NSCLC therapy (targeting PD-L1), while pembrolizumab was introduced as a first-line therapy for NSCLC without the presence of driver mutations (50). In addition, durvalumab received FDA approval for use as a second-line immune checkpoint inhibitor in 2018. Then in 2021, the FDA approved a new immune checkpoint inhibitor, cemiplimab, a human IgG4 anti-PD1 mAb, for advanced NSCLC with PD-L1 expression of at least 50% (EMPOWER-Lung 1 study; (51)). Previously, it had already been used for the treatment of locally advanced and metastatic cutaneous squamous cell carcinoma (CSCC). In different clinical studies, cemiplimab was demonstrated to be a new potential treatment for NSCLC (see review (29)) (Table 1).

Table 1: FDA-approved immune checkpoint inhibitors for the treatment of NSCLC with corresponding clinical trials. [Table and legend reprinted from Rodak et al. (29)(CC BY-NC-ND 4.0)]

Checkpoint Inhibitor	Target	Line of Treatment	Indications	Clinical Trial-Based Approval	FDA Approval Year
Nivolumab	PD-1	second-line	metastatic squamous NSCLC after chemotherapy;	CheckMate 017 (NCT01642004)	2015
		second-line	extension to non-squamous NSCLC;	CheckMate 057 (NCT1673867)	
Pembrolizumab	PD-1	first-line	metastatic NSCLC; with no EGFR or ALK mutation; TPS ≥ 50%;	KEYNOTE-024 (NCT02142738)	2016
		second-line	progression after chemotherapy or TKI in metastatic NSCLC; with TPS ≥ 1%;	KEYNOTE-010 (NCT01905657)	
		first-line	unresectable stage III or metastatic NSCLC; no possible definitive chemoradiation; with no EGFR or ALK mutations; TPS ≥ 1%;	KEYNOTE-042 (NCT02220894)	2019
Atezolizumab	PDL-1	second-line	metastatic NSCLC with progression on/after chemotherapy or TKIS;	OAK (NCT02008227) POLAR (NCT01903993)	2016
		first-line	combined with chemotherapy; metastatic non-squamous NSCLC; with no EGFR or ALK mutation;	Impower150 (NCT02366143)	2018
Durvalumab	PDL-1	second-line	unresectable Stage III NSCLC; with no progression after chemoradiation therapy;	PACIFIC (NCT02125461)	2018
Ipilimumab	CTLA-4	first-line	only in the combination with nivolumab; metastatic NSCLC; with no EGFR or ALK mutation; TPS ≥ 1%;	CheckMate 227 (NCT02477826)	2020
Cemiplimab	PD-1	first-line	advanced NSCLC; TPS ≥ 50%	EMPOWER-Lung 1 (NCT03088540)	2021

Since only a small number of patients (approximately 20%) gain a long-term benefit from immunotherapy, there is a significant demand for enhanced biomarkers with prognostic and predictive value (3, 52).

1.4. Tumor-derived ICI-related biomarkers

While ICIs therapy has demonstrated strong anti-tumor efficacy, certain patients do not exhibit the intended response to this therapeutic intervention. Consequently, increased attention has been devoted to the identification and development of predictive biomarkers for response to immunotherapy. Currently, primary predictive markers for ICIs response include PD-L1 expression, high tumor mutational burden (TMB), microsatellite instability (MSI), CD8 infiltration, and PD-L1 amplification (reviewed in (53-56)).

1.4.1. PD-1/PD-L1 expression

In addition to targeted molecular testing of specific gene regions, ESMO recommends the assessing PD-L1 expression in patients with advanced NSCLC for therapeutic decision-making (19), which is the current to select NSCLC patients, who most achieve a benefit from immunotherapy.

PD-1 and PD-L1 are important proteins for maintaining immune homeostasis (57) by inhibiting immune cell hyperactivation and preventing autoimmune disease through the PD-1/PD-L1 pathway (58). Nonetheless, within the tumor microenvironment cancer cells use the PD-1/PD-L1 pathway to evade immune surveillance (59). The overexpressed PD-L1 on cancer cells attaches to the PD-1 receptors found on lymphocytes infiltrating the tumor and impedes the activation of the T cells (60, 61) (Figure 2).

Emerging evidence indicates that the addition of immune checkpoint inhibitors to platinum-based dual chemotherapy yields therapeutic advantages in both lung adenocarcinoma (41) and squamous cell carcinomas (62), irrespective of PD-L1 expression status. However, clinical outcomes were less robust in patients with low PD-L1 expression considering subgroups. Despite their importance as a predictor of efficacy, many clinical trials testing checkpoint inhibitors as monotherapeutics have shown that some patients with high PD-L1 expression still do not benefit from these agents.

Even among patients whose tumors express high levels of PD-L1 (≥50% of tumor cells), than more than half of cases do not exhibit a prolonged response to pembrolizumab treatment (41, 63, 64). Similarly, first-line monotherapy with nivolumab demonstrated a 4-year OS rate of 14% (95% CI: 11–17%) across all patients. This rate increased to 19% in those with PD-L1 expression ≥1%, but paradoxically dropped to 11% in patients with PD-L1 expression above 1% (65, 66).

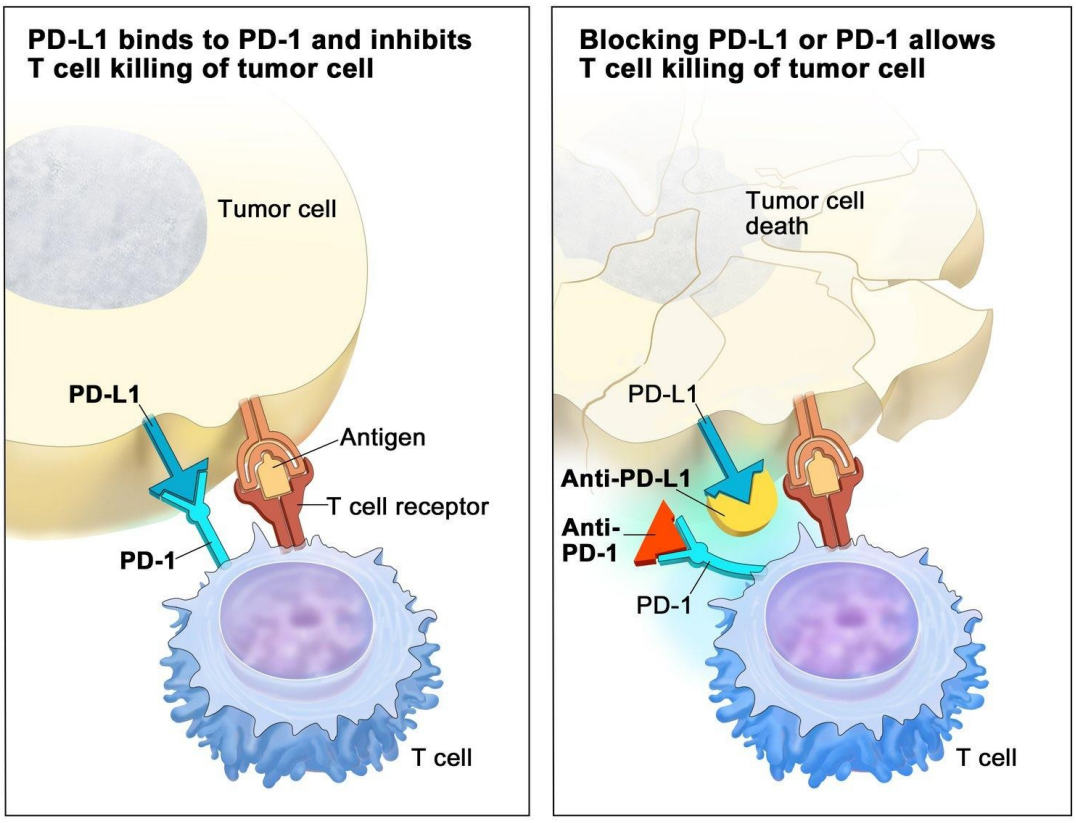

Figure 2: Checkpoint proteins, such as PD-L1 on tumor cells and PD-1 on T cells, help keep immune responses in check. The binding of PD-L1 to PD-1 keeps T cells from killing tumor cells in the body (left panel). Blocking the binding of PD-L1 to PD-1 with an immune checkpoint inhibitor (anti-PD-L1 or anti-PD-1) allows the T cells to kill tumor cells (right panel). [Reprinted with permission from ©2015 Terese Winslow LLC, U.S. Govt has certain rights].

1.4.2. Tumor mutational burden

The tumor mutational burden (TMB) serves as an additional predictive biomarker for response to ICIs and is defined as the number of non-synonymous somatic mutations found per tumor genome coding region, expressed as mutations per megabase (mut/Mb) (67, 68). The presence of non-synonymous somatic variations can lead to aberrant proteins, some of which

are no longer recognized as endogenous by the immune system. These proteins can become neoantigens that activate the anti-tumor immune response (69). TMB increases the likelihood of generating a diverse set of neoantigens, which in turn enhances the probability of effective T-cell activation and tumor recognition (64, 70). Since its first identification as a potential biomarker for ICI in melanoma by Snyder et al. in 2014, several studies have emphasized an association of a high TMB and the effectiveness of ICIs, suggesting its potential as a predictive biomarker (71). The FDA granted tissue-agnostic approval for pembrolizumab for the treatment of patients with unresectable or metastatic cancers with a TMB ≥10 mutations/Mb solid tumors (72). The FDA's decision was based on the objective response rate (ORR) data from 102 patients, primarily with 81 microsatellite stability tumors across nine cancer types, treated in the phase 2 KEYNOTE-158 trial (73). The largest subgroup (33%) consisted of SCLC. In the TMB-high group, ORR was observed in 30 out of 102 patients (29%, 95% CI 21-39), compared to 43 out of 688 patients in non-TMB-high group (6%; 95% CI 5-8) (73). Despite promising data, there are still many challenges for the further development of TMB as a clinical biomarker, as PD-L1 expression and TMB show limited correlation in most cancer subtypes (74-76).

1.4.3. Other biomarkers

Other tumor derived biomarkers include microsatellite instability (MSI) and deficiency of DNA damage and repair-related genes. Microsatellites are short tandem repeat sequences with 10–50 repetitions of a small DNA motif found throughout the genome (77). MSI is caused by defects in the mismatch repair pathway, leading to deficient mismatch repair (dMMR), proliferation of microsatellite replication errors, and diffuse MSI. When this repair mechanism is impaired, mutations accumulate across the genome, leading to a higher TMB and the generation of neoantigens. This has led researchers to speculate that the abundance of mutated neoantigens in dMMR cancers makes them susceptible to immune checkpoint blockade, irrespective of the tissue of origin of the cancer (78).

Several studies demonstrated that patients with dMMR exhibit enhanced responses to PD-1 inhibitor treatment. In a phase II study, the PD-1 inhibitor pembrolizumab has demonstrated effectiveness in treating metastatic tumors, whether or not they exhibit dMMR (79). In

advanced dMMR cases across twelve different tumor types, PD-1 inhibitor treatment resulted in radiological remission in 53% and complete response in 21% of patients, respectively (80, 81). Although recent data indicated that up to 14 tumor types display MSI, suggesting a widespread occurrence of MSI in various cancers (80, 81), MSI is most common in endometrial cancer and colon carcinoma. In contrast, only 0.8% of lung cancers present MSI (82).

DNA damage response (DDR) related genes play an important role in the human DNA damage repair mechanisms. Inability to promptly and precisely repair DNA damage may lead to diverse genomic abnormalities, such as point mutations, chromosomal translocations, and the acquisition or loss of chromosomal segments or entire chromosomes. In some cases, these genomic alterations produce changes in cell physiology that drive tumor initiation (reviewed in (83)). Hugo and colleagues showed that loss-of-function (LoF) mutations in *BRCA2*, a gene crucial in DNA damage repair, were significantly enriched in melanomas responsive to anti-PD-1 treatment. Among 38 patients with advanced metastatic melanoma undergoing PD-1 therapy, 28% of those who exhibited a positive therapeutic response had *BRCA2* mutations, while only 6% of those without a therapeutic response had such mutations (84).

Mutations in the tumor suppressor genes *TP53* and *STK11* are frequently observed in lung adenocarcinoma, often concurrently with *KRAS* mutations (reviewed in detail in (85, 86)). Studies suggest that NSCLC tumors harboring *TP53* or *KRAS* mutations have increased PD-L1 expression compared to wild-type tumors (87-89). Notably, Dong et al. suggested using *TP53* and *KRAS* mutations in lung adenocarcinoma to guide PD-1/PD-L1 antibody immunotherapy (90).

1.5. Liquid biopsy

In the last decade, liquid biopsy has emerged as a revolutionary paradigm in cancer diagnostics, offering a less invasive alternative to conventional tissue biopsies. Liquid biopsies are referred to as the detection and/or analysis of circulating tumor cells (CTC) and as well as cell-free DNA (cfDNA), cell-free RNA (cfRNA), extracellular vesicles, proteins, lipids and metabolites present in biofluids (91-96). Although liquid biopsies can be obtained from various body fluids, including serum, cerebrospinal fluid, pleural fluid, saliva, urine, stool and ascites (96, 97), this study specifically focuses on cfDNA from blood plasma samples.

1.5.1. Cell-free circulating tumor DNA

Liquid biopsy represents a promising avenue for improving cancer diagnostics as it offers a comprehensive and less invasive means of obtaining important genetic information for diseases such as NSCLC (see recent reviews (95, 98))

A promising analyte in a liquid biopsy is cfDNA, particularly circulating tumor DNA (ctDNA), which represents tumor-derived fragments within the cfDNA pool. ctDNA offers significant potential due to its ability to reflect the genetic and epigenetic alterations of tumors, such as mutations, copy number variations, methylation patterns, and chromosomal rearrangements. These characteristics make ctDNA a powerful tool for cancer detection, prognosis, monitoring treatment response, and identifying resistance mechanisms (see reviews (94, 95)).

Cell-cfDNA release into the bloodstream is a consequence of cancer cell death, primarily through processes such as apoptosis and necrosis. (99-104). Several studies have consistently reported that cfDNA typically has an average fragment size of 160 to 180 base pairs (bp) (105-107), which is consistent with the size of DNA wrapped around a nucleosome (approximately 142 bp) plus a linker (approximately 20 bp). This size closely resembles the DNA shed by apoptotic cells (108). A previous study not only confirmed the presence of cfDNA in the 160-180 bp range, but also detected cfDNA with an average size of about 320-360 bp (105). However, it is more likely that these larger DNA fragments originate from dinucleosomes than from necrosis, which is associated with DNA fragment sizes greater than 10,000 bp. In conclusion, the preponderance of evidence suggests that apoptosis is likely to be the primary source of cfDNA (95).

Research on the size profiling has indicated that cfDNA originating from cancer cells tends to be shorter compared to that released from non-cancerous cells (109-111). Since ctDNA is thought to be released from multiple tumor lesions including primary and metastatic lesions, it typically encompasses a comprehensive range of genetic and epigenetic alterations from the tumor, making it a valuable resource for disease monitoring (112). Consequently, ctDNA has the potential to reflect both intra-tumor heterogeneity and spatially separated metastases, thereby overcoming the limitations associated with traditional tissue biopsies (94, 96, 113), which only provide a snapshot of the tumor´s genome. Furthermore, ctDNA has been

shown to correlate with tumor burden. Owing to its short half-life, it is thought to be immediate reflector of tumor burden changes (114, 115), facilitating serial monitoring of treatment response and has been shown to be a reliable biomarker for the detection of minimal residual disease and the prediction of early relapse (116-118).

1.5.2. Challenges of ctDNA analysis

Several challenges can affect the clinical utility ctDNA analysis. One notable source of discrepancy between the molecular profiles of cfDNA and corresponding tumor or metastatic tissue is clonal hematopoiesis (CH) - a phenomenon characterized by the disproportionate expansion of blood cells derived from a single hematopoietic clone (119-122). As individuals age, somatic mutations can accumulate in white blood cells, and if these mutations confer a selective advantage, clonal expansion may occur. This process can lead to the emergence of detectable variants in cfDNA. Approximately 10% of individuals over the age of 65 harbor clonal hematopoiesis of indeterminate potential (CHIP) - a non-malignant form of clonal hematopoiesis involving mutations in genes frequently associated with cancer (123, 124).

As ctDNA is released into the bloodstream alongside a background of cell-free DNA (cfDNA) fragments primarily originating from the hematopoietic system and represent the predominant source of cfDNA under both physiological and pathological conditions (99, 100). CHIP-associated variants may overlap with those detected in ctDNA. This poses a risk of false-positive genotyping in plasma-based analyses (125-127).

A comprehensive pan-cancer study, which included more than 10,000 patients and utilized next generation sequencing to compared plasma-derived cfDNA with genomic material from peripheral blood mononuclear cells (PBMCs). The analysis revealed that 14% of cfDNA samples presented with CH-related variants. This finding highlights the importance of distinguishing between cfDNA alterations arising from CH and those that are tumor-specific. Ongoing research is focused on developing analytical methods capable of making this distinction. (128). Therefore, paired genotyping of the patient's PBMCs is recommended to exclude a clonal hematopoiesis - related variant and to avoid a misleading diagnosis (129).

1.5.3. Methodological approaches for ctDNA analysis

ctDNA levels can vary widely not only among tumor types, but also within the same entity Notably, even patients with metastases may present unexpectedly low fractions of ctDNA (105, 115, 130). Various cancer types, such as renal cell carcinoma, certain lung cancers or brain cancer, are typically associated with low ctDNA levels, which may limit the clinical applicability of liquid biopsy in these contexts (115). In contrast, advanced colorectal cancer, breast cancer, prostate cancer and melanoma shed high levels of ctDNA, making them perfect candidates for routine clinical use (131). Due to the often low proportion of tumor-derived DNA in the circulating cfDNA (93-95), the need arose to develop methods with high sensitivity.

Generally, two technologies for the analysis of cfDNA are available, differing primarily in their analytical sensitivity and genomic coverage (Figure 3) (132, 133). Targeted assays focus on the analysis of hotspots or gene panels, while untargeted approaches rely on whole exome (WES) or whole genome sequencing (WGS). Targeted methods are frequently used to quantify variant allele frequency (VAF) by focusing on selected genes or genomic regions of interest (VAF) (134). The advent of massively parallel NGS technologies, such as amplicon-based (135) or hybrid capture sequencing (136, 137), has unlocked the full potential of mutation-based analysis. This advance allows the simultaneous examination of multiple cancer-specific mutations with heightened analytical sensitivity (138). Recent advancements, particularly the integration of unique molecular identifiers (UMIs), have further improved detection accuracy by minimizing sequencing artifacts. UMIs correct for technical errors introduced during library preparation and thus allow for the tumor-agnostic detection of rare variants with sensitivities reaching as low as 0.1% (136, 137, 139). This improvement is especially valuable for identifying low-frequency variants in liquid biopsy samples, where tumor-derived DNA is often present in minimal amounts (94, 95).

ON the other hand, WGS - as a representative untargeted approach - offers a broad overview of the genomic landscape, allowing for the examination of somatic copy number alterations (SCNA) and structural changes (133). Similarly, WES has proven effective useful in identifying *de novo* alterations and identifying potentially actionable clinical targets for monitoring tumor progression during therapy (139). In general, untargeted sequencing methodologies do not

rely on prior knowledge of the tumor genome and are effective in capturing tumor heterogeneity. Nonetheless, genome-wide ctDNA profiling is limited by its requirement for a relatively high fraction of tumor-derived DNA in the bloodstream - often above 3–10% - to yield accurate and clinically meaningful results, making it less effective in low-shedding tumors (132) (Figure 3).

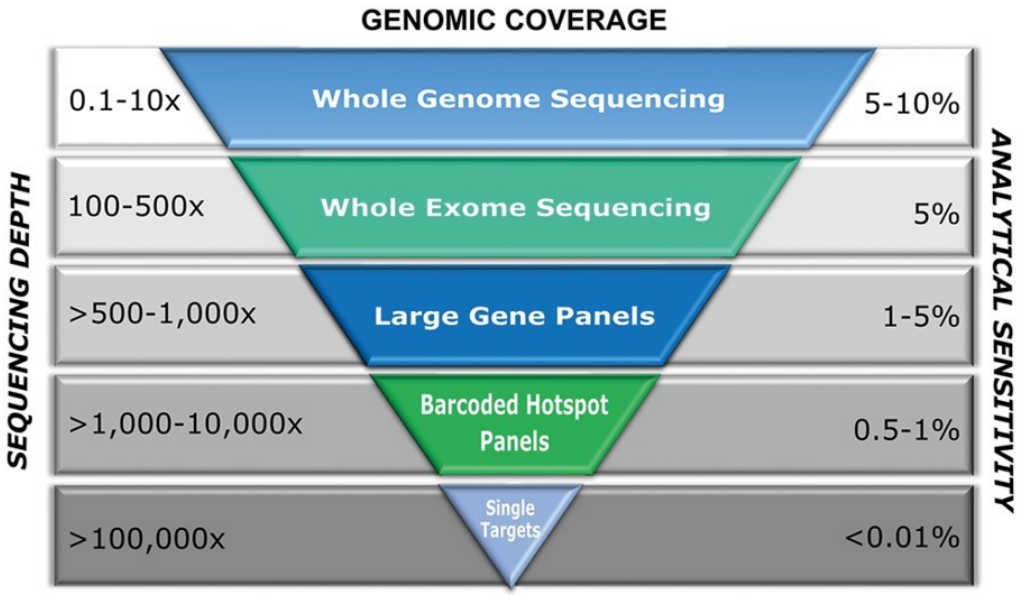

Figure 3: Genomic coverage of different ctDNA detection methods.
Illustration depicting the correlation between escalating sequencing depth and enhanced analytical sensitivity. Increased genome coverage is associated with decreasing analytical sensitivity. While the analysis of single targets or hotspots can be performed with high resolution, there is still a lack of analytical sensitivity when sequencing the entire exome or genome. [Reprinted from Zhou & Moser et al. (132) (CC BY-NC-ND 4.0)]

To inform about actionable mutations for targeted therapies, resistance mechanisms, and eligibility for immunotherapies, comprehensive genomic profiling (CGP) from cfDNA has gained traction in the past decade. CGP from ctDNA is particularly useful because it offers a non-invasive method to obtain comprehensive genetic data when tumor tissue is unavailable or insufficient.

Several CGP assays have been approved by the FDA such as the FoundationOne® CDx assay by Foundation Medicine, Inc. (Cambrigde, MA, USA) or the MSK-ACCESS ctDNA profiling test (Memorial Sloan Kettering Cancer Center, New York, NY, USA). These assays support the detection of all types of molecular alterations (e.g., single nucleotide variants, small and large

Indels, copy number alterations and structural variants) as well as complex biomarkers such as MSI, loss of heterozygosity and TMB (140, 141).

In addition to FDA-approved assays, laboratories engage in the development of proprietary tests known as laboratory-developed tests (LDTs). These *in vitro* diagnostic assessments for tumor biomarkers are conceived, fabricated, and utilized within a singular laboratory. The obtained results can then be shared with clinicians to guide patient care. Divergent from FDA-regulated diagnostic tests, LDTs are exempt from equivalent scrutiny, potentially leading to variations in analytical validity and clinical utility due to the absence of standardized evaluation procedures. Although laboratories performing LDTs must be certified and many of these tests are reliable, they are not held to the same standards as other diagnostic tests that are reviewed by the FDA and the analytical validity and clinical utility of these tests are not always thoroughly reviewed (142-144). However, the development of LDTs is not possible in every laboratory due to financial and personnel costs, which is why commercially available kits have to be used.

1.5.4. Circulating tumor cells

Besides ctDNA, another predictor for cancer development and progression is the enumeration of CTCs, which is most commonly performed using the CellSearch® System (Menarini Silicon Biosystems), a clinical system used to detect and count CTCs in a blood sample. Given the extremely low concentration of CTCs in the bloodstream, especially in comparison to the vast number of white and red blood cells, it is crucial to employ an assay that can reliably detect and enumerate CTCs within the background of normal cells. One effective strategy for enriching CTCs involves targeting the epithelial cell adhesion molecule (EpCAM), a surface marker that is commonly expressed on epithelial-derived tumor cells but largely absent on leukocytes, thereby enabling selective isolation (145-148). It is the first and only FDA-approved method for clinical use to date and mainly used in cancers like breast, prostate and colorectal (149-152). Clinical relevance has also likewise been shown in cases of metastatic SCLC and NSCLC (153, 154). In one of the first studies investigating CTCs, Cristofanilli et al. (2004) demonstrated that metastatic breast cancer patients with ≥5 CTCs per 7.5 mL of blood had shorter progression-free and overall survival than those with lower counts. A decrease in

CTC levels following treatment initiation indicated a favorable therapeutic response (152). Around the same time, Allard et al. confirmed the analytical validity of the CellSearch® system, showing high specificity and sensitivity in distinguishing cancer patients from healthy controls (155). Further research by De Bono et al. in castration-resistant prostate cancer identified CTCs as a stronger predictor of overall survival than PSA decline (156). Similarly, in metastatic colorectal cancer, a threshold of ≥3 CTCs effectively stratified patients by prognosis (157). While EpCAM-based techniques can detect CTCs originating from epithelial tumors, numerous CTCs in patients with various cancer types exhibit limited epithelial features, including low or absent EpCAM expression (158-160). This can be due to limitations in antibody efficiency (161) and the cells' phenotypic flexibility. For example, CTCs undergoing epithelial-to-mesenchymal transition may lose epithelial markers like EpCAM or E-cadherin and gain mesenchymal markers like N-cadherin, making them harder to detect (reviewed in (162)). Detection rates also differ by cancer type—$EpCAM^+$ CTCs are more common in breast, prostate, and small cell lung cancers but less so in pancreatic, colorectal, and non-small cell lung cancers (163). According to Krebs et al., only 7% of stage IIIB NSCLC patients had ≥ 2 CTCs in 7.5 mL of blood, and even among stage IV patients, this proportion was just 32% (153)). Nonetheless, higher CTC counts (≥2 or ≥5) were linked to shorter PFS and OS (153, 164). Despite significant advances in CTC enrichment and characterization, their integration into routine clinical practice remains limited, largely confined to translational research settings. Ongoing developments in single-cell analysis, alternative capture technologies, and the exploration of functional and molecular CTC properties continue to expand their potential applications (162).

2. AIMS

Accurately identifying patients who are likely to benefit from immune checkpoint inhibitor (ICI) therapy can help avoid unnecessary treatment, thereby reducing toxicity risks and minimizing healthcare costs. Therefore, the primary objective of this thesis was to investigate whether a decline in ctDNA levels was associated with a positive treatment response, suggesting its potential as an early indicator of therapeutic efficacy. A key focus was to assess the alignment between radiographic response and molecular response as measured by ctDNA, and to compare clinical outcomes between patients who demonstrated a ctDNA response and those who did not.

To this end, we first sought to identify the best performing Next Generation Sequencing (NGS)-based cfDNA assay in terms of sensitivity and specificity through extensive validation. A wide range of assays, including ddPCR, MassARRAY and various NGS-based kits were evaluated in three experimental setups. The best performing assay was used to retrospectively analyze a cohort of NCSLC patients undergoing ICI treatment.

To this end, we conducted an extensive validation to determine the most effective NGS-based cfDNA assay. Multiple platforms, including ddPCR, MassARRAY, and various NGS-based kits, were assessed with respect to their analytical performance across three experimental models. The assay demonstrating the highest performance was subsequently employed for retrospective analysis of a cohort of NSCLC patients treated with immune checkpoint inhibitors.

Specific aims were:

- To find the best performing NGS-based assay for ctDNA detection.
- To test the clinical utility of the selected NGS-based assay for predicting and monitoring response to ICI treatment in plasma DNA from NSCLC patients.
- To evaluate whether dynamic changes in ctDNA levels can serve as early indicators of treatment response to ICI therapy in NSCLC.
- To assess the agreement between ctDNA response and radiographic tumor response.

- To assess differences in overall survival (OS) and progression-free survival (PFS) between patients with a ctDNA response and those without.
- To investigate baseline ctDNA levels in association with survival.
- To perform a landmark analysis at two months after treatment initiation to evaluate survival outcomes, using this clinically meaningful time point to inform decisions regarding treatment continuation.

3. MATERIALS AND METHODS

3.1. Reference material

Two sets of commercially available ctDNA reference standards, covering different numbers of variants mutations across multiple genes commonly found in cancer with distinct allele frequencies, were used. The standard materials consisted of a synthetic mixture of fragmented DNA around a length of 170 bp that closely mimics the characteristics of ctDNA found in patient blood samples.

The Seraseq® ctDNA Reference Material v2 (SeraCare Life Sciences, Milford, MA, USA) consisted of 40 variants across 28 genes at various VAFs including 2%, 1%, 0.5%, 0.25%, 0.125% as well as an additional wild-type (WT) sample. The Seraseq® ctDNA Reference Material v2 comes in a 5 ml human plasma-like matrix called SeraCon™ Matribase, from which DNA was isolated with the QIAamp Circulating Nucleic Acid Kit (QIAGEN, Hilden, Germany) according to manufacturer`s instructions. The concentration was measured by Qubit dsDNA High Sensitivity Assay (Thermo Fisher Scientific, Waltham, MA, USA). Variants included in the Seraseq® ctDNA Reference material v2 and covered by each NGS panel are listed in Table 2 (165).

Table 2: Mutations in the Seraseq® ctDNA reference material v2 covered by the various NGS kits included in the study. Each kit's detection of a specific mutation is indicated with "YES". [Table and legend adapted from Cancers (Weber et al. (165))]

Gene	cds (HGVS)	Amino Acid Change	Mutation Type	NebNext Direct Cancer Hotspot (n=37)	QIASeq Actionable Panel (n=25)	Avenio Targeted Kit (n=17)	Oncomine LungcfDNA Assay (n=13)	GeneRead QIAact Lung UMI Panel (n=12)
AKT1	c.49G>A	p.(Glu17Lys)	SNV	YES	YES			YES
APC	c.4348C>T	p.(Arg1450*)	SNV	YES		YES		
BRAF	c.1799T>A	p.(Val600Glu)	SNV	YES	YES	YES	YES	YES
CTNNB1	c.121A>G	p.(Thr41Ala)	SNV	YES	YES			
EGFR	c.2369C>T	p.(Thr790Met)	SNV	YES	YES	YES	YES	YES
EGFR	c.2573T>G	p.(Leu858Arg)	SNV	YES	YES	YES	YES	YES
FGFR3	c.746C>G	p.(Ser249Cys)	SNV	YES				
FLT3	c.2503G>T	p.(Asp835Tyr)	SNV	YES				
FOXL2	c.402C>G	p.(Cys134Trp)	SNV		YES			
GNA11	c.626A>T	p.(Gln209Leu)	SNV	YES	YES			
GNAQ	c.626A>C	p.(Gln209Pro)	SNV	YES	YES			
GNAS	c.601C>T	p.(Arg201Cys)	SNV	YES				
IDH1	c.394C>T	p.(Arg132Cys)	SNV	YES	YES			
JAK2	c.1849G>T	p.(Val617Phe)	SNV	YES				
KIT	c.2447A>T	p.(Asp816Val)	SNV	YES	YES	YES		YES
KRAS	c.35G>A	p.(Gly12Asp)	SNV	YES	YES	YES	YES	YES
MPL	c.1544G>T	p.(Trp515Leu)	SNV	YES				
NRAS	c.182A>G	p.(Gln61Arg)	SNV	YES	YES	YES	YES	YES
PDGFRA	c.2525A>T	p.(Asp842Val)	SNV	YES		YES		YES
PIK3CA	c.1633G>A	p.(Glu545Lys)	SNV	YES	YES		YES	YES
PIK3CA	c.3140A>G	p.(His1047Arg)	SNV	YES	YES		YES	YES
RET	c.2753T>C	p.(Met918Thr)	SNV	YES	YES	YES		
TP53	c.524G>A	p.(Arg175His)	SNV	YES	YES	YES	YES	
TP53	c.818G>A	p.(Arg273His)	SNV	YES	YES	YES	YES	
TP53	c.743G>A	p.(Arg248Gln)	SNV	YES	YES	YES	YES	
ATM	c.1058_1059del	p.(Cys353Serfs*5)	Deletion	YES				
EGFR	c.2236_2250del	p.(Glu746_Ala750del)	Deletion	YES	YES	YES	YES	YES
TP53	c.723del	p.(Cys242Alafs*5)	Deletion	YES	YES			
PTEN	c.800del	p.(Lys267Argfs*9)	Deletion	YES				
TP53	c.263del	p.(Ser90Profs*33)	Deletion	YES	YES			
EGFR	c.(2310_2311insGGT)	p.(Asp770_Asn771insGly)	Insertion	YES	YES	YES	YES	YES
ERBB2	c.2313_2324dup	p.(Tyr772_Ala775dup)	Insertion	YES	YES	YES	YES	
NPM1	c.860_863dup	p.(Trp288Cysfs*12)	Insertion	YES				
PDGFRA	c.1694_1695insA	p.(Ser566Glnfs*6)	Insertion	YES	YES			
PIK3CA	c.3204_3205insA	p.(*1069Metext*3)	Insertion	YES	YES			
PTEN	c.741_742insA	p.(Pro248Thrfs*5)	Insertion	YES				
SMAD4	c.1394_1395insT	p.(Ala466Glyfs*28)	Insertion	YES				
APC	c.4666dup	p.(Thr1556Asnfs*3)	Insertion	YES				
NCOA4-RET			Gene Fusion			YES		
TPR-ALK			Gene Fusion			YES		

The Seraseq® ctDNA Complete™ Reference Material covered 25 variants, i.e. somatic nucleotide variants (SNVs), Indels, selected somatic copy number alterations (SCNAs) and fusions in 16 genes at specified VAFs (5%, 2.5%, 1%, 0.5%, 0.1%, WT) and do not require DNA extraction as it is already supplied as purified cfDNA in buffer. The mutations included in the reference material are listed in Table 3.

Table 3: Mutations in Seraseq® ctDNA Complete™ reference material covered by the AVENIO Targeted and the AVENIO Expanded assay. Each kit's detection of a specific mutation is indicated with an "X". [Table and legend adapted from Cancers (Weber et al. (165))]

Gene	cds (HGVS)	Amino Acid Change	Mutation Type	Avenio Targeted Kit (n=19)	Avenio Expanded Kit (n=22)
AKT1	c.49G>A	p.(Glu17Lys)	SNV		X
ALK	c.3604G>A	p.(Gly1202Arg)	SNV	X	X
ALK	c.3522C>A	p.(Phe1174Leu)	SNV	X	X
BRAF	c.1799T>A	p.(Val600Glu)	SNV	X	X
EGFR	c.2369C>T	p.(Thr790Met)	SNV	X	X
EGFR	c.2573T>G	p.(Leu858Arg)	SNV	X	X
KIT	c.2447A>T	p.(Asp816Val)	SNV	X	X
KRAS	c.183A>C	p.(Gln61His)	SNV	X	X
KRAS	c.35G>A	p.(Gly12Asp)	SNV	X	X
KRAS	c.34G>T	p.(Gly12Cys)	SNV	X	X
NRAS	c.182A>G	p.(Gln61Arg)	SNV	X	X
PIK3CA	c.3140A>G	p.(His1047Arg)	SNV		X
BRCA1	c.1961del	p.(Lys654Serfs*47)	Deletion	X	
BRCA2	c.7934del	p.(Arg2645Asnfs*3)	Deletion		
EGFR	c.2235_2249del	p.(Glu746_Ala750del)	Deletion	X	X
EGFR	c.2240_2257del	p.(Leu747_Pro753delinsSer)	Deletion	X	X
EGFR	c.2254_2277del	p.(Ser752_Ile759del)	Deletion	X	X
ERBB2	c.2313_2324dup	p.(Tyr772_Ala775dup)	Insertion	X	X
PIK3CA	c.3204_3205insA	p.(*1069Metext*3)	Insertion		X
ERBB2			CNV	X	X
MET			CNV	X	X
MYC			CNV		
EML4-ALKv1			Gene Fusion	X	X
CD74-ROS1			Gene Fusion		X
NCOA4-RET			Gene Fusion	X	X

3.2. Ethics and patient cohort

Patients with advanced (Stage IIIB-IV) non-small cell lung cancer (n=177) were recruited from December 2015 to May 2018 under the supervision of Harry Groen and Ed Schuuring and treated with ICI at the University Medical Center Groningen (UMCG), The Netherlands. Patients who received pembrolizumab as a first-line treatment, nivolumab as a second-line treatment, and atezolizumab as a second- or third-line treatment were included. For each patient, peripheral blood samples were collected prospectively prior to ICI treatment initiation (baseline, t_0) and after two cycles of treatment at first response evaluation (on average four weeks for nivolumab and six weeks for pembrolizumab, t_1). A total of ten patients were

excluded because of failure in analysis, library preparation, or inadequate timing of blood collection, resulting in 167 evaluable patients. In total, 334 plasma samples with advanced stage NSCLC were evaluable. Additionally, we included PBMCs of all 167 patients in our analysis (66).

In addition to blood samples, tumor tissue from 116 patients was obtained by bronchoscopy, transthoracic biopsy or wedge resection, or endoscopic ultrasound, processed, and diagnosed according to routine pathology procedures at UMCG. Patients with known targetable driver mutations such as *EGFR, BRAF, MET* mutations, or *ALK, ROS1, RET* gene rearrangements established from available primary tumor or lymph node metastasis tissues were excluded from the study. When available, tumor PD-L1 status - the percentage of PD-L1 positive tumor cells - was determined (66).

The ISO-certified biobank initiative (9001:2008 Healthcare) was approved by the medical ethics committee of the UMCG, the Netherlands (no. 2010/109), conducted according to the Declaration of Helsinki and made available to the CANCER-ID consortium (66, 166). All patients provided written informed consent for sample collection for research purposes (66).

3.3. Evaluation of response to the treatment

Patients underwent Fluorodeoxyglucose (FDG)-PET/CT before ICI treatment and CT every 6-8 weeks after treatment initiation. Tumor staging was determined with CT scans in accordance with the RECIST criteria (version 1.1, (31)). FDG-PET scans were used to determine the number of metastases in each patient. Patient response was categorized according to whether the tumor shrank, stayed the same, or increased in size, and were stratified into early responders (ER) and durable clinical responders (DCR) based on the duration of their response. Early responders showed complete response (CR) or partial tumor response (PR) at first staging. The DCR group was defined as CR, PR or sustained stable disease (SD) for more than 6 months. Patients who did not have a response durable response (non-durable responders, NDR) experienced disease progression (progressive disease, PD) within the first six months of treatment with ICI. Non-responders (NR) showed no response at first tumor assessment. In a subset of patients, response assessment was not performed due to very rapid disease

progression (not evaluable, NE) and therefore these patients were included in the progressive disease group. Progression-free survival (PFS) was defined from the day of first ICI treatment until tumor progression as determined by imaging or death. OS was defined from the first day of ICI administration until death. Patients who did not meet the primary endpoint were censored on the day of the last follow-up visit (66).

3.4. Blood sample collection, processing and isolation of cfDNA

3.4.1. Plasma extraction

Peripheral whole blood samples were collected at the UMCG from patients in sterile tubes coated with ethylenediaminetetraacetid acid (EDTA) (BD Biosciences, Franklin Lakes, NJ, USA) or in cell-free DNA blood collection tubes (BCTs) (Streck, Omaha, NE, USA). EDTA samples were processed within four hours of venipuncture. To separate lymphocytes from plasma, samples were first centrifuged at at 820×g for 10 min at 4°C. The resulting supernatant underwent a second centrifugation at 16,000×g at 4°C for another ten minutes to remove residual cellular debris. Plasma was then aliquoted into 1 mL portions and stored at −80 °C until cfDNA isolation (167). Cell-free DNA BCTs were processed within 24 hours following the same protocol, with the exception of an initial centrifugation at 1600×g in accordance with the manufacturer's guidelines. All centrifugation steps were conducted at room temperature (66).

3.4.2. cfDNA extraction

cfDNA was isolated at our laboratory from an average of 1.8 ml plasma (range 0.5 – 2.2 ml) using the QIAamp Circulating Nucleic Acid Kit (n=331 samples) or the PAXgene Blood ccfDNA Kit on the QIAsymphony device (both QIAGEN) (n=17 samples) and quantified using the Qubit dsDNA High Sensitivity Assay Kit (Thermo Fisher Scientific) in accordance with the manufacturer´s instruction (66).

DNA was isolated from 5 ml Seraseq® ctDNA Reference Material v2 with the QIAamp Circulating Nucleic Acid Kit (QIAGEN) according to manufacturer's instructions and the DNA concentration was measured using the Qubit dsDNA High Sensitivity Assay (Thermo Fisher Scientific).

3.5. Lymphocyte collection from EDTA blood and gDNA isolation

To correct for germline variants and variants derived from clonal hematopoiesis, genomic DNA (gDNA) from buffy coats was additionally analyzed. To this end, the mononuclear and red blood cell fraction were transferred into a 50 ml tube after the first centrifugation step for plasma extraction, Ammonium-chloride-potassium (ACK) buffer was added to the blood in a ratio of 3:1 (blood:lysis), incubated at 4°C for approximately 20 minutes, and centrifuged at 1000 rpm for 10 minutes. The supernatant was transferred to a new 50 mL tube, and the remaining cell pellet was resuspended in 10 mL of fresh ACK lysis buffer, followed by centrifugation under the same conditions. After removing the supernatant, the pellet was again resuspended in 1 mL of ACK buffer and centrifuged at 1000 rpm for 10 minutes at 4 °C. The final supernatant was carefully removed, and the resulting pellet was stored at –80 °C.

gDNA was subsequently isolated from the buffy coat - the leukocyte-enriched fraction of whole blood - using the Gentra Puregene Blood Kit (QIAGEN), according to the manual with minor modifications. Specifically, Proteinase K was added during the extraction process to enhance white blood cell lysis, and nuclease-free water was used for elution of the purified DNA. The concentration of gDNA was determined using the Qubit dsDNA Broad Range Assay Kit (Thermo Fisher Scientific) (66).

3.6. Assay validation and selection

To assess the performance of cfDNA-sequencing assays, we validated different mutation analysis platforms using commercially available highly multiplexed reference standards with distinct mutations at defined allele frequencies. To this end, we designed different experimental setups to evaluate the performance of reference material for inter- and intra-assay comparisons as well as between and within laboratories (Figure 4).

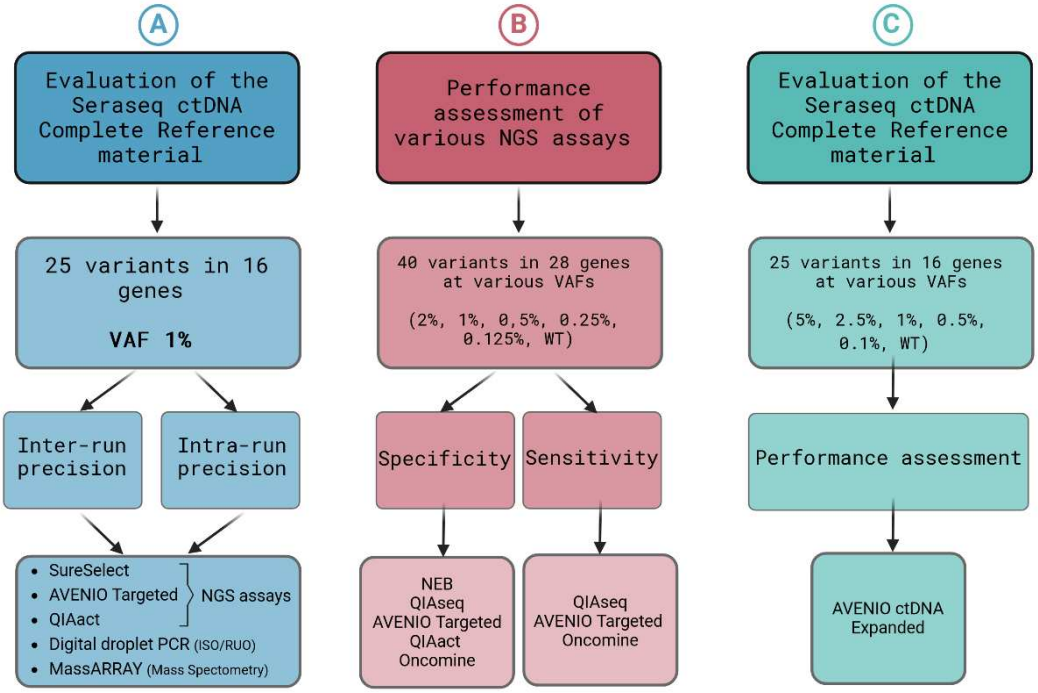

Figure 4: Experimental setup to assess Seraseq® reference material.
(A) A multicenter analysis of the Seraseq® ctDNA Complete™ Reference material was conducted using three NGS assays, two digital droplet PCR assays and the MassArray. To assess intra-run precision, the 1% variant allele frequency (VAF) reference sample was analyzed within a single workflow. Inter-run reproducibility was evaluated by processing the same material in three independent workflow runs. **(B)** The Seraseq® ctDNA Reference Material v2 was tested across five commercial mutation detection assays targeting clinically significant genes to determine their sensitivity and specificity. **(C)** Evaluation of the Seraseq® ctDNA Complete™ Reference Material's performance using the AVENIO ctDNA Expanded panel. [Figure and legend adapted from Cancers (Weber et al. (165))]

Several mutation analysis assays were used for the different study setups. While data from the AVENIO platform (Roche, Basel, Switzerland), QIAseq Human Actionable Solid Tumor assay (QIAGEN) and NEBNext Direct Cancer HotSpot Panel for Illumina (New England Biolabs, Ipswich, MA, USA) were generated in our lab, sample preparation and sequencing for a customized SureSelectXT panel (Agilent Technologies, Santa Clara, CA, USA), QIAact Lung UMI Panel (QIAGEN), Oncomine Lung cfDNA™ Assay (Thermo Fisher Scientific), two droplet digital PCR (ddPCR) assays (Bio-Rad, Hercules, CA, USA), the UltraSeek lung panel (MassARRAY, Agenda Bioscience) were performed by collaborating partners of Cancer-ID as specified in Table 4 and in accordance with the manufacturer's instructions (165).

Table 4: Overview of Cancer-ID partner sites and the mutation analysis assays they conducted [Table adapted from Weber et al. (165)]

Laboratory	ID	Assay	Platform	Study Setup
Agena	Agena	UltraSeek Lung panel (Agena Bioscience)	MassARRAY	A
BAYER	BAYER	Digital droplet PCR	Bio-Rad	A
Cancer Research UK Manchester Institute	UNIMAN	SureSelect CT Custom Kit (Agilent Technologies)	Illumina	A
Institute of Human Genetics, Medical University of Graz	MUG	AVENIO ctDNA Targeted Kit (Roche)	Illumina	A, B
		AVENIO ctDNA Expanded Kit (Roche)		C
		QIAseq Human Actionable Solid tumor assay (QIAGEN)		B
		NEBNext Direct Cancer HotSpot Panel (New England Biolabs)		B
Institute of Pathology, Medical University of Graz	MUG	QIAact Lung UMI Panel (QIAGEN)	GeneReader	A, B
		Oncomine cfDNA Lung Panel (Thermo Fisher Scientific)	Ion Torrent	B
Department of Pathology, University Medical Center Groningen	UMCG	Droplet digital droplet PCR	Bio-Rad	A

This work was done within the framework of the Innovative Medicines Initiative (IMI) program CANCER-ID. In addition, we assessed the performance of several NGS assays in terms of sensitivity and specificity. The aim was to find the best performing assay for further studies and clinical validation. The best performing assay was used to present a comprehensive mutation profiling of plasma ctDNA from patients treated with ICI therapy (66, 165).

The NGS assays used in our laboratory—QIAseq Human Actionable Solid Tumor Assay (QIAGEN), NEBNext Direct Cancer HotSpot Panel for Illumina (New England Biolabs), and both the AVENIO ctDNA Targeted and Expanded Kits (Roche) are described in detail below.

3.6.1. QIAseq™ Human Actionable Solid Tumor Assay (QIAGEN)

The QIAseq™ Human Actionable Solid Tumor Panel is a gene panel designed for the detection of somatic mutations in solid tumors, targeting exonic regions including 10 bases of the intron/exon boundary of 23 tumor suppressor genes and oncogenes, with a total panel size of

15,160 base pairs and enriches 773 variants in 12 exons. QIAGEN reports a specificity of 90.48% and a uniformity of 99.85% for this panel.

Fifteen nanograms of Seraseq® ctDNA Reference Material v2 were used for library preparation, following the QIAseq Targeted DNA Panel Handbook (QIAGEN, version 05/2017), In brief, after enzymatic fragmentation, end-repair and A-tailing was performed followed by an enrichment using a set of 651 target-specific primers. The resulting libraries were amplified through 23 cycles of universal PCR, and fragment sizes were assessed with the Bioanalyzer High Sensitivity DNA Kit (Agilent Technologies).
Sequencing was carried out on the Illumina NextSeq 550 platform (San Diego, CA, USA) using a Mid Output Kit, generating 150 bp paired-end reads across six libraries. Each library yielded an average of 22.4 million raw reads (range: 18.0–28.6 million), with a mean consensus read depth of 2900× (range: 1899–3412) (165). Data analysis was conducted using the QIAGEN GeneGlobe Analysis Hub, with smCounter v1(3) employed to accurately identify true variants by correcting for sequencing errors through Unique Molecular Identifier (UMI) tagging. Variants that failed to meet the predefined quality thresholds set by smCounter were excluded from further analysis. All remaining variants identified in the reference material were manually reviewed using the Integrative Genomics Viewer (IGV), version 2.3.58 (165).

3.6.2. NEBNext Direct™ Cancer HotSpot Panel for Illumina (New England Biolabs)

The NEBNext Direct™ Cancer Hotspot Panel targets 190 commonly mutated positions from 50 cancer genes (165). This panel uses a hybridization-based workflow that combines capture with library preparation, reducing false positive variants by incorporating UMIs. New England Biolabs states a 100% detection rate of 168 true variants over a range of 2-100% VAF.

Library preparation was performed using 15 ng of SeraCare reference material v2 following the manufacturer's recommendations (manual version 2.0), with fragment size and quantification assessed via Bioanalyzer High Sensitivity DNA Kit (Agilent Technologies) and qPCR using Illumina adapter-specific primers, respectively. Equimolarly pooled libraries were sequenced in a 75 bp paired-end mode on the Illumina NextSeq 550 instrument. On average, 24.8 million raw reads (range 23.5 million – 26.4 million) were obtained per sample. UMI sequences were added to the BAM files using the AnnotateBamWithUmis function from the

fgbio package (https://fulcrumgenomics.github.io/fgbio/) and variant calling was performed using the GATK MuTect2 pipeline (Broad Institute, https://software.broadinstitute.org/cancer/cga/mutect) with tumor-only mode. A mean depth of 2099 reads (range 1217-4361) were achieved. VCF files were annotated with annovar. All positions with variants included in the SeraCare reference material v2 covered by the panel were visually inspected using IGV (version 2.3.58) (165).

3.6.3. AVENIO ctDNA Targeted and Expanded Kit (Roche)

The AVENIO ctDNA kits are next-generation sequencing-based assays optimized for NSCLC and colorectal cancer, but also suitable for other cancer types aligned with the U.S. National Comprehensive Cancer Network (NCCN) guidelines (168, 169) and new cancer biomarkers. The kits enable the detection of all types of genetic aberrations such as SNVs, Indels (insertions and deletions), CNVs (Copy number variations) and fusions from cfDNA from solid tumors. The AVENIO ctDNA Targeted Kit is used for pan-cancer research applications and contains 17 genes in 81kb including SNVs. The AVENIO ctDNA Expanded Kit contains 77 genes in 192 kb, including 17 guideline-driven biomarkers and 60 novel biomarkers examined in clinical trials and detects Indels, gene fusions and CNVs in specific regions.

The AVENIO assays use hybrid capture-targeted enrichment techniques in an end-to-end process from cfDNA isolation to analysis. The AVENIO CAPPseq technology has integrated digital error suppression (iDES) by combining molecular barcoding with *in silico* error suppression techniques (136, 137). According to the vendor, the assays detect SNVs with an allele frequency of 0.5% with >99% sensitivity and specificity using 10-50ng of mixed cell lines and a minimum of 40 million and 60 million reads for the AVENIO ctDNA Targeted and Expanded assays, respectively.

Library preparation for both assays was performed in accordance with the manufacturers´ recommendation. Briefly, unique sample adapters were ligated to cfDNA, followed by overnight incubation and post-ligation bead-based cleanup. After PCR amplification, quality metrics such as library size and concentration were verified using the 7500 DNA Kit on the Agilent Bioanalyzer and the Qubit dsDNA High Sensitivity Assay from Thermo Fisher Scientific. After the quality control check, the samples were either frozen at -15 to -20°C until further

use or immediately transferred for overnight hybridization. After binding to streptavidin beads and post-hybridization washes, the target enrichment was completed by a PCR amplification and clean-up of the enriched sample. The concentration of the enriched library was again determined using the Qubit dsDNA High Sensitivity Assay (Thermo Fisher Scientific) and the size of the library was determined with the Bioanalyzer High Sensitivity Kit (Agilent Technologies). Libraries were pooled equimolarly by concentration (66, 165).

The AVENIO ctDNA Targeted Kit was used to evaluate the Seraseq® ctDNA Complete™ Reference material (Setup A) and to assess specificity and sensitivity with the Seraseq® ctDNA Reference Material v2 (Setup B). Setup A employed 20 ng of the Seraseq® ctDNA Complete™ Reference Material for library preparation. On average 20.0 million raw read pairs per sample were obtained, with a range spanning from 18.2 million to 23.5 million. Following the generation of consensus reads, a mean unique depth of 4002 reads was achieved, exhibiting a range from 2967 to 4603 (165).
For the ctDNA Reference Material v2, 15 ng input DNA was used. After library quantification, the reference materials were sequenced in pools of 16 samples on an Illumina NextSeq 550 with a High Output v2 300 cycles it in paired-end mode (165), which yielded in an average of 22.2 million raw read pairs per sample, ranging from 20.2 million to 27.5 million. Subsequent to the consensus read generation process, a mean unique depth of 5075 reads was observed, with a range extending from 4544 to 6288 reads (165).

A total of 15 ng of Seraseq® ctDNA Complete™ Reference Material were used for the library preparation (Setup C). The reference materials were sequenced in pools of 12 samples on an Illumina NextSeq 550 with a High Output v2 300 cycles in paired-end mode (2 x 150 bp) resulting in a mean unique depth of 4569x (range, 4028-5026). A total of 22/25 mutations (12 SNVs, five Indels, two gene amplifications, i.e. *ERBB2* and *MET*) and three translocations (*EML4-ALKv1*, *NCOA4-RET*, *CD74-ROS1*) included in the reference material were covered by the AVENIO ctDNA Expanded panel (66, 165).

For the clinical validation study, AVENIO ctDNA Expanded libraries were prepared from cfDNA from NSCLC patients using an average input of 34.4 ng (range, 5.4–53.2 ng). To correct for

germline variants and those associated with clonal hematopoiesis, gDNA from PBMCs was additionally sequenced. Genomic DNA from PBMCs were enzymatically fragmentated prior to library preparation. Up to 200 ng of DNA was fragmented in a single reaction. A master mix consisting of KAPA Fragmentation Buffer (10X) and KAPA Fragmentation Enzyme in a 1:2 ratio (Roche) was added to the DNA and incubated at 37°C for 30 minutes. After incubation, a stop solution was added followed by a 3x Bead Clean-up with KAPA Pure Beads (Roche). After cleaning with 80% ethanol, beads were dried, resuspended in nuclease free water, and incubated at 37°C for ten minutes to elute the DNA from the beads. The concentration was measured using the Qubit dsDNA High Sensitivity assay and the size distribution was checked with the High Sensitivity DNA Bioanalyzer. On average 46.6 ng (range, 5.0-55) was used for library preparation (66).

Patient-derived cfDNA and PBMC samples were sequenced using 150 bp paired-end reads. Library pools consisted of eight samples for cfDNA and nine for PBMCs when sequenced on an Illumina HiSeq system. Additional pools of 11 to 12 libraries were processed on an Illumina NextSeq 550 platform. To enhance sequencing diversity and calibration, 10% PhiX Sequencing Control v3 (Illumina) was included in each sequencing run (66, 165). On average, cfDNA samples produced 34.3 million read pairs (range: 11.3–52.3 million), while PBMC samples generated 33.0 million read pairs (range: 12.5–48.6 million). After generating consensus reads, cfDNA libraries reached a mean sequencing depth of 4294× (range: 951–9303×), and PBMC libraries reached a mean depth of 4256× (range: 637–6831×) (66).

3.6.4. AVENIO ctDNA Targeted and Expanded data analysis

Raw sequencing data from the Targeted and Expanded kit were analyzed using the AVENIO ctDNA Analysis Software (Roche, version 1.1.0). Variant calls were generated using a custom somatic variant filter set. This filter removed variants present with >1% mutated population allele frequency listed in frequency databases (Exome Aggregation Consortium (ExAC), Genome Aggregation Database (gnomAD), 1000genomes) along with common single nucleotide polymorphisms (SNPs) as defined in the Single Nucleotide Polymorphism Database (dbSNP). In contrast to the default filter settings provided by Roche, the somatic variant settings included also variants which are not defined in the Catalogue of Somatic Mutations

in Cancer (COSMIC) or The Cancer Genome Atlas Program (TCGA) and somatic mutations, particularly in tumor suppressor genes would therefore not be reported by the default algorithm (66, 165).

Various filter settings were used to differentiate between somatic variants from the tumor and variants arising from clonal hematopoiesis in order to avoid false-positive results in the tumor-specific variant set. Following the default filtering procedures applied by the AVENIO Oncology software, the remaining plasma DNA variants were cross-referenced with variant calls from the PBMCs to identify rare germline alterations. Variants with a minor population allele frequency greater than 0.1% were filtered out. Moreover, variants in PBMCs that were single time point specific and had less than 10 alternate reads were removed. On the other hand, mutations that were present at both time points in the plasma samples and in the PBMCs were retained, regardless of the number of mutated reads. To sum up, variants that were found in both cfDNA and PBMCs with VAFs ranging from 0.1% to 10% were categorized as variants associated with clonal hematopoiesis (66, 165). A graphical representation of the filter steps is shown in Figure 5.

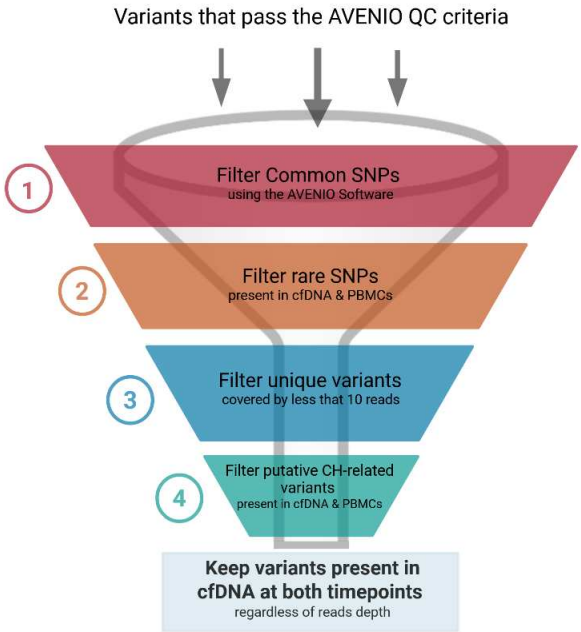

Figure 5: Somatic custom filter settings.
The filter removes variants present with >1% mutated population allele frequency listed in frequency databases (ExAC, gnomAD, 1000genomes) along with common SNPs as defined in dbSNP. Remaining plasma DNA variant calls were compared to PBMC variant calls to detect rare germline variants (<0.1% allele frequency). Unique variants at one time point, covered by <10 alternative reads, were filtered out, while mutations present at both time points were retained regardless of read count.

3.7. Assessment of ctDNA levels and molecular response

We employed different proxies to analyze its association with radiographic response and survival. ctDNA levels were assessed using two metrics: VAF, which represents the proportion of sequencing reads that contain the alternate allele relative to the total number of reads at that specific site (170, 171); and mutant molecules per milliliter of plasma (MM), which refers to the absolute number of DNA molecules carrying a specific genetic mutation detected in 1 milliliter of plasma (172). The average of all detected variants per patient (referred to as aMM and aVAF) and the highest variant's value per patient (referred to as hMM and hVAF) were established for both proxies. To ensure accuracy, a minimum threshold of 25% was set for observing ctDNA changes, considering a previously identified 20% technical variance in variant calling of the AVENIO assay (165). A more stringent cut-off of 50% was also applied based on previous reports (173-176). Survival analysis and forward stepwise Cox regression were calculated to determine the most appropriate surrogate for further analysis (66).

3.8. Tumor specimen handling and tissue NGS

Tumor tissue profiling data were available from 116 patients. Tumor specimens were acquired through a variety of methods including bronchoscopies, transthoracic biopsies, wedge resections, or endoscopic ultrasound procedures. Tissue samples underwent standard pathology procedures for processing and diagnosis. From the original formalin-fixed paraffin-embedded (FFPE) tissue blocks, two to four section of 10 µm thickness were prepared, euch preceded and followed by a 4 µm section. The 4 µm slides were stained with hematoxylin and eosin and reviewed by a trained pathologist to confirm the presence of a tumor-rich area containing more than 20% tumor cells. Genomic DNA was then extracted from the FFPE sections using the Cobas® DNA Sample Preparation Kit (Roche) and quantified with the Qubit dsDNA Broad Range Assay Kit (Thermo Fisher Scientific). In accordance with Dutch guidelines, tissue samples from all adenocarcinomas but not squamous cell lung cancer in patients with metastasized non-small cell lung cancer underwent predictive testing for *EGFR*, *BRAF*, *KRAS*, *ALK*, and *ROS* mutations, with results documented in the Dutch Pathology archives (66). Tumor-specific mutations, including SNVs and Indels, were identified through routine diagnostic next-generation sequencing conducted in an ISO15189-accredited laboratory.

Various hotspot panels, such as IonPGM-v01 (11 genes, 30 amplicons) and IonPGM-v02b (24 genes, 82 amplicons), were employed on the IonTorrent platform for the analysis of earlier tumors (66). More recent tumor specimens were analyzed using the smMIP PATHv2D panel (33 genes, 479 smMIPs) as previously described (177). This section of the study was carried out by colleagues at the UMCG.

3.9. Statistical analysis

Data processing and visualization utilized various statistical tools, including Microsoft Excel, Prism 7.0 by GraphPad Software, R Studio (version 3.5.2, *maftools*, *ggplot2*, *epiR* packages) and IBM SPSS Statistics version 29.0. Intra-run precision was determined by triplicate testing of a 1% VAF sample within a single mutation analytical run, while inter-run reproducibility was assessed across three separate workflows. The Coefficient of Variation (CV), calculated as the standard deviation divided by the mean, was used as a precision metric. Poisson (shot) noise was calculated using the formula sqrt[(1 - expected VAF)/(DNA copies x expected VAF)]. Concordance between expected and observed VAF was determined using *Lin's concordance correlation coefficient* via the *epiR* package in R Studio (version 1.2.1335). Visualization of false-positive variant calls was performed *maftools* in R (version 2.0.16).

Nonparametric Kruskal-Wallis and Mann-Whitney U test were applied to compare ctDNA levels at t_0 and t_1, various response groups, and concordance with clinical response. Agreement between ctDNA dynamics and therapeutic benefit was evaluated using the Cohen's kappa coefficient (κ). For differences in ctDNA response between responders and non-responders, the nonparametric Fisher’s exact test was used (66, 165).

PFS and OS were analyzed using the Kaplan–Meier method, with comparisons between groups performed using the log-rank test. Survival time was calculated from the initiation of ICI therapy until radiographic disease progression or death. Patients without an event were censored at their last follow-up visit. Multivariate Cox regression analysis was employed to account for clinical variables, including age at the initiation of ICI initiation, gender, smoking status, disease stage, metastasis count, tumor histology, treatment sequence, and ECOG performance status. Covariates were identified using a backward conditional selection method with a significance threshold of p = 0.1. The clinical model incorporated significant

predictors from the multivariate Cox regression analysis, and was further used to assess the impact of dynamic ctDNA response (defined as a ≥25% or ≥50% reduction), the presence of STK11/KEAP1 mutations, and PD-L1 expression. Corrected hazard ratios (HR <1 indicating extended survival), 95% confidence intervals (CI) and p-values were reported for the key variables. P-values equal to or less than 0.05 were deemed statistically significant (66, 165).

A landmark analysis was performed 60 days after treatment initiation to determine the impact of ctDNA levels on PFS and OS. The landmark method evaluates the effect of a time-dependent covariate at a specific point on survival outcomes (Figure 11B). The 60-day post-treatment period is critical for clinicians to make informed decisions about continuing ICI treatment, particularly when radiologic responses are unclear. Kaplan-Meier curves for PFS and OS using the 2-month landmark were calculated (66). At this time point, 60 days after the baseline measurement, data from 144 patients were available for OS and from 99 patients for PFS (66).

4. RESULTS

4.1. Assay validation and selection

To evaluate the effectiveness of cfDNA sequencing assays, we conducted validation studies across multiple mutation analysis platforms using commercially available reference standards containing known mutations at specified allele frequencies. For this purpose, we developed various experimental approaches to examine the reference material's suitability for comparisons both within and across assays, as well as between different laboratories and within individual labs (Figure 4). This work was done within the framework of the IMI program CANCER-ID. In addition, we assessed the performance of several NGS assays in terms of sensitivity and specificity. The aim was to find the best performing assay for further studies and clinical validation. The best performing assay was used to present a comprehensive mutation profiling of plasma ctDNA from patients treated with ICI therapy (66, 165).

4.1.1. Setup A: Variants with a VAF of 1% were detected across all platforms

In this study design, the suitability of the Seraseq® ctDNA Complete™ reference material (VAF of 1%) for the evaluation of cfDNA assays was tested in a multicenter approach. To this end, five Cancer-ID partners tested the intra-run precision and inter-run reproducibility of three NGS panels, two ddPCR mutation analyses and the Ultraseek panel according to the manufacture's handbook (Figure 4). A detailed description of the laboratories and assays is listed in Table 4, while our laboratory tested the AVENIO ctDNA Targeted assay (Roche) in this study setup (165). This multicenter approach focused on the most clinically relevant mutations with a VAF of 1%, namely *BRAF* c.1799T>A p.V600E, *EGFR* c.2369C>T p.T790M, *EGFR* c.2573T>G p.L858R, *KRAS* c.34G>T p.G12C and *KRAS* c.35G>A p.G12D. To assess the precision of the panels, all samples were prepared in triplicate and sequenced in one run (intra-run) as well as in three separate sequencing runs (inter-run) (165). Focusing on the NGS assays, on average, 101.67 million raw read pairs per sample (range 55.56 –186.06 million) were obtained for the SureSelect custom assay, 20.0 million raw read pairs per sample (range 18.2-23.5 million) were obtained for the AVENIO ctDNA Targeted assay, and target regions were

covered with an average of 798 reads (range 664-969) for the GeneRead^{TM} QIAact Lung UMI panel (165).

All platforms consistently detected the five variants with an average VAF of 1.03% (ranging from 0.5-1.7%; Figure 6) (165). Inter-run variability was similar between the two ddPCR assays (with 8 ng input for each: Bayer CV of 24%, UMCG CV 30%) and two of the three NGS assays (with 20 ng input for each: SureSelect CV 26%, AVENIO CV 22%). However, MassARRAY (15ng input) showed the lowest variability (CV 19%), while the QIAact NGS assay with 20ng input showed the highest variability (CV 48%). All assays demonstrated slightly higher inter-run reproducibility compared to intra-run variability (Figure 7A).

Due to the impact of limited cfDNA input on the sensitivity and precision of molecular profiling, we further investigated how DNA input quantity influences variability in ddPCR assays. To quantify the extent of variability attributable to random sampling error, we accounted for shot noise based on the Poisson distribution. Reducing the input from 8 ng to 4 ng and 2 ng led to a noticeable decline in assay precision, whereas increasing the input amount improved the reliability of variant detection (Figure 7B) (165).

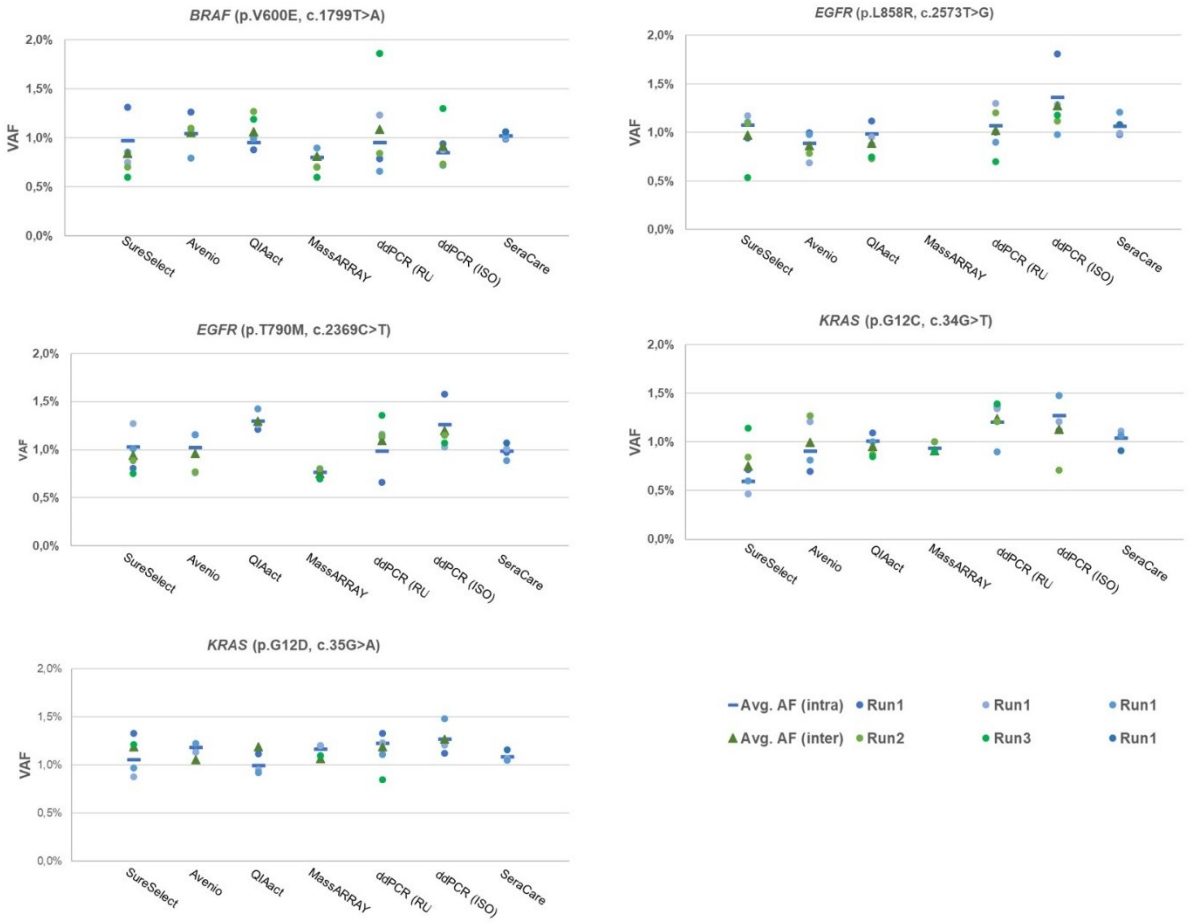

Figure 6: Precision within a single run (intra-run) and reproducibility across three different runs (inter-run) of various assays, showcasing their performance in detecting mutations at a set VAF of 1%.
Displayed are the variant allele frequencies (VAF) for five clinically significant mutations: *BRAF* V600E, *EGFR* T790M, *EGFR* L858R, *KRAS* G12C, and *KRAS* G12D, included in the Seraseq® ctDNA Complete™ reference material. The assays used include the SureSelect custom panel (Agilent Technologies), AVENIO ctDNA Targeted assay (Roche), QIAact Lung UMI Panel (QIAGEN), two droplet digital PCR (ddPCR) assays (one research use only and one ISO15189 validated), and the UltraSeek lung panel (MassARRAY). [Figure originally reprinted and legend adapted from Cancers (Weber et al. (165))]

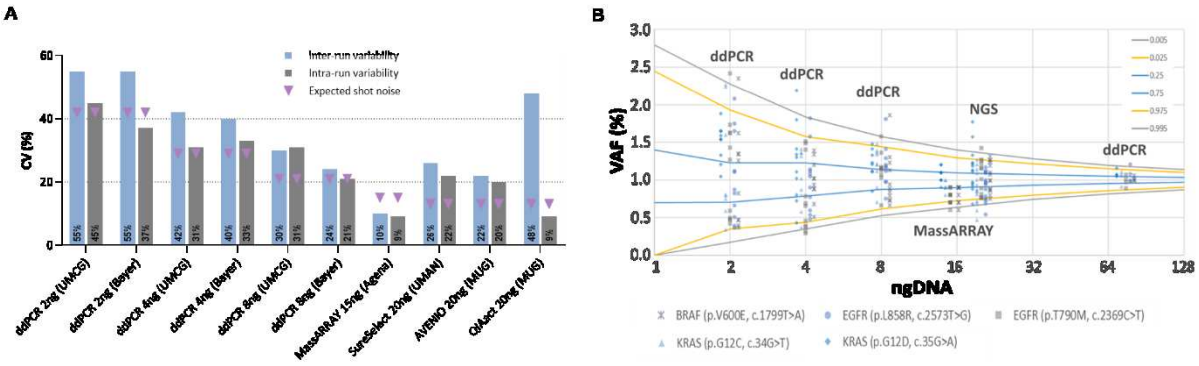

Figure 7: Variability assessment of qPCR-based and NGS assays using five clinically relevant mutations.
The SeraCare Seraseq® ctDNA Complete™ reference material (VAF1%) was used to evaluate assay performance across two digital droplet PCR assays (ddPCR) -one ISO15189-accredited [ISO (UMCG)] and one for research use only [RUO (Bayer)]- alongside the MassARRAY (UltraSeek lung panel) and three NGS platforms (a custom SureSelect panel, AVENIO cfDNA Targeted kit, and the QIAact Lung UMI Panel). The analysis focused on five clinically relevant mutations, i.e., *BRAF* c.1799T>A V600E, *EGFR* c.2369C>T T790M, *EGFR* c.2573T>G L858R, *KRAS* c.34G>T G12C and *KRASc*.35G>A G12D (**A**) The coefficients of variation (CV) is shown for each assay, capturing both inter-and intra-run variability, along with the expected random fluctuation (Poisson shot noise) based on the number of mutant input molecules present. (**B**) VAFs across different DNA input amounts are displayed for the three NGS panels (20 ng), the MassARRAY (15 ng), and two ddPCR assays (8, 4, 2 ng). The data illustrate that variability increases as DNA input decreases. Overlayed are the respective VAF ranges as well as an inverse binomial distribution based on the trials (number of DNA copies), event probability (0.01 for 1% VAF), and the location along the cumulative distribution function (colored line, e.g., 2.5th percentile would be 0.025). For example, when sampling a 4-ng input DNA, one can expect to observe a 1% variant between VAFs of 0.44% and 1.57% with a likelihood of 95%, or between 0.35% and 1.85% with a likelihood of and 99%. [Figure and legend adapted from Weber et al. (165)]

4.1.2. Setup B: Sensitivity assessment of different mutation assays

To identify the most suitable assay for clinical validation, the analytical performance of five commercially available NGS-based mutation detection assays was compared. These included the AVENIO ctDNA Targeted Kit (“Avenio Targeted”), QIAseq Human Actionable Solid Tumor Assay (“QIAseq”), NEBNext Direct Cancer Hotspot Panel (“NEB”), QIAact Lung UMI Panel (“QIAact”), and the Oncomine cfDNA Lung Panel (“Oncomine”). For benchmarking, the Seraseq® ctDNA Reference Material v2 was used. The assays yielded different sequencing depths across targeted regions, with median depths ranging from 2099× to 798× for NEB, QIAseq, Avenio Targeted, Oncomine, and QIAact, respectively (165). In summary, the Oncomine assay detected all 13 variants down to a VAF of 0.25%, while missing two at 0.125% (Figure 8A). The AVENIO ctDNA Targeted Assay identified all 15 variants covered in the ctDNA reference material v2 at VAFs of 2% and 1%, with decreasing detection rates at lower VAFs, but still calling 60% of the expected variant at a VAF of 0.125% (Figure 8B). QIAseq showed slightly lower detection rates (Figure 8C), while QIAact and NEB assays exhibited considerably lower rates, attributed to differences in sequencing depth (Figure 8D, E). In addition to the

Seraseq® ctDNA reference material v2, AVENIO ctDNA Targeted was tested with the Seraseq® ctDNA Complete™ reference material, which includes a slightly different mutation set and various VAFs. The detection rate remained similar to that of v2, but there was an improvement in concordance (*pc* = 0.946) (Figure 8F). Overall, there was high concordance between expected and observed VAFs across assays, except for the NEB kit (Oncomine: *pc* = 0.948, AVENIO ctDNA Targeted: *pc* = 0.839, QIAseq: *pc* = 0.873, QIAact: *pc* = 0.782, NEB: *pc* = 0.271) (Figure 8G) (165).

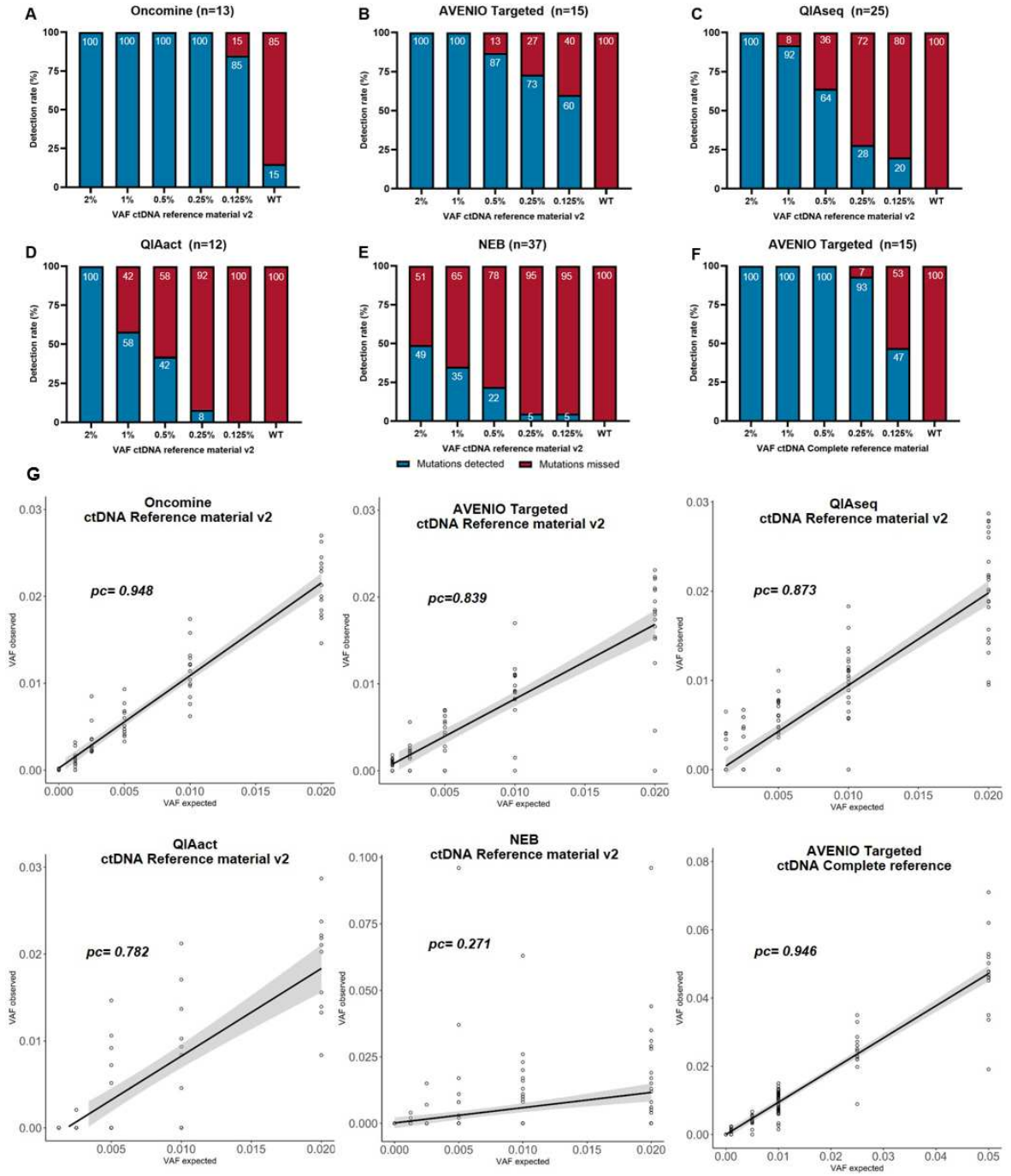

Figure 8: Detection performance of five mutation assays (A-F) and concordance of expected versus observed VAFs (G). It illustrates the detection rates of mutations, including (SNVs) and insertions/deletions (Indels), in the Seraseq® ctDNA Reference Material v2 across different variant allele frequencies (VAF). The panels show the detection rates for the Oncomine Lung cfDNA Assay **(A),** the AVENIO Targeted ctDNA Kit **(B),** the QIAseq Human Actionable Solid Tumor Panel **(C),** the GeneRead QIAact Lung UMI Panel **(D)**, and the NebNext Direct Cancer Hotspot Panel **(E)**, respectively. Panel **F** shows the detection rates for mutations in the Seraseq® ctDNA Complete™ reference material for the AVENIO Targeted ctDNA kit only. The numbers in parentheses indicate the number of mutations covered in each assay. **(G)** Linear regression was employed to compare the VAF across different NGS mutation analysis platforms with the VAF reported by SeraCare. The Lin concordance correlation coefficient (pc) was computed for this assessment [Figure and legend adapted from Weber et al. (144)]

Variants were classified as true positives if they were present in the Seraseq® reference material, detected by the corresponding panel, and had a VAF equal to or above the established LOD. In contrast, variants exceeding the LOD but not included in the reference material were deemed false positives. At a 0.5% LOD, recall rates ranged from 79% to 100% for variants with VAFs of 1% and 2%, and from 61% to 73% for those with a 0.5% VAF.

Recall rates dropped significantly for variants with allele frequencies below 0.5% across all tested assays. While lowering the LOD to 0.2% and 0.1% preserved high sensitivity, it also led to a further decline in recall for low-frequency variants, primarily due to an increase in potential false positives (Figure 9, Table 5) (165).

False positive results can arise from a range of factors, including technical limitations, biological variation, and random sampling noise. The Seraseq® ctDNA Complete™ Reference Material, produced using a gentler synthesis method (178), is designed to reduce background noise compared to the earlier Seraseq® ctDNA Reference v2. When paired with the AVENIO ctDNA Targeted Kit, this reference material demonstrated enhanced accuracy, indicating that this combination may offer improved performance and lower false positive rates relative to other assay configurations (Figure 9, Table 5) (165). Generally, false positive calls were clustered around a VAF of 0.2% (Table 5), whereby some of these false positive calls recurred across multiple samples. Notably, the most common false positive calls were C > T transitions for AVENIO and QIAseq, whereas Oncomine predominantly showed C > A transversions (data shown in Weber et al. (165)).

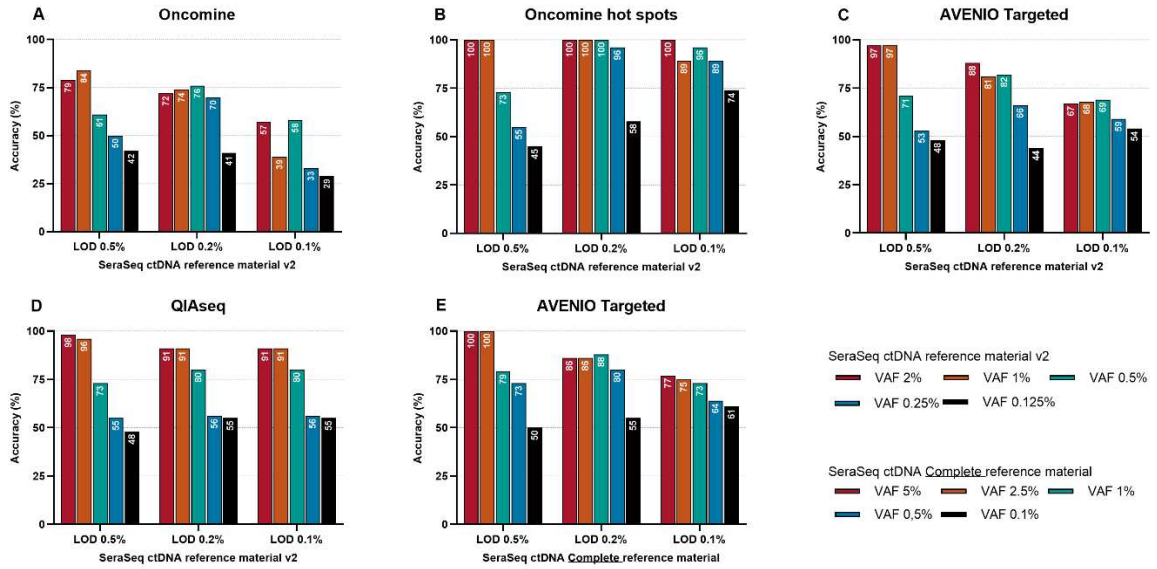

Figure 9: Accuracy rates of three NGS assays assessed with the Seraseq® ctDNA Reference material (A-D) and of the AVENIO ctDNA Targeted ctDNA assay assessed with the Seraseq® ctDNA Complete™ reference material (E).
Limits of detection (LOD) were set at 0.5%, 0.2%, and 0.1% VAF. Variants known to be present in the reference material and called with a VAF higher than the LOD were considered as true positives (TP). Variants with a VAF above the LOD but not reported in the reference material were considered as false positive. Accuracy was assessed for the following assays: **(A)** Oncomine Lung cfDNA assay ("Oncomine"), **(B)** Hotspot variants within the Oncomine Lung cfDNA assay ("Oncomine hot spots"), **(C, E)** AVENIO ctDNA Targeted assay ("AVENIO Targeted"), **(D)** QIAseq Actionable panel ("QIAseq") [Figure and legend adapted from Weber et al. (165)]

Table 5: False-positive variant detections across different LOD thresholds [Table originally published in Cancers, Weber et al. (165)]

LOD	0.50% *	0.20% *	0.10% *	Average VAF (Range) at LOD 0.1%
AVENIO Targeted Seraseq ctDNA reference material v2	0.8	5.6	13.6	0.21% (0.1–0.7)
AVENIO Targeted Seraseq ctDNA Complete	0	4.4	10.2	0.21% (0.1–0.4)
Oncomine (all regions)	5.2	9.8	35	0.23% (0.1–1.5)
Oncomine (hot spot regions)	0	0.2	1.8	NA
QIAseq	2.4	4.2	4.2	0.73% (0.2–2.4)

* Average numbers of false positive variant calls for all tested reference materials.

4.1.3. Setup C: AVENIO kits showed the best performance after assay validation

Since the AVENIO platform was considered most suited for the clinical validation study, the AVENIO ctDNA Expanded kit was additionally evaluated using 15 ng of the Seraseq® ctDNA Complete™ Reference Material, which covers different SNVs, Indels, copy number alterations and structural variants (Table 6). The agreement between the expected and observed VAF was high at 97% (determined by Lin's concordance correlation coefficient ρc = 0.97) (Figure 10).

The AVENIO ctDNA Expanded assay demonstrated robust performance by detecting all 17 SNVs and Indels at a minimum VAF of 0.5%. At a lower threshold of 0.1% VAF, 11 of the 17 mutations (65%) were still identified (Figure 10B). Notably, two gene fusions - EML4-ALKv1 and NCOA4-RET – could be successfully detected at VAFs of 0.5% and 1%, respectively, while the CD74-ROS1 fusion was missed at any VAF level (Table 6). These results confirm the assay's claimed sensitivity for variant detection down to 0.1% VAF (66, 165).

Table 6: Variant allele frequency (VAF) of mutations in Seraseq® ctDNA Complete™ reference material using the AVENIO Expanded assay. ND= not detected

Gene	CDS Mutation	AA Mutation	Type	Mutation covered in the Avenio ctDNA Expanded panel	VAF 5.00% expected	VAF 2.50% expected	VAF 1.00% expected	VAF 0.5% expected	VAF 0.1% expected	WT
AKT1	c.49G>A	p.E17K	SNV	YES	3.40%	1.79%	0.62%	0.25%	ND	ND
ALK	c.3604G>A	p.G1202R	SNV	YES	4.50%	2.62%	1.21%	0.67%	0.18%	ND
ALK	c.3522C>A	p.F1174L	SNV	YES	4.82%	2.37%	0.94%	0.67%	0.18%	ND
BRAF	c.1799T>A	p.V600E	SNV	YES	5.50%	2.82%	1.14%	0.61%	0.07%	ND
BRCA1	c.1961delA	p.K654fs*47	InDel	NO						
BRCA2	c.7934delG	p.R2645fs*3	SNV	NO						
EGFR	c.2235_2249del15	p.E746_A750delELREA	InDel	YES	5.60%	3.40%	1.40%	1.00%	0.19%	ND
EGFR	c.2240_2257del18	p.L747_P753>S	InDel	YES	5.10%	3.20%	1.20%	0.31%	0.13%	ND
EGFR	c.2254_2277del24	p.S752_I759delSPKANKEI	InDel	YES	4.60%	3.00%	1.10%	0.28%	ND	ND
EGFR	c.2369C>T	p.T790M	SNV	YES	4.21%	2.06%	0.82%	0.36%	0.19%	ND
EGFR	c.2573T>G	p.L858R	SNV	YES	4.92%	2.48%	0.78%	0.56%	ND	ND
ERBB2	c.2324_2325ins12	p.A775_G776insYVMA	InDel	YES	4.10%	2.30%	0.28%	0.18%	ND	ND
KIT	c.2447A>T	p.D816V	SNV	YES	4.60%	2.67%	0.80%	0.47%	0.06%	ND
KRAS	c.183A>C	p.Q61H	SNV	YES	4.10%	2.16%	0.81%	0.36%	ND	ND
KRAS	c.35G>A	p.G12D	SNV	YES	4.83%	2.36%	1.03%	0.49%	ND	ND
KRAS	c.34G>T	p.G12C	SNV	YES	4.27%	2.21%	0.95%	0.48%	0.04%	ND
NRAS	c.182A>G	p.Q61R	SNV	YES	5.21%	2.94%	0.91%	0.58%	0.12%	ND
PIK3CA	c.3140A>G	p.H1047R	SNV	YES	3.54%	1.74%	0.67%	0.30%	0.14%	ND
PIK3CA	c.3204_3205insA	p.N1068fs*4	InDel	YES	4.95%	2.40%	1.20%	0.47%	0.17%	ND
ERBB2			CNA	YES	DETECTED	DETECTED	ND	ND	ND	ND
MET			CNA	YES	DETECTED	DETECTED	ND	ND	ND	ND
MYC			CNA	NO						
EML4-ALKv1	Translocation	-	SV	YES	DETECTED	DETECTED	DETECTED	DETECTED	ND	ND
CD74-ROS1	Translocation	-	SV	YES	ND	ND	ND	ND	ND	ND
NCOA4-RET	Translocation	-	SV	YES	DETECTED	DETECTED	DETECTED	ND	ND	ND

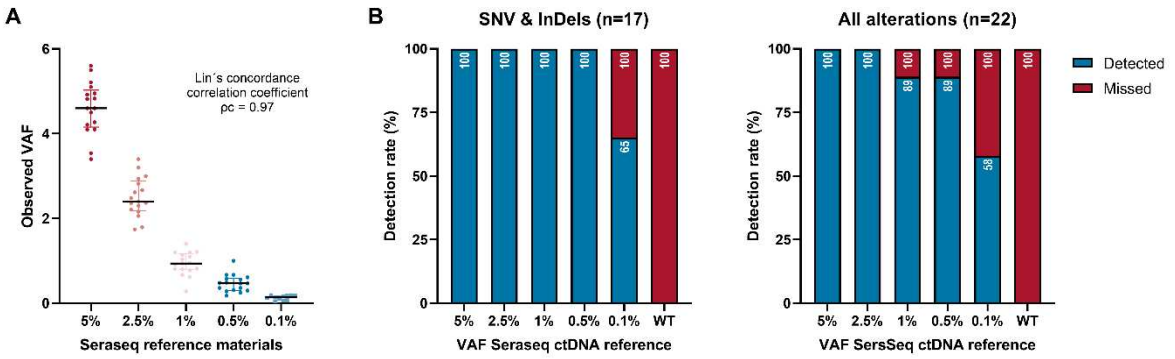

Figure 10: Evaluation of the AVENIO ctDNA Expanded Assay using the Seraseq® ctDNA Complete™ Reference Material. (**A**) Variant allele frequency (VAF) distribution for each mutation present in the Seraseq® ctDNA Complete™ reference material (**B**) Detection performance for single nucleotide variants (SNVs) and insertion-deletion mutations (Indels) (left), as well as the combined detection rate of all variants covered by the Seraseq® ctDNA Complete™ material (right), across different VAF levels. Number in brackets indicate the number of mutations covered by the AVENIO ctDNA Expanded panel. [Figure originally reprinted and legend adapted from JCO Precision Oncology (Weber et al. (66))]

4.2. ctDNA-based response evaluation in NSCLC undergoing ICI therapy

4.2.1. Patient characteristics

Of the 177 patients initially recruited, cfDNA from 167 patients was successfully analyzed at two key time points: (baseline, t_0), prior to the initiation of ICI therapy, and after two treatment cycles (t_1) - corresponding to an average of four weeks for nivolumab and six weeks for pembrolizumab. The median age of the analyzed cohort (n = 167) was 66 years (range: 29–87), with the majority being smokers (64.1%). Adenocarcinoma was the predominant histological subtype, accounting for 67.1% of cases. A total of 71.3% of patients received ICIs as second-line therapy, with nivolumab being the most frequently used agent. PD-L1 expression was assessed at baseline in 110 patients. Among them, 54 tumors (49.1%) were PD-L1 positive, with 20.9% exhibiting high expression (tumor proportion score [TPS] >50%). The remaining 56 patients (50.9%) had PD-L1–negative tumors (TPS <1%). An early response to treatment was observed in 44 patients (26.4%), and a durable clinical response was achieved in 60 patients (35.9%). Further details on baseline characteristics and study design are presented in Table 7 and Figure 11.

Table 7: Baseline patient characteristics (n=167). [Table reprinted from JCO Precision Oncology (Weber et al. (66))]

Variable	Parameter	No. of patients (%)
Age	Median (range)	66 (29-87)
Gender	Male	96 (57.5)
	Female	71 (42.5)
Performance score	0	69 (41.3)
	1	89 (53.3)
	2	8 (4.8)
	3	1 (0.6)
Smoking history	Smoker	107 (64.1)
	Ex-smoker	47 (28.1)
	Non-smoker	13 (7.8)
Stage	IIIB	22 (13.2)
	IV	145 (86.8)
Metastatic sites	0	3 (1.8)
	1	32 (19.2)
	2	55 (32.9)
	3	41 (24.5)
	≥4	36 (21.6)
Line of therapy	1st	13 (7.8)
	2nd	119 (71.2)
	3rd	35 (21.0)
Therapy	Nivolumab	140 (83.8)
	Pembrolizumab	15 (9.0)
	Atezolizumab	7 (4.2)
	Nivolumab plus ipilimumab	3 (1.8)
	Durvalumab	2 (1.2)
No. cycles	Mean (SD)	13 (15)
ICI therapy ended due to	Progressive disease	121 (72.5)
	Toxicity	25 (15.0)
	Two years duration	19 (11.4)
	Infection	2 (1.2)
Histology	Adenocarcinoma	112 (67.1)
	Squamous cell carcinoma	51 (30.5)
	Other	4 (2.4)
PD-L1 expression	<1%	56 (33.5)
	1-49%	31 (18.6)
	≥50%	23 (13.8)
	Not evaluable/ unknown	57 (34.1)
Tumor response	CR, complete response	8 (4.8)
	PR, partial response	36 (21.6)
	SD, stable disease	39 (23.4)
	PD, Progressive disease	70 (41.9)
	NE, not evaluable	14 (8.4)
Early response	Response at first CT	44 (26.3)
Durable response	SD + PR + CR ≥ 6 months	60 (35.9)

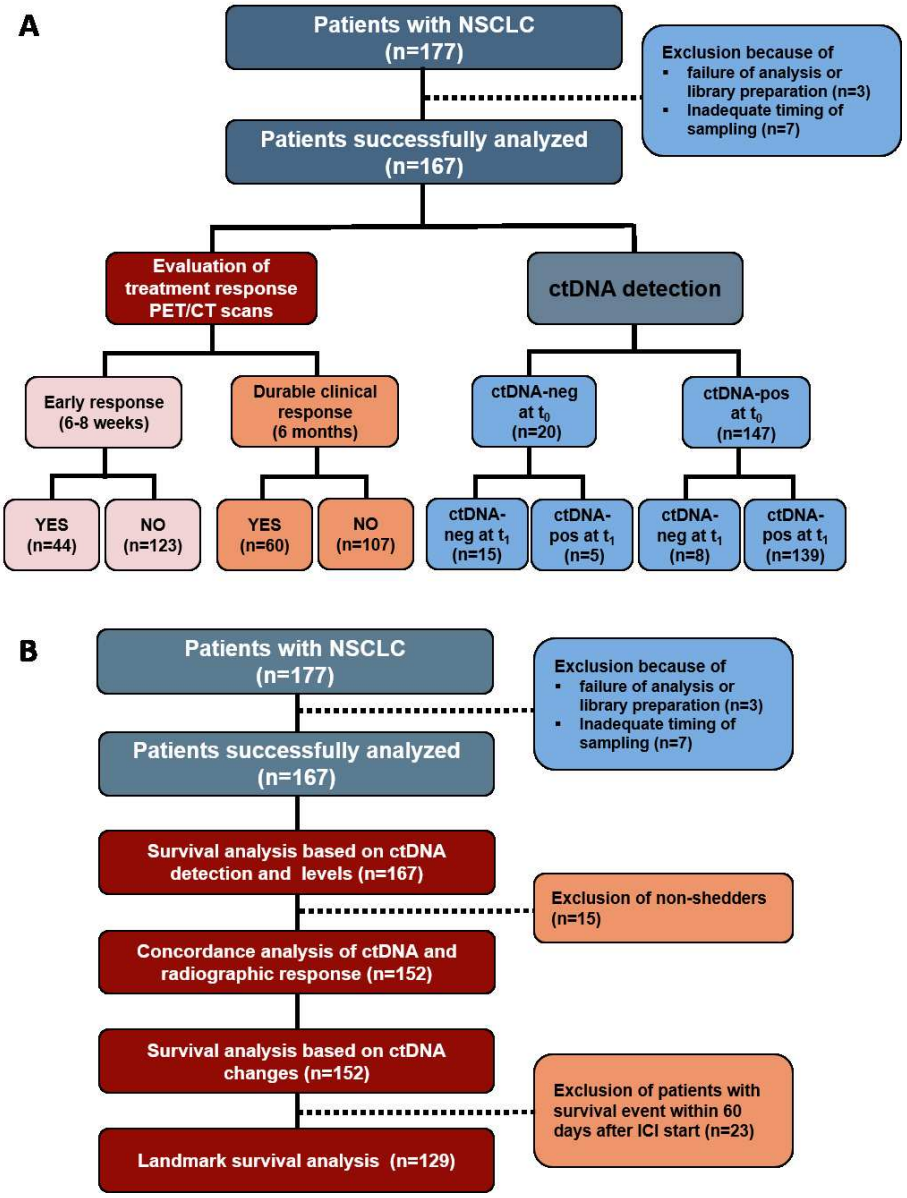

Figure 11: Flowchart and study design.
(**A**) Flowchart of patients included in the study. In 139 of 152 (91.4%) patients, at least one mutation was identified at both time points, and in 91 of 152 patients (59.9%), additional mutations unique to a single time point (either t_0 or t_1) were observed. (**B**) Analysis workflow of the study. CT computed tomography; ctDNA-neg, no tumor-specific somatic mutation detected; ctDNA-pos, detection of at least one mutation using the AVENIO ctDNA Expanded Kit; ctDNA, circulating tumor DNA; ICI, immune checkpoint inhibitor; NSCLC, non–small cell lung cancer; PET, positron emission tomography; t0, blood draw before initiation of ICI; t1, blood draw at first response assessment. [Figure and legend originally published and reprinted and adapted with permission from JCO Precision Oncology (Weber et al.(66)]

The final study cohort included 334 plasma samples and corresponding PBMCs from 167 patients with advanced stage NSCLC. The median PFS and OS for the entire cohort were 2.8 months (range: 0.2-61.6 months) and 8.2 months (range: 0.5-61.1 months), respectively (Figure 12A). The median PFS and OS calculated from a 2-months landmark was 7.9 months (range, 0.03 – 59.1) and 8.7 months (range, 0.2 – 59.1) (Figure 12B).

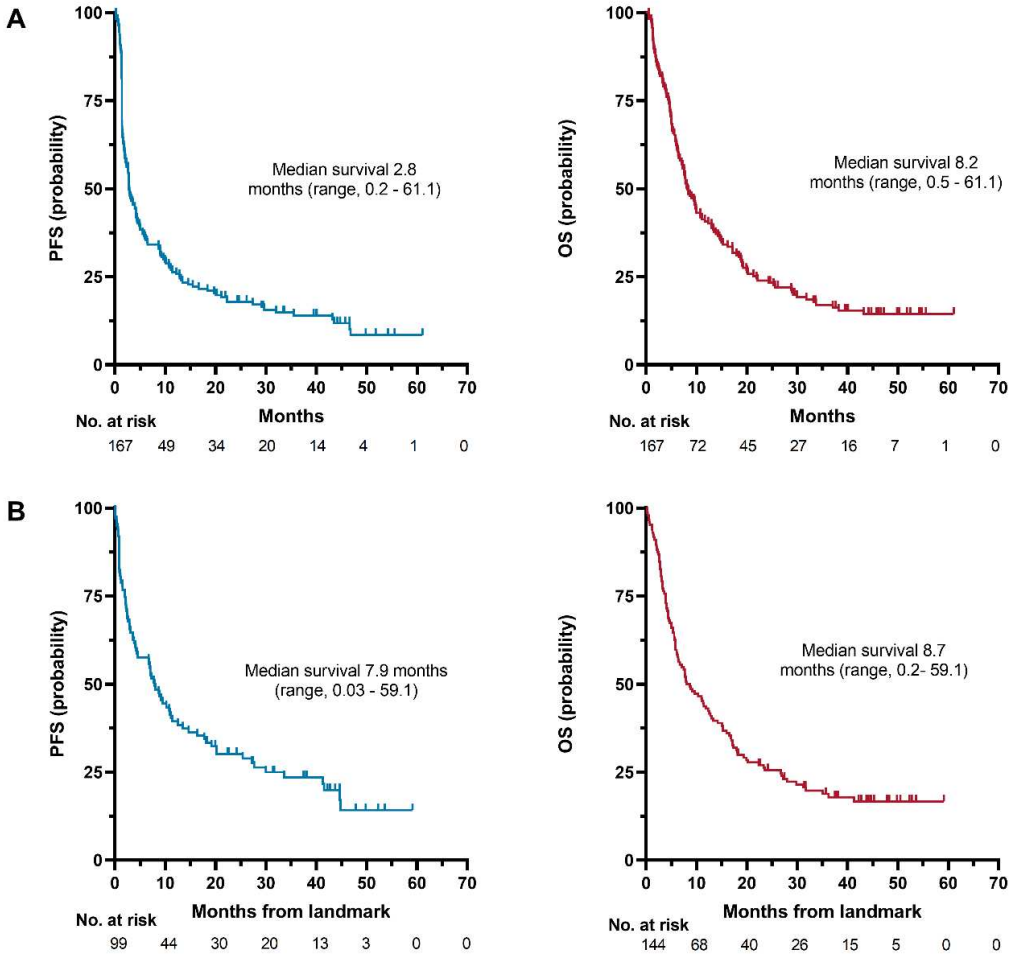

Figure 12: Survival curves of the lung cancer cohort.
Kaplan-Meier curves illustrating the progression-free survival (PFS) and overall survival (OS) of the patient cohort. (**A**) PFS (left) and OS (right) calculated from the start of therapy for 167 patients. (**B**) PFS (left, n=99 patients) and OS (right, n= 144 patients) calculated at a 2-month landmark. The number of patients at risk at various time points is indicated below each graph [Figures originally reprinted and legend adapted from Weber et al. (66)]

4.2.2. Correlation of ctDNA levels using various metrics while aMM provides the most accurate measurement

ctDNA levels were meticulously assessed as VAF and the number of mutant molecules per milliliter of plasma, respectively. For each metric, the average (aVAF, aMM) and highest (hVAF, hMM) values per patient were calculated. All metrics proved to be strongly correlated (Figure 13). Since our performance assessment demonstrated a 20% technical variance in variant calling (165), a minimum threshold of 25% for relative change in aMM from t_0 to t_1 was applied, along with a more stringent 50% cut-off, which had been shown to be informative in prior research (66).

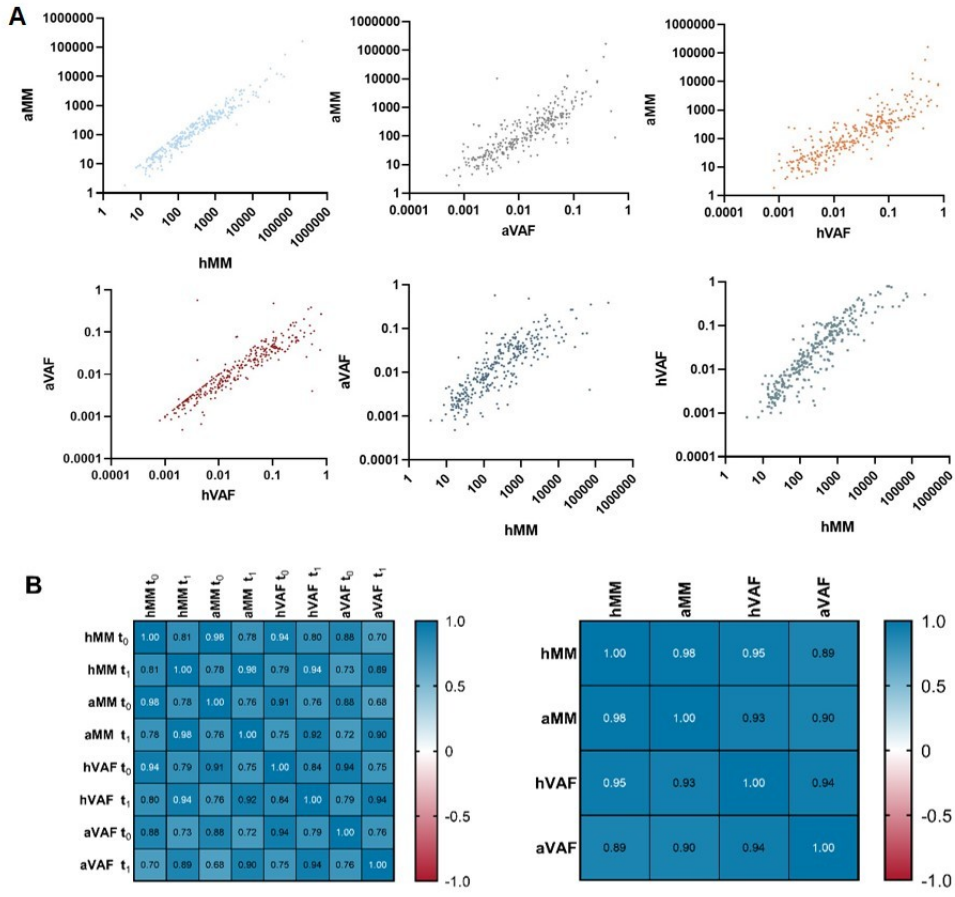

Figure 13: Correlation of the ctDNA values assessed using various measures.
(**A**) Linear regression of ctDNA levels as highest VAF (hVAF), average VAF of all mutations detected per patient (aVAF), highest number of mutant molecules per ml plasma (hMM) and average number of mutant molecules of all mutations per patient (aMM). (**B**) Heatmap depicting the Spearman correlation coefficients of pairwise comparisons: **Left**: Correlation matrix for individual time points (t_0, t_1). **Right**: Combined correlation matrix for both time points. The heatmaps use a color scale to represent the Spearman correlation coefficients, where blue stands for a strong positive correlation and red indicates a strong negative correlation. [Figures originally reprinted and legend adapted from JCO Precision Oncology (Weber et al. (66))]

Among all proxies, median aMM consistently demonstrated the strongest prognostic value in terms of OS, tested for the two time points as well as for 50% response (Table 8, Table 9). At baseline (t_0), its addition yielded a modest model improvement (−2Log Likelihood: 1223.6, P = 0.080), whereas at follow-up (t_1), it significantly improved the model fit (−2 Log Likelihood: 1202.0, P < 0.001). This progression marks aMM as the most discriminative ctDNA metric for OS in this cohort. In comparison, other proxies such as hMM, aVAF, and hVAF also reached statistical significance at t_1, but with less pronounced improvements in model fit (e.g., hMM: 1213.7; aVAF: 1213.5; hVAF: 1216.3). At t_0, none of these showed significant contributions to survival prediction (Table 8) (66).

Table 8: Stepwise Cox regression analysis aimed at determining which ctDNA metric (median aMM, hMM, aVAF, hVAF) best discriminates overall survival (OS) at two time points (t_0 and t_1). [Table and legend adapted from Weber et al. (66)]

ctDNA metrics included in the model*	Time point	-2Log Likelihood for OS
Median aMM	t_0	1223.6 (*P*=0.080**)
	t_1	1202.0 (*P* <0.001**)
Median hMM	t_0	1225.8 (n.s.)
	t_1	1213.7(*P* <0.001)
Median aVAF	t_0	1226.1 (n.s.)
	t_1	1213.5 (*P*<0.001)
Median hVAF	t_0	1225.5 (n.s.)
	t_1	1216.3 (*P*=0.001)

* Median values of the ctDNA-based metrics aVAF, hVAF, aMM, and hMM were used as cut-off points in a cohort of 167 patients. Models were adjusted for clinically significant relevant factors including sex, number of metastasic sites and performance status. ** ctDNA metrics analyzed within the multivariate model adjusted for clinical covariates. n.s., not significant

In a separate Cox regression analysis using a fixed 50% cut-off for each ctDNA proxy, median aMM again showed the strongest prognostic value for overall survival. Specifically, adding aMM to the multivariate model yielded the lowest −2 Log Likelihood value (1076.8**,** *P* < 0.0001), indicating the best model fit among all tested proxies. While hMM, hVAF, and aVAF also reached statistical significance (all *P* < 0.0001), their −2 Log Likelihood values were consistently higher (hMM: 1078.4; hVAF: 1085.4; aVAF: 1089.9) (Table 9) (66). These findings further corroborate aMM as the most robust and informative ctDNA proxy for predicting overall survival across modeling strategies.

Table 9: Stepwise Cox regression analysis used to evaluate which ctDNA proxy response (aMM, hMM, aVAF, hVAF) best predicts overall survival (OS), using 50% a cut-off for response. [Table originally reprinted and legend adapted from Weber et al. (66)]

ctDNA metrics included in the model*	Cut-off	-2Log Likelihood for OS
aMM	50%	1076.8** (*P*<0.0001)
hMM	50%	1078.4 (*P*<0.0001)
aVAF	50%	1089.9 (*P*<0.0001)
hVAF	50%	1085.4 (*P*<0.0001)

*A ≥50% response of ctDNA metrics- aVAF, hVAF, aMM, and hMM- was used at as the threshold in 152 patients (excluding 15 without detectable ctDNA) and **adjusted for key clinical variables (sex, number of metastasic sites and ECOG).

4.2.3. Prevalence of clonal hematopoiesis-related variants

Recent studies have indicated that somatic mutations derived from the expansion of clonal populations of blood cells, known as clonal hematopoiesis of indeterminate potential, can impact the specificity of ctDNA detection. This can lead to false positive results and decreased specificity in ctDNA-based assays (127, 179). Therefore, it is important to consider the impact of clonal hematopoiesis on ctDNA detection and to utilize appropriate methods for accurate interpretation of results. To make sure that the variant calls were specific to the tumor and not from other sources, we included PBMCs in our analysis. Variations present in both PBMCs and paired plasma samples were designated as clonal hematopoiesis (CH)-related and removed, as they were considered constitutional rather than tumor-specific (66). After excluding germline SNPs, 769 and 792 somatic variants were identified at time points t_0 and t_1, respectively. Of these, 648 of these variants were found at both time points, while 121 and 144 variants were unique to t_0 or t_1, respectively, resulting in a total of 913 detected variants (Figure 14) (66).

In 75 out of 167 patients (44.9%), 115 out of 913 somatic variants (12.6%) were identified in paired PBMCs and plasma across 43 genes. Most CH-related variants were found in the *TP53* gene. A total of 30 *TP53* mutations (20.8% of all identified *TP53* mutations) could be attributed to clonal hematopoiesis. Additionally, 29 out of 167 patients (17%) had more than one CH-related variant (Figure 14) (66, 119).

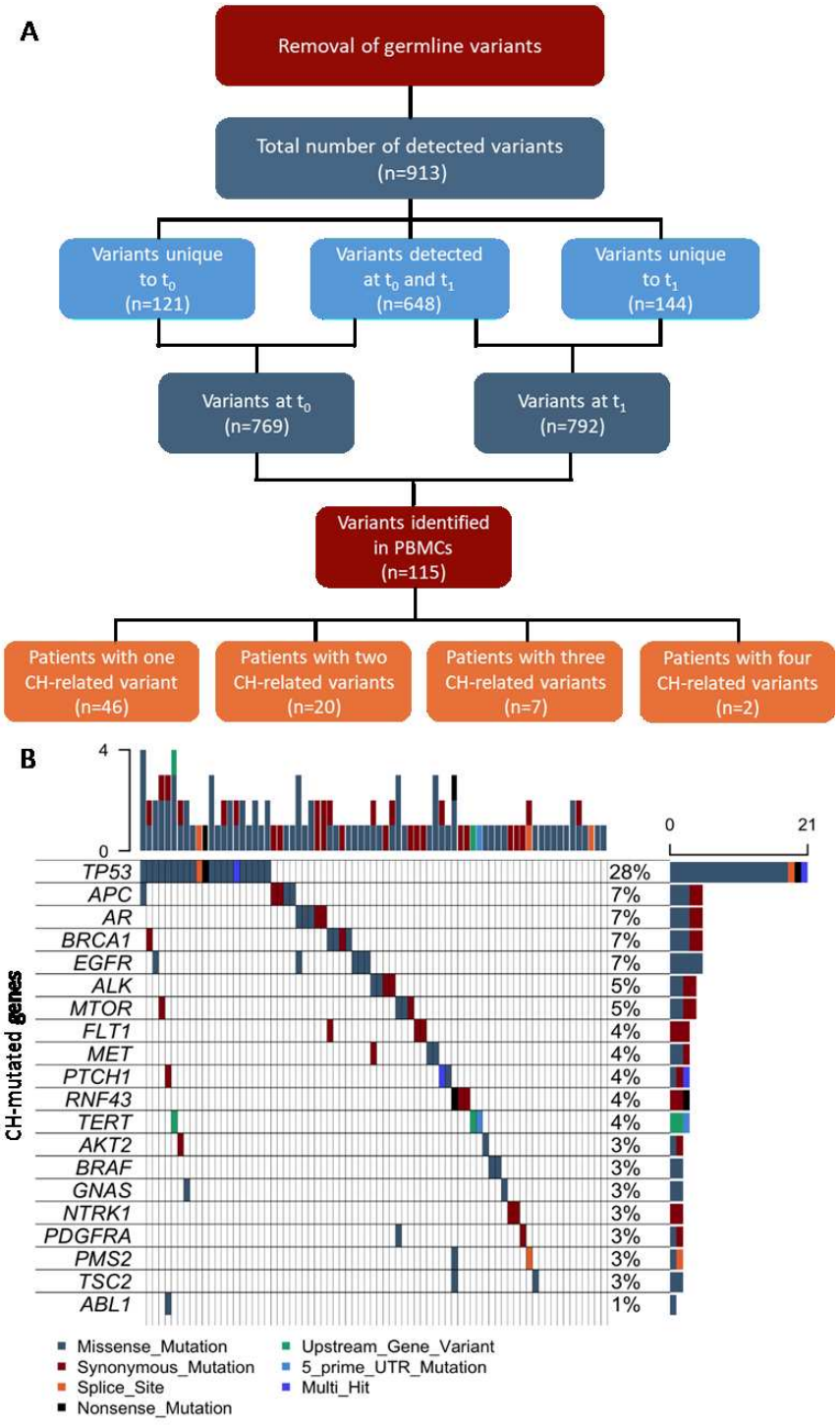

Figure 14: CH-related variants are frequently observed in patients with advanced NSCLC.
(**A**) After removal of germline variants, a total of 769 and 792 somatic variants were identified at t_0 and t_1, respectively. Of those, 648 were identified at both time points, whereas 121 and 144 variants were either unique to t0 or t1, respectively, resulting in a total of 913 detected variants. Of these, 115 variants from 75/167 patients were also detected in PBMCs with 30 of 167 patients having more than one CH-related variant. (**B**) Oncoprint of the most frequent CH-mutated genes. Shown is an overview of the top 20 altered genes and its genomic alterations (legend), in particular, genes (rows) affecting individual samples (columns). Of the 144 identified TP53 mutations in 114 patients, a total of 30 mutations in 21 patients were associated with CH. [Figure and legend adapted from JCO Precision Oncology (Weber et al. (66))]

Clonal hematological expansion was associated with age. Both, the number of patients and the total number of these variants were higher in those aged 65 years and older compared to younger patients (Figure 15A). The median VAF of CH-related mutations (0.59%) was notably lower compared to the median VAF of tumor-derived mutations (0.91%), the values ranging from 0.07% to 14.65% and 0.04% to 79.12%, respectively. Unlike tumor-specific variants, which changed on average 2.6-fold from t_0 to t_1 (range 0-218), the number of CH-related variants mostly remained stable over time (average fold change 0.95, range 0-3.0) (Figure 15B) (66). In line with previous reports, DNA fragments that hold tumor-specific variants have a slightly shorter lengths when compared to DNA fragments that carry CH-related variants (Kolmogorov-Smirnov test, P, 1 × 10−10) (179, 180) (Figure 15C).

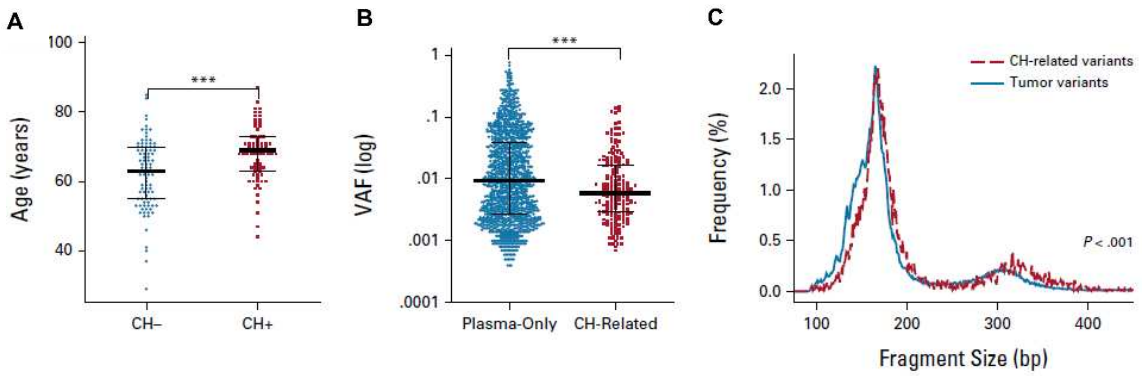

Figure 15: Comparison of age, variant allele frequency (VAF), and fragment size distribution between clonal hematopoiesis (CH)-related variants and tumor-specific variants.
(**A**) Dot plot showing the age distribution of patients without (CH-) and with (CH+) clonal hematopoiesis variants. The median age is significantly higher in patients with CH (CH+). (**B**) Logarithmic scale dot plot of variant allele frequencies (VAF) comparing plasma-only variants to CH-related variants. CH-related variants have a significantly lower median VAF than plasma-only variants. (**C**) Line graph depicting the frequency distribution of fragment sizes (in base pairs, bp) for CH-related variants (red line) and tumor-specific variants (blue line). Tumor-specific variants have shorter DNA fragment lengths compared to CH-related variants. Kolmogorov-Smirnov test, P <.001) [adapted from Weber et al. (66)].

While previous studies reported an association of CH-related variants with previous chemotherapy treatments or patient survival, in our cohort, no correlation was observed. The majority of patients with CHIP-related variants in our cohort were receiving second-line ICI therapy (70.7%), a smaller proportion were in third-line therapy (19.5%), only 8.1% were in first-line treatment, and 1.7% had received more than three prior lines (Figure 16A). CHIP-positive patients were more frequently observed in later lines of therapy, although the difference did not reach statistical significance (Chi^2 test, p = 0.35) (Figure 16B). There was no

significant difference in PFS and OS between patients with detected CH variants (“CHIP yes”) and those without detected CH variants (“CHIP no”) (Figure 16C) (66).

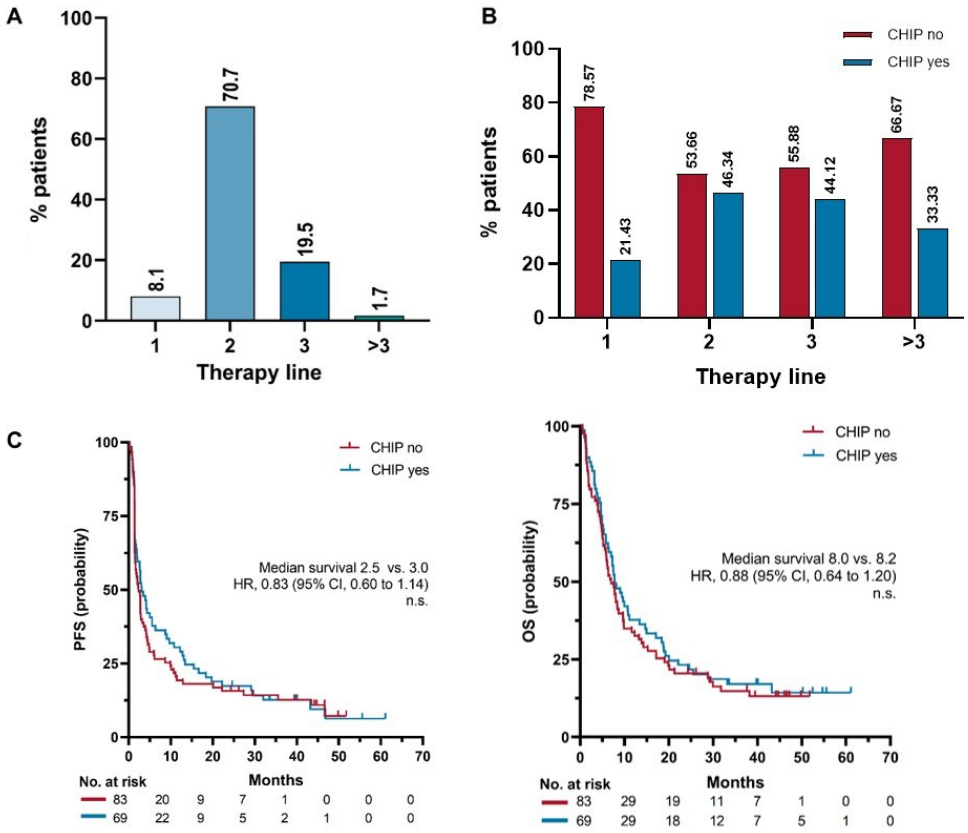

Figure 16: Distribution and clinical impact of CHIP variants in advanced NSCLC patients.
(**A**) Proportion of patients treated with ICI in the first, second, third, or beyond third-line setting (**B**) CHIP prevalence across therapy lines (**C**) Kaplan-Meier survival analysis showing no association between clonal hematopoiesis related variants and clinical outcome. Progression-free survival (PFS, left) and overall survival (OS, right) are compared between patients with (CHIP yes) and without (CHIP no) detectable CH-associated mutations. [Figure and legend adapted from Weber et al. (66)].

4.2.4. Molecular profiling and ctDNA levels of the cohort

In the first step, we determined the *de novo* mutation spectrum of the 167 NSCLC patients. At least one mutation could be detected in ctDNA in 91% of the patients (n=152), with an average number of 5.25 tumor-specific mutations per patient (median 4, range 1 – 68). Fifteen patients did not have detectable ctDNA at both time points and were defined as “non-shedders”. Notably, six of these non-shedders had variants related to clonal hematopoiesis, which would have led to incorrect classification of ctDNA-positive if these variants had not been excluded.

In a small percentage of patients (n=8, 5.3%), the level of tumor-derived ctDNA decreased from t_0 to t_1 to below the detection threshold, reaching 0. Additionally, ctDNA was only detectable at the second time point (t_1) in 5 patients (3.3%) but not at the first time point (t_0) (Figure 11A) (66).

Out of the 152 patients included, in 139 (91.4%) one or more mutations could be detected at both baseline and follow-up. In 91 patients (59.9%), additional mutations were identified that were exclusive to one of the two time points. The majority of these alterations were missense mutations, followed by nonsense and splice site variants. The most common nucleotide substitutions were C>T transitions, often linked to age-related deamination of 5-methylcytosine, and C>A transversions, typically associated with tobacco smoking (Figure 17A). The genes most frequently affected by mutations were *TP53*, *KRAS* and *KEAP1* (Figure 17B). Although our cohort was preselected and - if tumor mutation status was available a - excluded *EGFR* mutated patients**,** *EGFR* alterations were still detected in 20 patients (12%), including five actionable mutations such as L858R or exon 20 deletions. These patients would have been eligible for TKI therapy had tumor tissue genetic profiling been available at enrollment (66).

Genetic data from routine diagnostic work-up from tumor biopsies were obtainable from 116/167 NSCLC patients (69.5%) and compared to the molecular profiles obtained from plasma ctDNA. Among these, 71 patients (61.2%) had a total of 85 mutations in their tumor tissue, 64 of which were also detected in the plasma of 54 patients, resulting in a concordance rate of 75.3% (Figure 17C). This finding is consistent with data from previously published studies (181). Notably, in 17 patients whose tissue and plasma mutation profiles showed discordant results, plasma samples had significantly lower levels of ctDNA compared to concordant samples (aVAF: 0.2% versus 2.2%) (Figure 17D) (66).

Additionally, among 45 patients (38.8%) who did not have any mutations in their tumor tissue detected, six patients also presented a negative result in ctDNA, while 39 had at least one mutation detected. This can be explained by the fact the AVENIO Expanded kit includes a larger number of gene and does not rely on hotspot testing. The concordance between tissue and plasma molecular profiling is detailed in Table 10. In summary, the application of *de novo* mutation calling from plasma provides comprehensive molecular profiles (66).

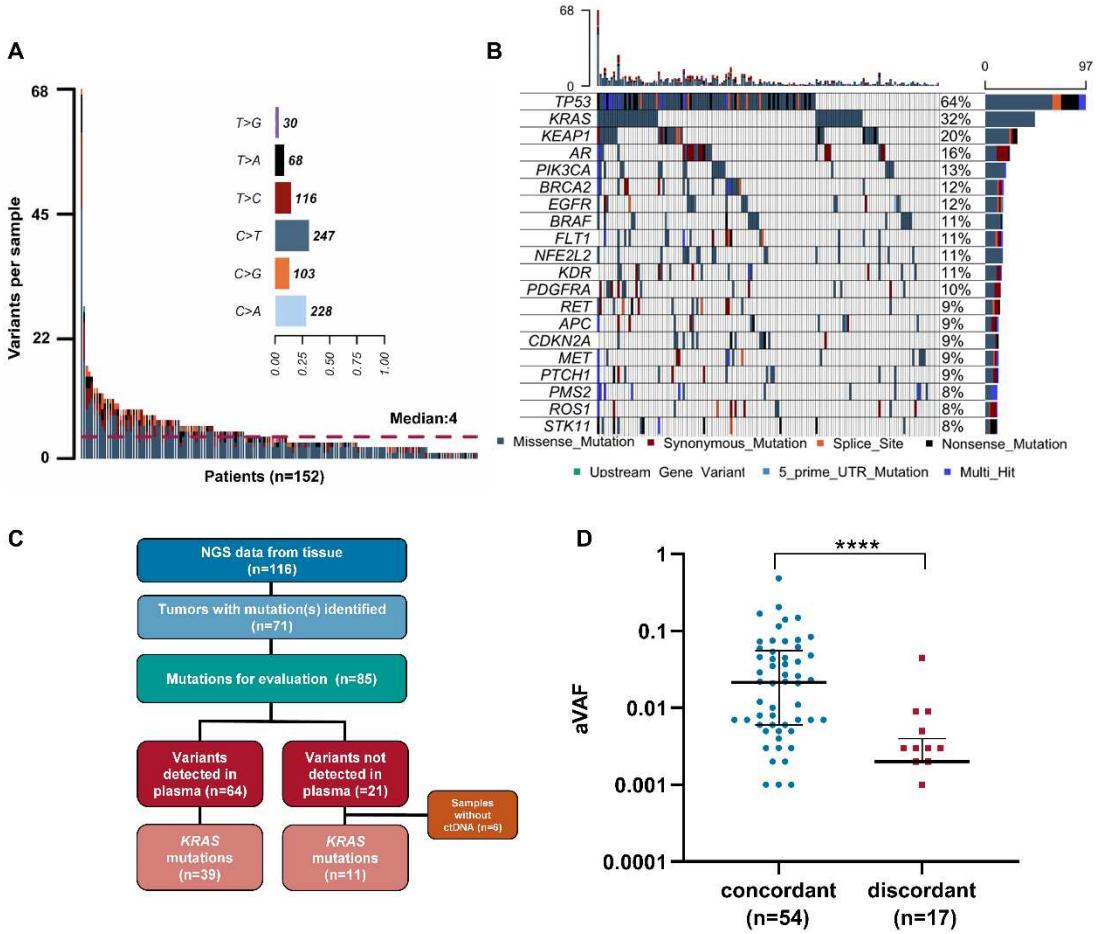

Figure 17: Molecular profiling of plasma samples and concordance with tumor tissue.
(A) After excluding clonal hematopoiesis related variants, an average of 5.2 mutations per patient (median 4, range 1 - 68) was identified. When applying AVENIO`s default filter settings, many mutations would have been missed and mutation detection was limited to 143/174 patients (82.2%) with a lower average of 2.17 mutations (median 2, range 1 - 10). Most detected variants were missense alterations, followed by nonsense and splice changes, while Indels were detected in only six patients. The most frequent nucleotide substitutions were C>T transitions. **(B**) Oncoprint displaying the 20 most frequently mutated genes after removal of CH-related variants. Each column represents an individual sample, and rows indicate gene-level alterations. The most commonly mutated genes included *TP53*, *KRAS*, and *KEAP1*. Despite the exclusion of patients with known activating *EGFR* mutations, *EGFR* alterations were found in 18 cases (10.7%). **(C)** Tumor tissue sequencing data were available for 116 of 167 patients (69.5%). At least one mutation was identified in 71 of these cases (61.2%). Among 50 KRAS mutations found in tumor tissue, 39 (78.0%) were also detected in plasma. In two cases, plasma profiling revealed a different KRAS mutation (G12V) compared to the corresponding tumor (Q22K and G12C). Overall, 64 of 85 tissue-detected mutations were also found in plasma, resulting in a concordance rate of 75.3% across 54 patients **(D)** ctDNA levels (based on average variant allele frequency, aVAF) in 71 plasma samples with matched tissue data are plotted. Samples with discordant tissue results (n=17) showed significantly higher ctDNA levels compared to concordant cases (n=54), with median aVAFs of 2.2% and 0.2%, respectively ($p < 0.0001$, two-tailed Mann–Whitney U test). ****$p \leq 0.0001$ [Figure reprinted and adapted with permission from JCO Precision Oncology, Weber et al. (66)].

Table 10: Concordance of tissue and plasma molecular profiling [Table and legend originally reprinted from Weber et al. (66)]; [1] [0=no concordance; 1=yes, at least one mutation is concordant; 2=NA, 3=no mutation in tumor detected]

ID	Mutation(s) detected in tumor tissue	Mutation(s) detected in plasma sample	Concordance[1]
852	KRAS: c.34G>T, p.(G12C)	KRAS: c.34G>T, p.(G12C)	1
951	No mutation detected		3
952	KRAS: c.38G>A, p.(G13D)	KRAS: c.38G>A, p.(G13D)	1
962	No mutation detected		3
964	NGS: not tested		2
965	NGS: not tested		2
979	BRAF: c.1406G>T, p.(G469V)	BRAF: c.1406G>T, p.(G469V)	1
981	No mutation detected		3
982	No mutation detected		3
985	NGS: not tested		2
990	No mutation detected		3
993	NGS: not tested		2
996	NGS: not tested		2
1001	BRAF: c.1799T>A, p.(V600E)	BRAF: c.1799T>A, p.(V600E)	1
1002	No mutation detected		3
1003	No mutation detected		3
1004	NGS: not tested		2
1008	KRAS: c.35G>C, p.(G12A)	KRAS: c.35G>C, p.(G12A)	1
1015	NGS: not tested		2
1016	NGS: not tested		2
1021	NGS: not tested		2
1022	NGS: not tested		2
1023	NGS: not tested		2
1024	EGFR: c.2573T>G, p.(L858R) EGFR: c.2369C>T, p.(T790M)	EGFR: c.2573T>G, p.(L858R) EGFR: c.2369C>T, p.(T790M)	1
1027	ERBB2: c.2223_2234dup, p.(Y742_A745dup)	ERBB2: c.2223_2234dup, p.(Y742_A745dup)	1
1029	EGFR: c.2126A>C, p.(E709A) EGFR: c.2155G>A, p.(G719S)	EGFR: c.2126A>C, p.(E709A) EGFR: c.2155G>A, p.(G719S)	1
1030	NGS: not tested		2
1031	NRAS: c.182A>G, p.(Q61R)	NRAS: c.182A>G, p.(Q61R)	1
1032	KRAS: c.35G>A, p.(G12D)	KRAS: c.35G>A, p.(G12D)	1
1033	NGS: not tested		2
1035	KRAS: c.34G>T, p.(G12C)	KRAS: c.34G>T, p.(G12C)	1
1037	NGS: not tested		2
1038	KRAS: c.183A>T, p.(Q61H)	KRAS: c.183A>T, p.(Q61H)	1
1043	No mutation detected		3
1047	NGS: not tested		2
1051	No mutation detected		3
1054	NGS: not tested		2
1057	No mutation detected		3
1063	NGS: not tested		2
1064	NGS: not tested		2
1066	KRAS: c.34G>T, p.(G12C)	KRAS: c.34G>T, p.(G12C)	1
1067	KRAS: c.34G>T, p.(G12C)	KRAS: c.34G>T, p.(G12C)	1
1068	KRAS: c.35G>A, p.(G12D)		0
1069	PIK3CA: c.1633G>A, p.(E545K)	PIK3CA: c.1633G>A, p.(E545K)	1
1070	No mutation detected		3
1071	KRAS: c.35G>C, p.(G12A)		0
1073	BRAF: c.1406G>C, p.(G469A)	BRAF: c.1406G>C, p.(G469A)	1
1075	NGS: not tested		2

1076	No mutation detected		3
1077	NGS: not tested		2
1080	No mutation detected		3
1081	No mutation detected		3
1083	KRAS: c.34G>T, p.(G12C)	KRAS: c.34G>T, p.(G12C)	1
1086	No mutation detected		3
1089	KRAS: c.34G>C, p.(G12R)		0
1090	KRAS: c.34_35delinsTT, p.(G12F)	KRAS: c.34_35delinsTT, p.(G12F)	1
1091	KRAS: c.35G>A, p.(G12D) PIK3CA: c.1633G>A, p.(E545K)	KRAS: c.35G>A, p.(G12D) PIK3CA: c.1633G>A, p.(E545K)	1
1092	NGS: not tested		2
1093	No mutation detected		3
1094	NGS: not tested		2
1096	KRAS: c.35G>A, p.(G12D)	KRAS: c.35G>A, p.(G12D)	1
1097	KRAS: c.35G>T, p.(G12V)	KRAS: c.35G>T, p.(G12V)	1
1098	KRAS: c.34G>T, p.(G12C)	KRAS: c.35G>T, p.(G12V)	0
1099	KRAS: c.34G>T, p.(G12C)	KRAS: c.34G>T, p.(G12C)	1
1100	NGS: not tested		2
1101	KRAS: c.34G>T, p.(G12C)		0
1103	KRAS: c.35G>T, p.(G12V)	KRAS: c.35G>T, p.(G12V)	1
1104	KRAS: c.34G>T, p.(G12C)	KRAS: c.34G>T, p.(G12C)	1
1105	TP53: c.469G>T, p.(V157F)	TP53: c.469G>T, p.(V157F)	1
1111	MET: c.3082G>C, p.(D1028H)		0
1112	NGS: not tested		2
1114	No mutation detected		3
1115	NGS: not tested		2
1116	KRAS: c.34G>T, p.(G12C)	KRAS: c.34G>T, p.(G12C)	1
1117	NGS: not tested		2
1118	NGS: not tested		2
1119	No mutation detected		3
1120	BRAF: c.1406G>C, p.(G469A) KRAS: c.440A>C, p.(K147T)	BRAF: c.1406G>C, p.(G469A) KRAS: c.440A>C, p.(K147T)	1
1124	No mutation detected		3
1127	BRAF: c.1397G>T, p.(G466V)	BRAF: c.1397G>T, p.(G466V)	1
1132	KRAS: c.35G>A, p.(G12D) BRAF: c.1406G>T, p.(G469V)	KRAS: c.35G>A, p.(G12D) BRAF: c.1406G>T, p.(G469V)	1
1133	KRAS: c.35G>T, p.(G12V)	KRAS: c.35G>T, p.(G12V)	1
1136	PIK3CA: c.1624G>A, p.(E542K)		0
1137	No mutation detected		3
1139	No mutation detected		3
1140	NGS: not tested		2
1141	BRAF: c.1799T>A, p.(V600E) MET: c.2962C>T, p.(R988C) IDH1: c.394C>T, p.(R132C)	BRAF: c.1799T>A, p.(V600E) IDH1: c.394C>T, p.(R132C)	1
1143	KRAS: c.34G>T, p.(G12C)		0
1145	NGS: not tested		2
1147	KRAS: c.34G>T, p.(G12C)	KRAS: c.34G>T, p.(G12C)	1
1149	NGS: not tested		2
1150	NGS: not tested		2
1151	No mutation detected		3
1153	KIT: c.1259G>C, p.(R420T)		0
1154	KRAS: c.34G>T, p.(G12C)	KRAS: c.34G>T, p.(G12C)	1
1158	No mutation detected		3
1166	KRAS: c.35G>T, p.(G12V) PIK3CA: c.1624G>A, p.(E542K)	KRAS: c.35G>T, p.(G12V) PIK3CA: c.1624G>A, p.(E542K)	1

1167	NGS: not tested		2
1168	BRAF: c.1799T>A, p.(V600E) PIK3CA: c.1624G>A, p.(E542K)	BRAF: c.1799T>A, p.(V600E) PIK3CA: c.1624G>A, p.(E542K)	1
1172	No mutation detected		3
1173	No mutation detected		3
7005	NGS: not tested		2
7006	BRAF: c.1799_1801del, p.(V600_K601delinsE)	BRAF: c.1799_1801del, p.(V600_K601delinsE)	1
7007	NGS: not tested		2
7008	KRAS: c.35G>T, p.(G12V)	KRAS: c.35G>T, p.(G12V)	1
7009	No mutation detected		3
7010	NGS: not tested		2
7011	No mutation detected		3
7016	KRAS: c.183A>T, p.(Q61H)	KRAS: c.183A>T, p.(Q61H)	1
7021	KRAS: c.35G>T, p.(G12V)		0
7022	KRAS: c.34G>T, p.(G12C) MAP2K1: c.149T>C, p.(L50P)	KRAS: c.34G>T, p.(G12C) MAP2K1: c.149T>C, p.(L50P)	1
7023	KRAS: c.34_35delinsTT, p.(G12F)	KRAS: c.34_35delinsTT, p.(G12F)	1
7024	KRAS: c.35G>T, p.(G12V)	KRAS: c.35G>T, p.(G12V)	1
7027	KRAS: c.182 A>T, p.(Q61L)	KRAS: c.182 A>T, p.(Q61L)	1
7030	No mutation detected		3
7034	No mutation detected		3
7035	No mutation detected		3
7036	NGS: not tested		2
7037	No mutation detected		3
7041	NGS: not tested		2
7043	NGS: not tested		2
7044	NGS: not tested		2
7049	KRAS: c.34G>T, p.(G12C)	KRAS: c.34G>T, p.(G12C)	1
7059	NGS: not tested		2
7067	No mutation detected		3
7069	NGS: not tested		2
7071	No mutation detected		3
7073	NGS: not tested		2
7074	No mutation detected		3
7075	No mutation detected		3
7079	NGS: not tested		2
7085	EGFR: c.2316_2321dup, p.(H773_V774dup)	EGFR: c.2316_2321dup, p.(H773_V774dup)	1
7090	No mutation detected		3
7091	NGS: not tested		2
7093	KRAS: c.34G>T, p.(G12C)	KRAS: c.34G>T, p.(G12C)	1
7098	No mutation detected		3
7099	No mutation detected		3
7103	KRAS: c.34G>T, p.(G12C)	KRAS: c.34G>T, p.(G12C)	1
7108	No mutation detected		3
7110	KRAS: c.35G>A, p.(G12D) IDH1: c.395G>T, p.(R132L)	KRAS: c.35G>A, p.(G12D) IDH1: c.395G>T, p.(R132L)	1
7111	BRAF: c.1781A>G, p.(D594G)		0
7117	KRAS: c.35G>A, p.(G12D)		0
7118	No mutation detected		3
7119	No mutation detected		3
7120	KRAS: c.34G>T, p.(G12C)	KRAS: c.34G>T, p.(G12C)	1
7121	No mutation detected		3
7123	No mutation detected		3
7125	KRAS: c.33_35delinsCGT, p.(G12V)		0

7126	KRAS: c.35G>C, p.(G12A)		0
7133	NGS: not tested		2
7135	KRAS: c.35G>T, p.(G12V)	KRAS: c.35G>T, p.(G12V)	1
7145	KRAS: c.64C>A, p.(Q22K)	KRAS: c.35G>T, p.(G12V)	0
7149	PIK3CA: c.1624G>A, p.(E542K)		0
7150	KRAS: c.34G>T, p.(G12C) BRAF: c.1397G>T, p.(G466V)	KRAS: c.34G>T, p.(G12C) BRAF: c.1397G>T, p.(G466V)	1
7151	No mutation detected		3
7153	NGS: not tested		2
7155	KRAS: c.38G>A, p.(G13D)	KRAS: c.38G>A, p.(G13D)	1
7160	NGS: not tested		2
7162	KRAS: c.35G>T, p.(G12V) TP53: c.524G>A, p.(R175H)	KRAS: c.35G>T, p.(G12V) TP53: c.524G>A, p.(R175H)	1
7178	ROS: c.6528_6529delinsGT, p.(G2177*) TP53: c.818G>T, p.(R273L)		0
7180	No mutation detected		3
7181	BRAF: c.1799T>A, p.(V600E)	BRAF: c.1799T>A, p.(V600E)	1
7183	NGS: not tested		2
7184	NGS: not tested		2
7185	KRAS: c.34G>T, p.(G12C)	KRAS: c.34G>T, p.(G12C)	1
7186	NGS: not tested		2
7187	NGS: not tested		2

4.2.5. Dynamics of ctDNA response patterns and impact of CH-related variants

Next, we investigated whether ctDNA level and their dynamics are predictive of response to ICI. Overall ctDNA levels at t_0 were predominantly low, with 50.9% (85/167) of patients having an average VAF (aVAF) <1% (median 0.9%; range, 0-48.4). The aMM per ml plasma ranged from 0-57,500 molecules per ml with a median of 77 (66).

Among responders, a significant decrease in aMM levels was observed from t_0 to the first response evaluation (t_1). Patients with a DCR showed a reduction from 36.6 to 14.6 aMM ($p = 0.0204$), while those with an ER had a drop from 45 to 13 aMM ($p = 0.0341$). In contrast, non-responders (NR, NDR) showed no significant change in aMM. However, the aMM levels at t_1 were significantly higher in non-responders (NR, NDR) compared to responders (DCR vs. NDR: 15 versus 159, $p<0.0001$*;* ER vs. NR: 101 vs. 13, $p<0.0001$). Detailed pre- and on-treatment ctDNA levels for all proxies can be found in Figure 18 (66).

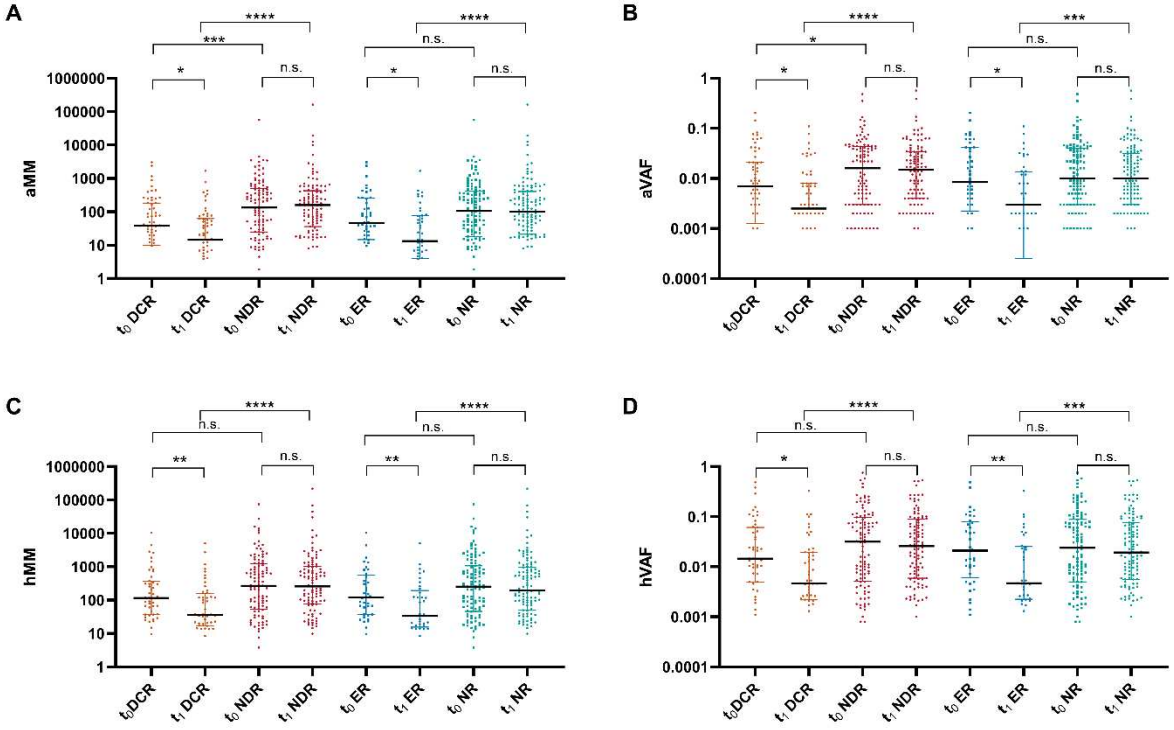

Figure 18*:* ctDNA level distributions stratified by treatment response and time point.
Patients were grouped based on response type and sampling time: DCR (durable clinical response), NDR (no durable response), ER (early response at first tumor evaluation), and NR (no early response). Timepoints included baseline (t_0, before initiation of IC] therapy) and early follow-up (t_1, approximately 4 weeks after treatment initiation). Pairwise comparisons between groups (t_0 vs. t_1, DCR vs. NDR, ER vs. NR) were conducted using the Mann–Whitney U test to evaluate four ctDNA metrics: **(A)** average number of mutant molecules per mL of plasma (aMM), **(B)** average variant allele frequency (aVAF),**(C)** highest number of mutant molecules per mL (hMM), and**(D)** highest variant allele frequency (hVAF). In patients who did not respond to treatment, ctDNA levels remained largely unchanged. However, a significant difference was observed for both early (aMM 45 versus 13, p=0.0341; aVAF 0.95% versus 0.30%, p=0.0129, hMM 36 versus 116, p=0.0081; hVAF 0.47% versus 1.45%, p=0.0108) and durable responders (aMM 36.6 versus 14.6, p=0.0204; aVAF 0.47 versus 2.10%, p=0.0240, hMM 34 versus 116, p=0.0087; hVAF 0.8% versus 0.3%, p=0.0099). Moreover, for all ctDNA metrics, levels of non-responder (NR and NDR) at t_1 were significantly higher than in responders (ER and DCR) aMM (ER: 101 versus 13, p<0.0001; aVAF 1.0% versus 0.30%, p=0.0010, hMM 260 versus 35, p=, p<0.0001; hVAF 2.59% versus 0.47%, , p<0.0001; DCR: aMM 15 versus 159, p<0.0001; aVAF 1.5% versus 0.30%, p=0.0010, hMM 196 versus 34, p=, p<0.0001; hVAF 1.93% versus 0.47%). n.s., not significant p>0.05; * p≤0.05; ** p≤0.01, *** p≤0.001, **** p≤0.000. [Figure reprinted from JCO Precision Oncology; legend adapted (Weber et al. (66))].

The analysis of ctDNA response patterns from t_0 to t_1 revealed that a majority of treatment responders (DCR and ER) presented a decrease of ctDNA levels, while non-responders (NDR and NR) exhibited variable mutation dynamics (Figure 19A, Figure 19B, Figure 20). When patients were categorized based on a ≥50% decrease or increase in aMM levels, 54.5% of the cohort fell into one of these categories and 45.5% pf patients had changes less than 50% (Figure 19C). When CH-related variants were not excluded, this ratio decreased further, which led to a misclassification of 20 patients as either responders or non-responders based on their molecular response (Figure 21). This underscores the significance of incorporating PBMCs in the analysis to mitigate CH-related variant interference. For instance, patient #1147 initially showed a 116% increase in aMM from t_0 to t_1, which was corrected to a 50.8% decrease and aligned with a subsequent molecular response after excluding CH variants. The patient also displayed a durable partial response as indicated by the radiographic findings, which aligns with the ctDNA change picture after CH variants exclusion (Figure 19D) (66).

The likelihood of early and durable responders showing a 50% molecular decrease without CH-variants was 4.46 and 3.63 times higher, respectively, compared to non-responders (Fisher's exact test, P values of 0.0003 and 0.0009, respectively) (Figure 19E). However, the correlation between early/durable radiographic responses and molecular responses of 25% and 50% from the baseline to the first measurement showed only moderate agreement (Cohen's kappa coefficients of 0.31 and 0.28 for a 50% ctDNA response, and 0.27 and 0.23 for 25% ctDNA response, respectively) (Figure 19) (66).

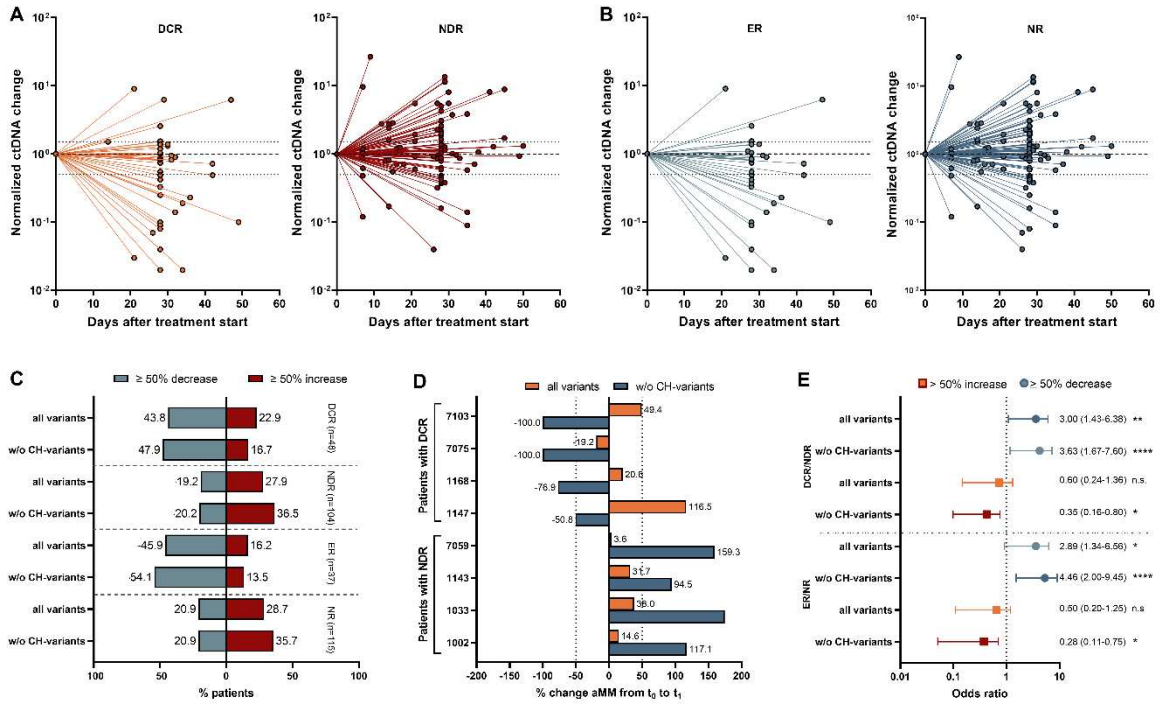

Figure 19: **Correlation of dynamic ctDNA changes with response to ICI**.
(A) Normalized ctDNA levels (aMM, average mutant molecules per mL plasma) relative to pre-treatment levels in different patient response groups: durable clinical responders (DCR), non-durable responders (NDR) and **(B)** early responders (ER) and non-responders (NR). The dashed line represents no change in ctDNA levels, while the dotted lines mark the 50% cut-offs for ctDNA decrease and increase. In **(C)** the fraction of patients, stratified by early and durable responders, that experienced a ≥ 50% ctDNA decrease (left) or increase (right) is plotted. Data is shown for all variants, including CH-related variants, as well as for a corrected variant call set that excludes CH-related variants. **(D)** shows the percentage change in average mutant molecule frequency (aMM) from baseline (t_0) to first follow-up (t_1) for exemplary patients stratified by their response to treatment. The data is presented for all variants (including CH-related variants) as well as for a corrected variant call set excluding CH-related variants, with significant differences observed between the call sets. **(E)** Displayed are the odds ratios (ORs) for responders versus non-responders with a 50% increase or decrease in all variants, including CH-related variants, and a corrected variant call set excluding CH-related variants. These ORs were calculated using a two-sided Fisher's exact test with a 95% confidence interval (CI). n.s., not significant $p > 0.05$; * $p \leq 0.05$; ** $p \leq 0.01$, *** $p \leq 0.001$, **** $p \leq 0.0001$. CH, clonal hematopoiesis, ctDNA, circulating tumor DNA, t_0, blood draw before ICI therapy start, t_1 = blood draw at first response evaluation [Figure and legend adapted from JCO Precision Oncology (Weber et al. (66))]

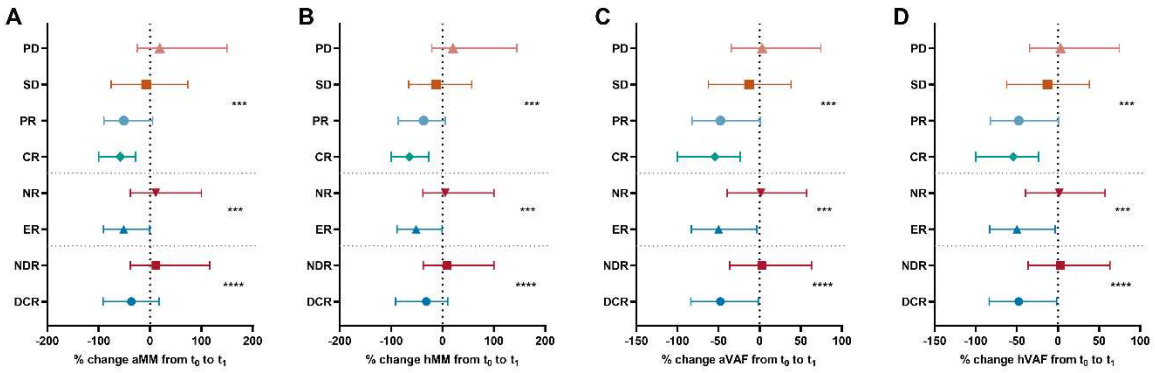

Figure 20: ctDNA molecular responses differ between responders and non-responders. Median percentage changes from baseline (t_0) to follow-up (t_1) are shown for:**(A)** average mutant molecules per mL plasma (aMM), **(B)** highest mutant molecules per mL plasma (hMM), **(C)** average variant allele frequency (aVAF), and**(D)** highest variant allele frequency (hVAF), with interquartile ranges. Patients are stratified by treatment response categories. While most responders show a clear molecular decline in ctDNA levels, non-responders display variable or inconsistent changes. Clinical subgroups include: PD (progressive disease), SD (stable disease), PR (partial response), CR (complete response), NR (no early response), ER (early response), NDR (no durable response), and DCR (durable clinical response). Statistical analysis was performed using the Mann–Whitney U test for pairwise comparisons (ER vs. NR; DCR vs. NDR) and the Kruskal–Wallis test for group-wise comparisons (PD, SD, PR, CR); n.s., not significant p>0.05; * p≤0.05; ** p≤0.01, *** p≤0.001, **** p≤0.0001 [Reprinted and adapted from JCO Precision Oncology (Weber et al. (66))].

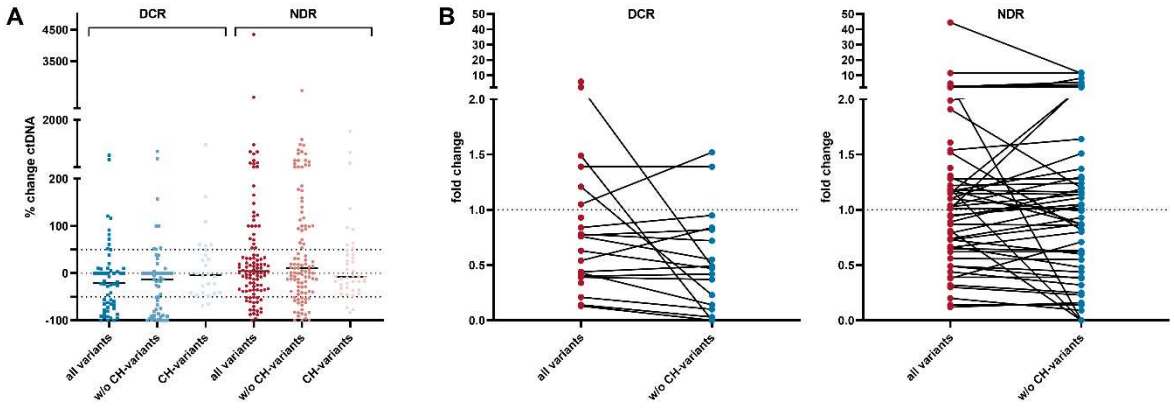

Figure 21: Impact of clonal hematopoiesis (CH)-related variants on interpretation of ctDNA response. (A) Percent change in ctDNA levels is shown for patients with durable clinical response (DCR) and those without (NDR), based on three variant call sets: all detected variants, a filtered set excluding CH-associated variants, and CH-related variants alone. **(B)** Fold changes in variant levels are displayed for both the complete set of mutations and the CH-corrected dataset. In some patients, excluding CH-related variants significantly altered the interpretation of molecular response. [Reprinted originally from JCO Precision Oncology; legend adapted (Weber et al. (66))].

4.2.6. Prognostic value of molecular ctDNA response for survival outcomes

In addition to evaluating the predictive utility of ctDNA, we assessed the prognostic significance of molecular ctDNA response in relation to survival outcomes. To this end, several molecular response thresholds were tested to determine optimal cut-offs distinguishing responders from non-responders. Notably, patients classified as “non-shedder”, with no ctDNA detected at both timepoints (n=15), had improved OS and PFS compared to patients with detectable ctDNA (“shedder”). Median PFS was 9.2 months in non-shedders versus 2.8 months in shedders (HR: 0.49; 95% CI: 0.30–0.79; p = 0.0231). Median OS was 21.9 months in non-shedders compared to 7.7 months in shedders (HR: 0.55; 95% CI: 0.32–0.84; p = 0.0342). Additionally, patients with ctDNA levels exceeding the median aMM value showed significantly reduced progression-free and overall survival at both timepoints (Figure 22) (66).

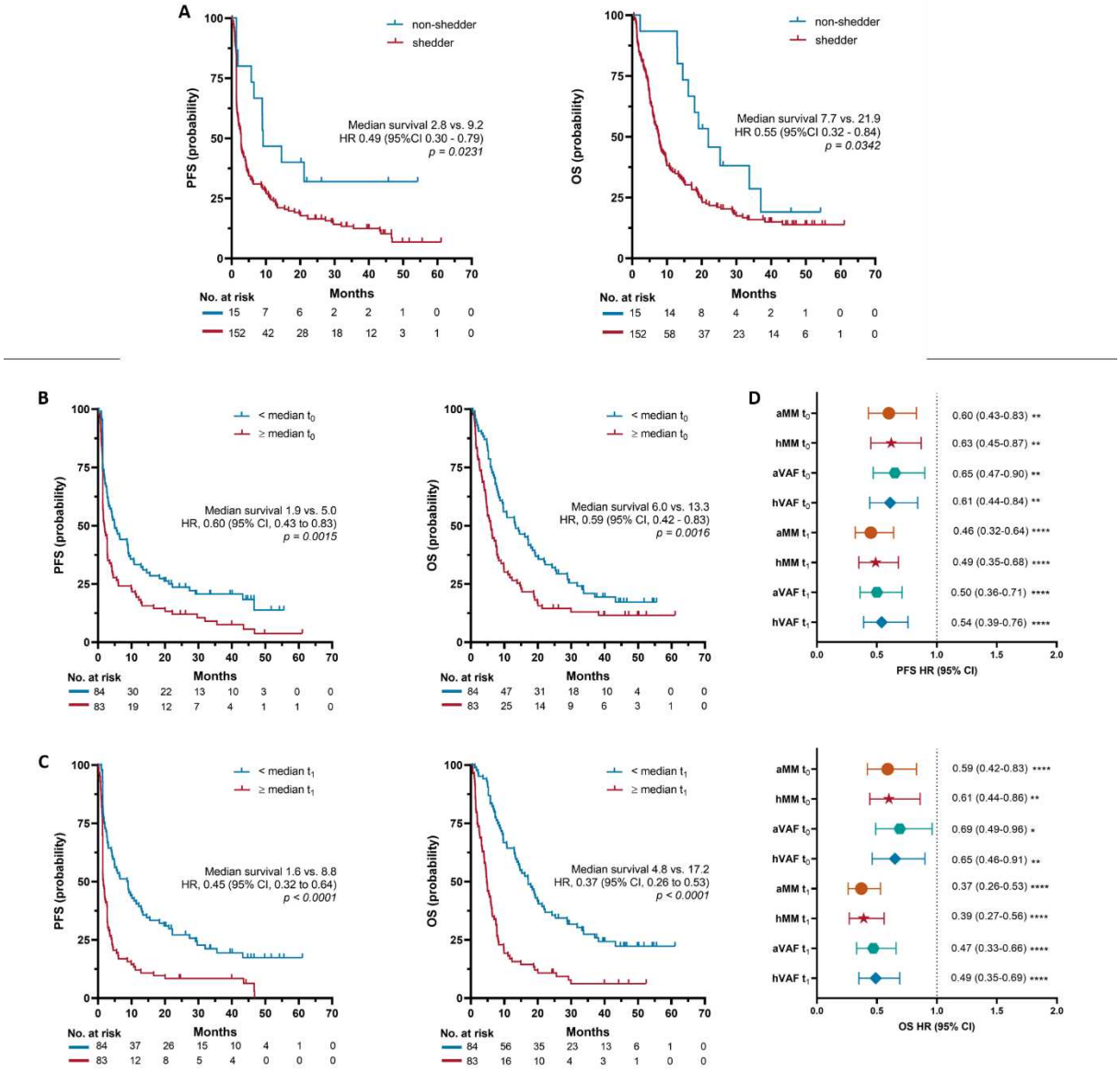

Figure 22: Elevated ctDNA is linked to poorer survival outcomes, while low or absent ctDNA correlates with improved prognosis

Kaplan- Meier curves in panel **A** compare non-shedders (no ctDNA detected) and shedders (ctDNA detected) of the full cohort (n=167 patients), indicating longer median PFS (2.8 vs. 9.2 months, p=0.0231) and OS (7.7 vs. 21.9 months, p=0.0342) in non-shedders. **B** evaluated patients with ctDNA levels below and above the median for t_0 (aMM median=77), showing better PFS (9.1 vs. 5.0 months, p=0.0015) and OS (6.0 vs. 13.3 months, p=0.0016) in patients with lower levels (PFS, HR of 0,60 (95% CI, 0.43-0.83, p=0.0015; OS, HR of 0.59 (95% CI, 0.42-0.83, p=0.0016)). Panel **C** compares patients stratified on median ctDNA level (aMM median = 70) and demonstrates superior outcomes for those below the median, with PFS of 1.6 vs. 8.8 months (p<0.0001) and OS of 4.8 vs. 17.2 months (p < 0.0001) at t_1. At t_1, the survival difference was even more pronounced (PFS HR 0.45, 95% CI, 0.32-0.64, p<0.0001 and OS HR 0.37, 95% CI, 0.26-0.55, p<0.0001) than in t_0. **D** shows the hazard ratios (HR) and 95% confidence intervals (CI) for all 4 proxies stratified by the median ctDNA level for PFS and OS. HR, hazard ratio, CI, confidence interval, P-values are calculated from log-rank tests. *p≤0.05, ** p≤0.01, *** p≤0.001, ****p≤0.0001 [Figure and legend adapted from Weber et al. (66)].

Subsequently, patients were categories based on changes in their ctDNA levels in four groups:

- no ctDNA at both time points (“non-shedders”)
- a decrease of more than 50% from t_0 to t_1
- an increase of more than 50%,
- changes falling within these two thresholds (intermediate group)

Patients who achieved a ctDNA decrease of ≥50% showed similar OS and PFS to those without detectable ctDNA, whereas patients with a ctDNA increase or a decrease of less than 50% had substantially poorer survival outcomes (Figure 23A). Similar trends were observed when applying a 25% response threshold, though the effect on PFS was less pronounced, as shown in Figure 23B (66).

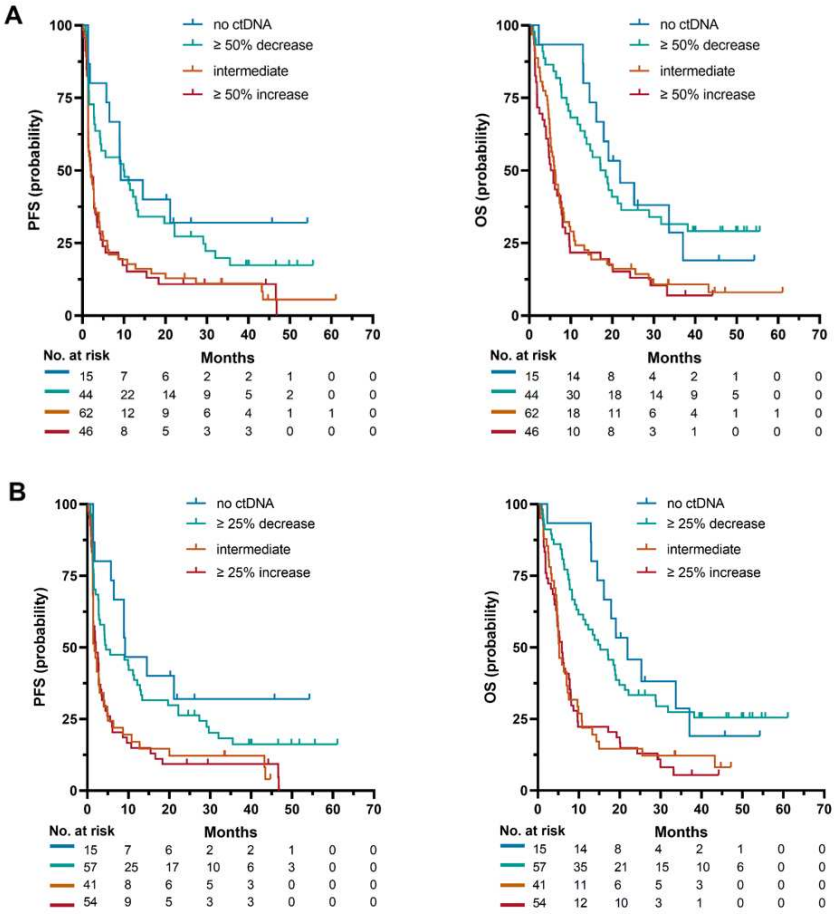

Figure 23: Changes in ctDNA levels during ICI treatment correlate with patient survival
(**A**) Kaplan-Meier analysis of PFS (left plot) and OS (right plot) of all 167 patients, grouped by ctDNA dynamics between baseline (t_0) and follow-up (t_1). Patients were stratified into four categories: no detectable ctDNA at both time points (blue), a ≥50% reduction in the average number of mutant molecules (green), a ≥50% increase (red), and those with intermediate changes not meeting the 50% threshold (orange). (**B**) The same survival analysis was repeated using a 25% threshold for defining increase or decrease in ctDNA levels. [Figure and legend reprinted and adapted from Weber et al. (66)].

Stratifying patients simply by ≥50% versus <50% ctDNA decrease revealed significant differences in survival. Among patients with <50% reduction (based on all variants), median PFS was 2.6 months and OS was 6.4 months, compared to 7.7 months and 16.2 months in patients with ≥50% decrease. Importantly, these distinctions became even more pronounced when CH- related variants were excluded ("w/o CH-variants"). When stratifying patients based on a 50% molecular ctDNA response and exclude CH-associated variants, those with <50% decrease had a median PFS of 2.0 months and OS of 5.9 months, compared to 10.0 months and 18.4 months, respectively, in patients with ≥50% aMM decrease (Figure 24A). Applying a 25% decrease threshold yielded similar trends, but with weaker PFS discrimination - based on

all variants. Without CH variants, PFS improved from 1.9 to 4.5 months (HR 0.57, 95% CI 0.41–0.80), and OS improved from 5.4 to 15.2 months (HR 0.48, 95% CI 0.33–0.65) when patients showed a ≥50% molecular ctDNA response. Inclusion of CH variants again reduced the predictive separation (Figure 24B) (66).

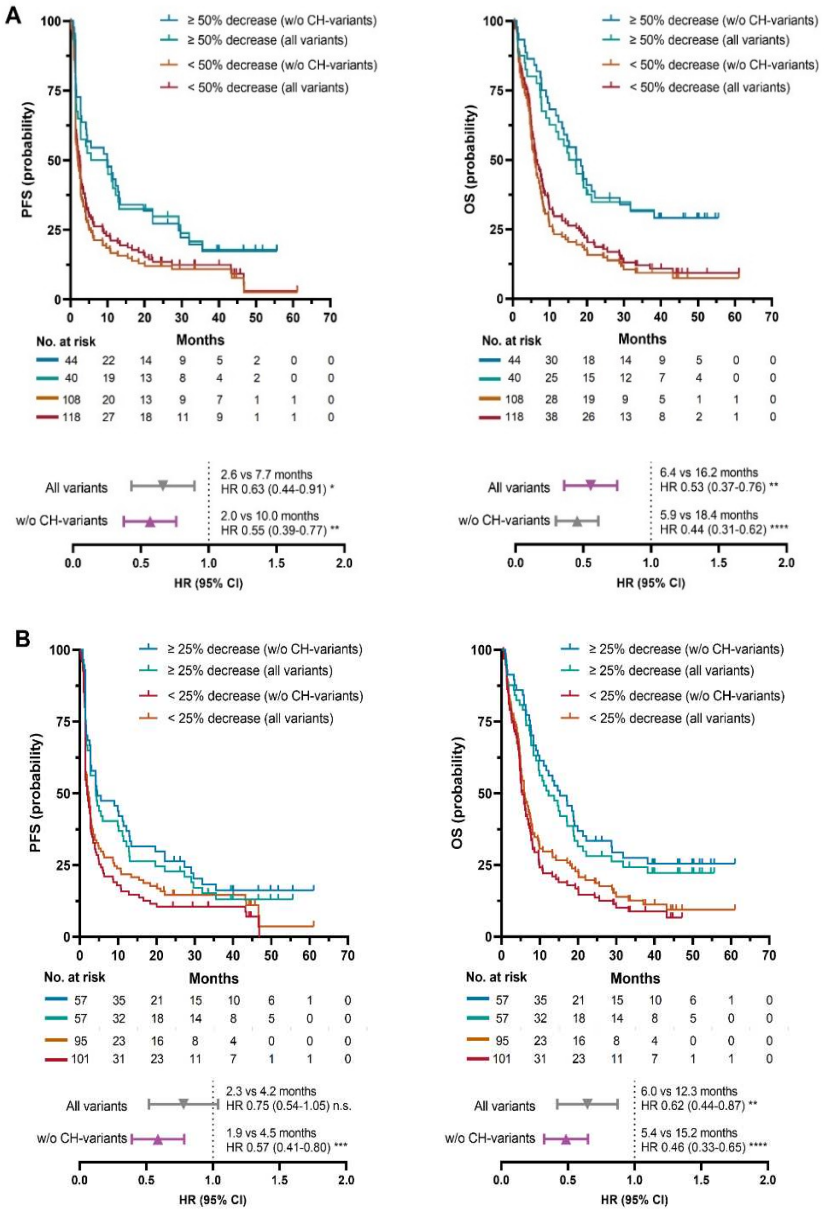

Figure 24: Impact of molecular ctDNA response thresholds on survival outcomes with and without exclusion of CHIP-related variants. (A) Kaplan–Meier curves for progression-free survival (PFS, left) and overall survival (OS, right) stratified by a ≥50% ctDNA aMM decrease from baseline (t_0) to follow-up (t_1) (n=152 patients). Patients achieving ≥50% decrease exhibited significantly improved survival compared to those with <50% decrease. Exclusion of clonal hematopoiesis (CH)-related variants further enhanced stratification. **B**) Same as in (A), but using 25% cut-off. Hazard ratios (HR), 95% confidence intervals (CI), and median survival times are indicated for both uncorrected ("all variants") and CH-corrected analyses ("w/o CH-variants"). *p≤0.05; **p≤0.01; ***p≤0.0001; n.s. not significant; p values were calculated from log-rank tests. ctDNA, circulating tumor DNA [Figure and legend reprinted and adapted from Weber et al. (66)].

To further investigate the prognostic value of early molecular response, additionally a 2-month landmark analysis (60 days after t_0) was performed and revealed a clear separation between the four groups. Patients with a ≥50% reduction in ctDNA or undetectable ctDNA throughout treatment had the longest survival, whereas a ≥50% ctDNA increase was associated with poorest PFS and OS (Figure 25A). When stratifying patients by ≥50% ctDNA decrease versus <50% ctDNA decrease, median PFS and OS were shorter in patients with <50% decrease in aMM (all variants: 4.3 and 5.9 months, respectively) compared to those with a ≥50% decrease (all variants: 11.1 and 16.9 months, respectively). It was also observed that the separation of survival curves was less distinct when CH-related variants remained included in the analysis. Specifically, patients with a ≥50% decrease in ctDNA-levels – after correction for CH variants – showed a median PFS of 11.3 months compared to 3.1 months in those with less than 50% decrease (HR 0.59; 95% CI: 0.37-0.94; $p < 0.05$*). Similarly, median OS was 16.9 months for patients with ≥50% decrease compared to 5.3 months with less than 50% decrease (HR 0.45; 95% CI: 0.30-0.65; $p < 0.0001$***). These findings emphasize the importance of eliminating CH-associated alterations to optimize the prognostic utility of ctDNA response evaluation (Figure 25B) (66).

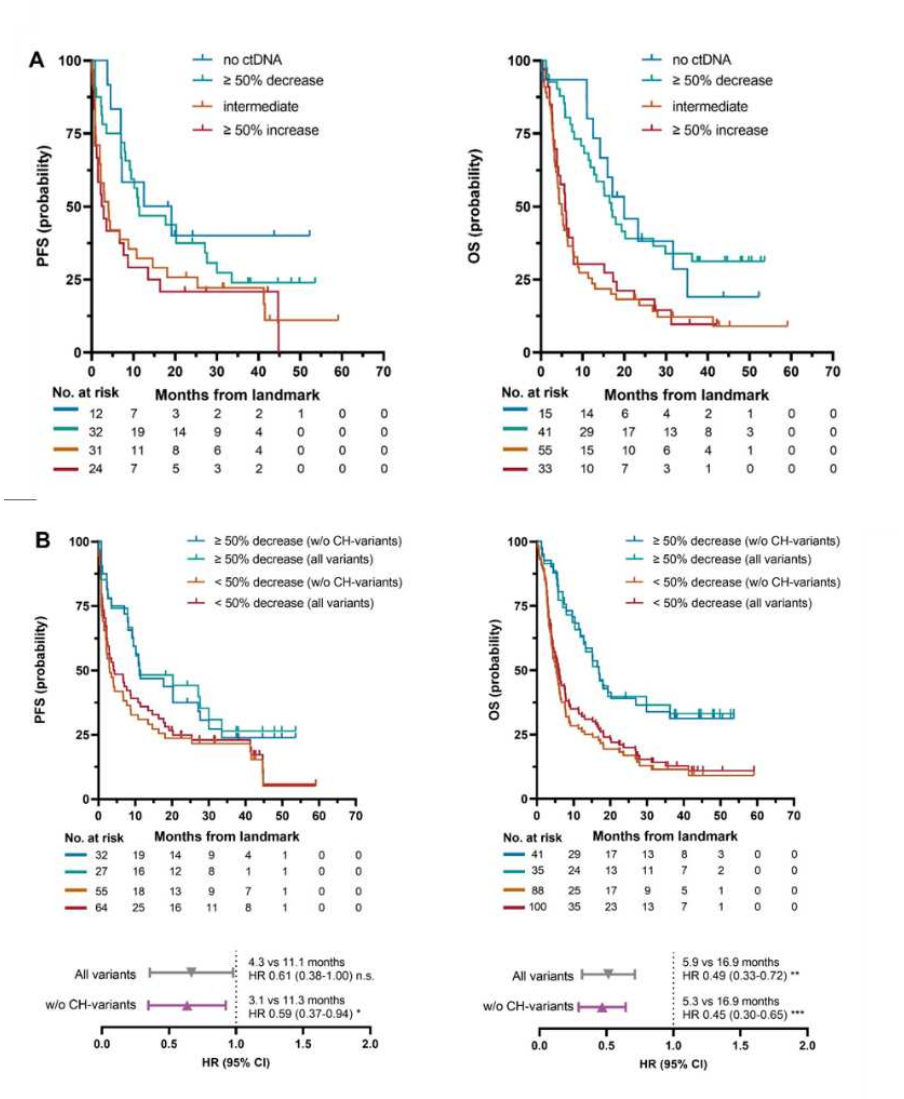

Figure 25: On treatment ctDNA dynamics are linked to survival outcomes.
(**A**) Kaplan Meier plots of progression-free survival (PFS) and overall survival (OS) for a 2-month landmark cohort (n=129), categorized by ctDNA absence from baseline (t_0) to follow-up (t_1). Groups include patients with absence of ctDNA at both time points (blue), those with a ≥50% reduction in the average number of mutant molecules (aMM, green), those with a ≥50% increase of aMM (red) and patients with intermediate changes not meeting either threshold (orange). (**B**) Kaplan–Meier curves for PFS (left) and OS (right) stratified by a ≥50% ctDNA aMM decrease from t_0 to t_1. Patients without CH-variants achieving ≥50% decrease exhibited significantly improved survival compared to those with <50% decrease. Hazard ratios (HR), 95% confidence intervals (CI), and median survival times are indicated for both uncorrected ("all variants") and CH-corrected analyses ("w/o CH-variants"). *p≤0.05; **p≤0.01; ***p≤0.0001; n.s. not significant; p values were calculated from log-rank tests. ctDNA, circulating tumor DNA. [Figure and legend reprinted and adapted from JCO Precision Oncology (Weber et al. (66))].

4.2.7. Tumor-guided versus *de novo* mutation calling

Multiple studies have demonstrated that a tumor-informed approach can enhance clinical outcomes by improving survival and more accurately distinguishing between responders and non-responders to therapy. To evaluate its effectiveness, we compared this strategy with *de novo* mutation calling from plasma ctDNA to determine which method more reliably identifies treatment response (66).

For the tumor-informed method, only mutations that were concordant between tumor tissue and plasma - after excluding variants associated with CH - were considered. Seventy-one patients fulfilled these criteria and were categorized into durable clinical response (DCR) and non-durable response (NDR) groups (66).

As depicted in Figure 26 and Figure 27 , the change of the aMM from t_0 to t_1 and the survival analysis for both the tumor-guided approach and the *de novo* mutation calling from plasma alone produced similar results. The tumor-informed approach shows that patients with less than a 50% aMM decrease had a median progression-free survival time of 1.9 months, while those with more than 50% aMM decrease had a significantly longer median survival of 11.4 months. Similar results were observed with the *de novo* mutation calling from plasma, showing a PFS time of 1.6 months for patients with less than a 50% decrease and 12.9 months for those with ≥50% decrease. When considering overall survival (OS), there were no substantial differences between the two approaches. Thus, the tumor-informed approach does not provide better stratification of responders and non-responders compared to the CH-corrected *de novo* approach (66).

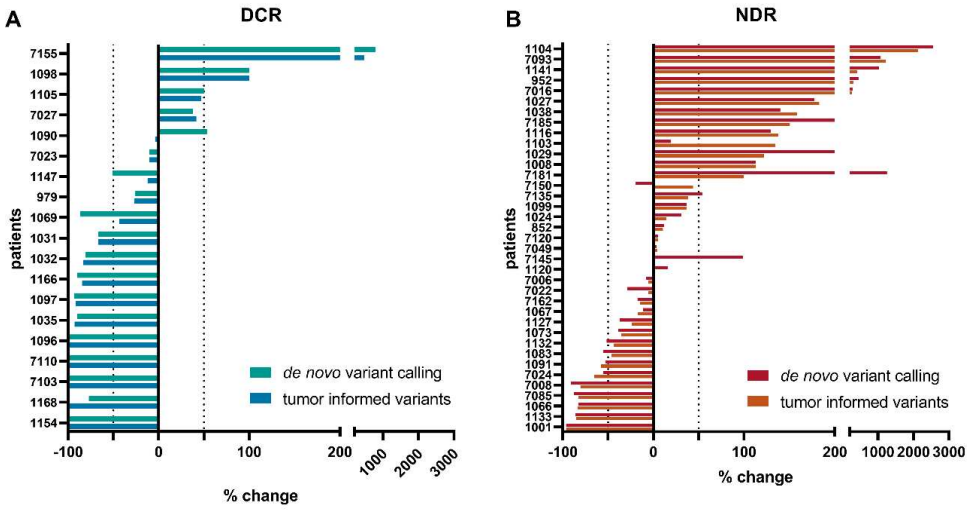

Figure 26: *De novo* mutation calling from plasma yields results comparable results to a tumor-guided strategy. Percentage change in the average mutant molecules counts is shown for 71 patients, stratified by clinical outcome: **(A)** patients with durable clinical response (DCR) and **(B)** without durable clinical response (NDR). ctDNA dynamics were evaluated using both *de novo* approach – based solely on plasma data without prior tumor mutation knowledge- and a tumor-guided method, which included only variants confirmed in both tumor tissue and plasma. [Figure and legend adapted with permission from JCO Precision Oncology (Weber et al. (66))]

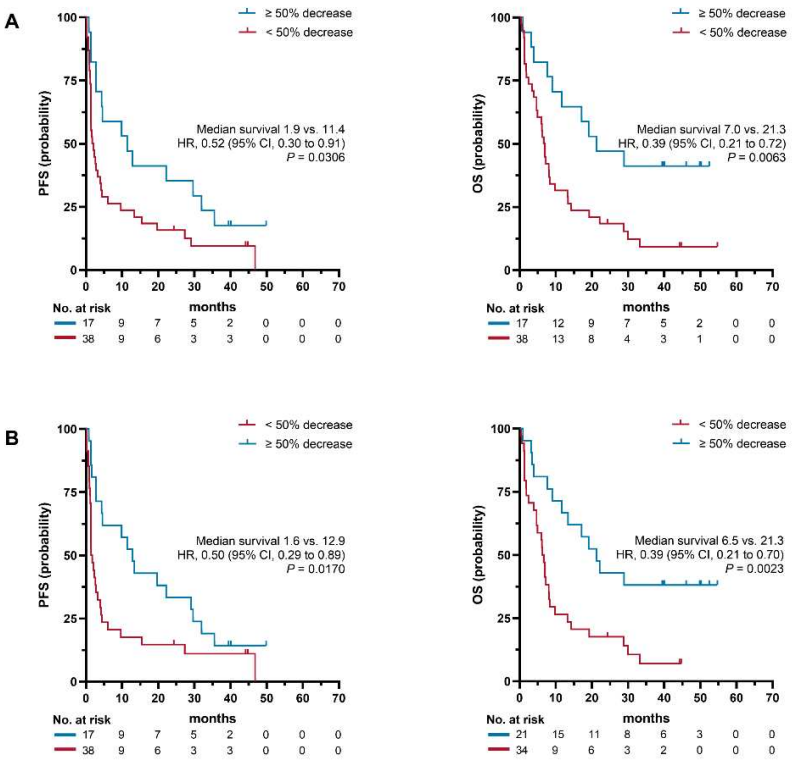

Figure 27: *De novo* variant calling offers comparable patient stratification performance to the tumor-guided approach. Kaplan-Meier curves of PFS (left) and OS (right) of patients with available tumor molecular profiling data and concordantly detected mutations in tissue and plasma (n=55 patients) stratified by a ≥ 50% decrease in average number of mutant molecules (aMM) from t_0 to t_1. (**A**) Only variants identified in the tumor were used to calculate the molecular response (tumor-informed variant call set) (**B**) All variants (but corrected for variants related to clonal hematopoiesis) were used to calculated the molecular response (*de novo* variant call set). [Figure and legend originally reprinted from Weber et al. (66)]

4.2.8. *STK11* and/or *KEAP1* mutations are associated with poor prognosis

To explore the prognostic impact of *STK11* and *KEAP1* mutations, patients were stratified based on the presence of mutations detected in plasma at either t_0 and/or t_1. Mutations in these genes were found to significantly impact patient survival, affecting both PFS and OS. Patients harboring these mutations had reduced PFS (1.5 vs. 4.1 months; HR: 0.53, 95% CI: 0.34–0.83) and OS (5.7 vs. 9.7 months; HR: 0.48, 95% CI: 0.31–0.75) compared to mutation-negative patients. Landmark analysis (60 days after t_0) confirmed the negative impact of *STK11* and *KEAP1* mutations on PFS and OS, with patients harboring these mutations experiencing worse outcomes compared to those without them (PFS: 4.4 vs. 8.7 months (HR: 0.48, 95% CI: 0.36–0.97); OS: 4.4 vs. 11.4 months (HR: 0.42, 95% CI: 0.25–0.72) (Figure 28). In contrast to previous reports, the presence of *NFE2L2* mutations did not influence the stratification of patient outcomes (data not shown) (66).

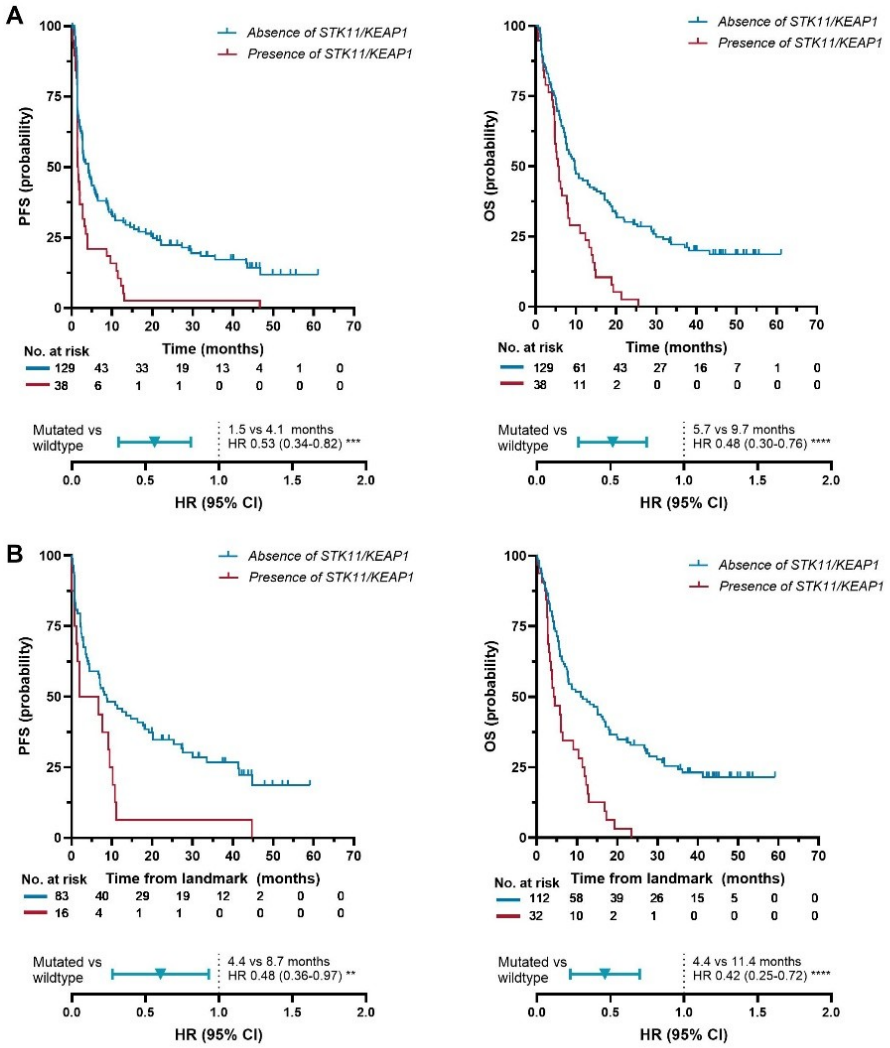

Figure 28: Impact of *STK11* and *KEAP1* mutations on survival outcomes
Kaplan-Meier plots show progression-free survival (PFS) and overall survival (OS), stratified by the presence of *STK11* and/or *KEAP1* mutations at baseline (t_0) and/or follow-up (t_1) of **(A)** the full cohort (n=167 patients) (B) same stratification as in **(A)** but using a 2-month landmark to calculate PFS and OS. HR, hazard ratio plus 95% CI; p values were calculated from log-rank tests. OS, overall survival. PFS, progression-free survival [Figure and legend reprinted and adapted from Weber et al. (66)]

4.2.9. Multivariate analysis of biomarkers

A multivariate Cox regression model was performed to evaluate the impact of clinical characteristics on survival (n=167 patients). Performance status was independently associated with survival, with higher ECOG scores predicting worse outcomes (HR 1.60, 95% CI: 1.21–2.12; $p < 0.001$). Sex was associated with a modest survival benefit (HR 0.69, 95% CI: 0.48–0.99; $p = 0.049$). In addition, the number of metastatic sites was also significantly associated with inferior outcomes (HR: 1.16, 95% CI:1.02–1.33; $p = 0.026$). In contrast, age at treatment initiation, disease stage, and histology were not significantly associated with survival in this model. The overall model was statistically significant (Chi-square = 26.62; $p < 0.001$, df=6).

Table 11: Multivariate Cox regression analysis of clinical factors associated with survival. Hazard ratios (HR), 95% confidence intervals (CI) and p-values for ECOG performance status, sex, number of metastases, age, stage and histology. Significant associations were observed for performance status, sex and number of metastatic sites ($p < 0.1$)

Clinical factor		**HR (95% CI)**	**p-values**
ECOG Performance score	0/1/2	1.60 (1.21-2.12)	< 0.001
Sex	Male/Female	0.69 (0.485-0.99)	0.049
Number of metastatic sites	0/1/2/3/>4	1.16 (1.019-1.331)	0.026
Age of treatment start	years	1.02 (0.996-1.035)	n.s.
Disease stage	IIIB/IV	0.79 (0.464-1.332)	n.s.
Histology	Adenocarcinoma/ Squamous cell carcinoma/other	1.11 (0.816-1.514)	n.s.

n.s., not significant

In addition, a multivariate Cox regression model was performed to assess the combined prognostic impact of clinical parameters, ctDNA dynamics, and molecular alterations on PFS and OS of 152 NSCLC patients.

A decrease in aMM levels of at least 50% was strongly associated with improved PFS (HR: 0.57, 95% confidence interval (CI): 0.39–0.84; $p = 0.004$), indicating that molecular response was an independent predictor of favorable outcome. However, the presence of *STK11*/*KEAP1* mutations was also independently associated with shorter PFS (HR: 1.64, 95% CI: 1.11–2.42; $p = 0.014$), highlighting the adverse prognostic impact of these genomic alterations (Table 12) (66).

For OS, molecular ctDNA response was again strongly predictive. Patients achieving a ≥ 50% decrease in aMM had a significantly longer OS (HR: 0.37; 95% CI: 0.24–0.57; p < 0.001). STK11/KEAP1 mutations remained independently associated with worse OS (HR: 1.72; 95% CI: 1.15–2.56; p = 0.008) (Table 13) (66).

Table 12: Impact of dynamic ctDNA response and *STK11/KEAP1* mutation status on progression-free survival (PFS), adjusted for clinical parameters, in 152 patients with advanced NSCLC receiving immune checkpoint inhibitors. [Table reprinted from Weber et al., JCO Precision Oncology (66)]

Clinical factor		**HR (95% CI)**	***P*-values**
Gender	Male/Female	0.80 (0.56-1.14)	n.s.
Metastases	Number	1.06 (0.93-1.21)	n.s.
Performance score	0/1/2	1.55 (1.15-2.10)	*0.004*
Change of aMM[1]	≥50% decrease	0.57 (0.39-0.84)	*0.004*
	<50% decrease		
Presence of *STK11/KEAP1* variants	yes	1.64 (1.11-2.42)	*0.014*
	no		

[1] aMM, average mutant molecules corrected for clonal hematopoiesis, n.s., not significant

Table 13: Influence of dynamic ctDNA response and *STK11/KEAP1* mutation status on overall survival (OS), adjusted for clinical parameters, in 152 patients with advanced NSCLC undergoing ICI therapy. [Table reprinted from Weber et al., JCO Precision Oncology (66)]

Clinical factor		**HR (95% CI)**	***P*-values**
Gender	Male/Female	0.79 (0.55-1.12)	n.s.
Metastases	Number	1.11 (0.98-1.27)	n.s.
Performance score	0/1/2	2.06 (1.51-2.81)	*<0.001*
Change of aMM[1]	≥50% decrease	0.37 (0.24-0.57)	*<0.001*
	<50% decrease		
Presence of *STK11/KEAP1* variants	yes	1.72 (1.15-2.56)	*0.008*
	no		

[1] aMM, average mutant molecules corrected for clonal hematopoiesis

The next Cox regression analysis on OS was performed, integrating PD-L1 expression (TPS ≥50% vs. <50%) and change in aMM. PD-L1 expression, assessed by standard immunohistochemistry on tumor tissue, was available for 110 patients. In this multivariate model, PD-L1 expression ≥50% was not independently associated with OS (HR: 0.78; 95% CI: 0.58–1.04; p = n.s) (Table 14) (66). In addition, a landmark Cox regression analysis was performed for OS including 129 patients. Of the total cohort of 167 patients, 57 were excluded due to missing PD-L1 data, and an additional 14 patients were excluded based on the 60-day landmark definition. The landmark analysis confirmed similar associations as observed in the primary multivariate OS model incorporation PD-L1 expression (Table 15) (66).

Table 14: Effect of dynamic ctDNA changes on overall survival (OS), adjusted for clinical parameters, in 110 patients* with advanced NSCLC and available PD-L1 expression data. [Reprinted from Weber et al. (66)]

Clinical factor		**HR (95% CI)**	***P-values***
Gender	Male/Female	0.78 (0.50-1.20)	n.s.
Metastases	Number	1.22 (1.04-1.43)	0.020
Performance score	0/1/2	1.75 (1.23-2.47)	0.002
Change of aMM[1]	≥50% decrease	0.37 (0.23-0.59)	<0.0001
	<50% decrease		
PD-L1 expression	≥50%	0.78 (0.58-1.04)	n.s.
	<50%		

[1] aMM, average mutant molecules corrected for clonal hematopoiesis; n.s., not significant; *57 patients had no PD-L1 data,

Table 15: Effect of dynamic ctDNA changes and PD-L1 expression on landmark overall survival (OS), adjusted for clinical variables, in 96 patients*. [Reprinted from Weber et al. (66)]

Clinical factor		**HR (95% CI)**	***P-values***
Gender	Male/Female	0.84 (0.52-1.35)	n.s.
Metastases	Number	1.14 (0.95-1.36)	n.s.
Performance score	0/1/2	1.45 (0.99-2.14)	n.s.
Change of aMM[1]	≥50% decrease	0.49 (0.29-0.80)	0.005
	<50% decrease		
PD-L1 expression	≥50% TPS	0.79 (0.58-1.08)	n.s.
	<50% TPS		

[1] aMM, average mutant molecules corrected for clonal hematopoiesis; n.s., not significant; *57 patients had no PD-L1 data and 14 patients were excluded because of the landmark of 60 days.

5. DISCUSSION

Liquid biopsy, particularly the analysis of cfDNA, has become a pivotal method for non-invasive cancer diagnostics and monitoring. Since several clinical guidelines now include ctDNA used cases, ctDNA is currently nearing the point of becoming a standard clinical practice for companion diagnostics in cancer (19, 169, 182-185). Despite these advancements, ctDNA testing still faces key challenges before it can be fully incorporated into routine patient care. One major limitation is the high cost and technical complexity of ultra-deep sequencing, which is often required to detect mutations at low VAFs - particularly relevant in early-stage disease, low shedding tumors, or in the context of MRD. Additionally, there is a critical need for standardized protocols and quality control measures to ensure reproducibility and reliability across institutions, platforms, and laboratories. Variability in pre-analytical factors (e.g., blood collection, cfDNA extraction), bioinformatic pipelines, and variant interpretation can significantly influence test results and clinical decision-making.

As the landscape of predictive biomarkers in oncology continues to expand, the role of next-generation sequencing (NGS) is becoming increasingly prominent. NGS technologies allow for the simultaneous detection of multiple genomic alterations, including single nucleotide variants, insertions/deletions, copy number alterations, and gene fusions. These are now routinely used alongside traditional diagnostic tools such as immunohistochemistry (IHC) for protein expression, fluorescence in situ hybridization (FISH) for gene rearrangements, and RNA-based fusion detection assays—particularly in formalin-fixed paraffin-embedded (FFPE) tissue samples (reviewed in (186, 187)). Today, a growing number of commercially available cfDNA-based NGS assays—such as Guardant360®, FoundationOne® Liquid CDx, AVENIO®, and QIAseq—have entered the market and are progressively being integrated into clinical oncology workflows. These assays vary in target content, depth of coverage, sensitivity thresholds, and regulatory approval status, and their selection often depends on the specific clinical context (e.g., tumor type, treatment history, available tissue). As ongoing studies continue to validate their utility across broader patient populations and treatment settings,

cfDNA-based NGS testing is expected to play an increasingly central role in personalized cancer care (reviewed in (94, 95)).

5.1. Analytical performance assessment

Analytical validation of ctDNA assays is a critical process due to the unique challenges posed by the low concentrations and complex nature of ctDNA in patient plasma. The first part of our study critically examined the impact of different types of cfDNA reference materials on the performance of liquid biopsy NGS assays at different laboratories, emphasizing the importance of using well-defined reference materials for assay validation with regard to sensitivity and specificity. We evaluated various commercial mutation analysis platforms and reference materials, focusing on their analytical performance for liquid biopsy profiling (165). This is essential for ensuring reliable detection of actionable mutations in cancer patients, facilitating better clinical decision-making. We conducted a comprehensive evaluation across three experimental setups, testing various platforms in different laboratories. These platforms included digital droplet PCR, MassARRAY, and several NGS assays. The Seraseq® reference materials used in this study encompass a range of clinically significant mutations, many of which are essential for guiding current treatment decisions. Our findings highlight variability in sensitivity and specificity across different platforms, emphasizing the need for extensive validation before clinical implementation.

We demonstrated that the use of reference materials with predefined VAFs is highly effective for evaluating the performance of both PCR-based and NGS-based mutation analysis platforms, even with only three replicates. At a VAF of 1%, ddPCR and MassARRAY showed high sensitivity and lowest variability. Coefficient of variation (CV) for intra-run comparisons using a minimum input of 8ng DNA ranged from 9-31% across all platforms, while the range for intra-run comparisons was slightly higher (CV 10-48%). NGS platforms demonstrated considerable variability, with some assays performing better in terms of sensitivity and specificity. This variability necessitates rigorous benchmarking against standardized reference materials. However, the reference materials allowed for consistent inter- and intra-assay comparisons, ensuring reliability and reproducibility of mutation detection. Overall, NGS assays offer a significantly greater amount of clinically relevant information compared to

traditional targeted ddPCR assays. However, it is important to note that NGS assays are generally more expensive than PCR assays (165).

One significant hurdle in molecular profiling is the limited amount of cfDNA available for most analyses, which critically impacts the analytical performance. Our findings confirm that the amount of template DNA has a direct impact on assay performance: higher input amounts (≥8 ng) yielded more accurate variant allele frequency (VAF) estimates, whereas lower inputs (2–4 ng) were associated with greater variability in results (165). The sensitivity of detecting mutant copies in NGS assays is heavily dependent on the total DNA input amount, as this determines the number of molecules analyzed. Our analysis also underscored the critical role of sequencing depth. For instance, identifying three mutated copies at a 0.1% limit of detection (LOD) requires at least 20 ng of input cfDNA with a sequencing depth of 3000x. While it is possible to use lower amounts of cfDNA, the LOD must be adjusted accordingly. Importantly, when using unique molecular identifiers (UMIs) for error correction, increasing the DNA input demands a proportional increase in sequencing coverage in order to maintain a consistent number of replicates per UMI, which is essential for reliable variant calling. These considerations highlight the delicate balance between DNA input, sequencing depth, and error suppression in achieving high sensitivity and specificity in cfDNA-based NGS assays.

Furthermore, we emphasized the importance of finding the best performing assay from the variety of commercially available providers. Therefore, we evaluated the performance of five commercially available mutation assays (AVENIO Targeted, QIAseq, NEB, QIAact, Oncomine) using 15ng of Seraseq® ctDNA reference material v2 at a single center (MUG), focusing on their sensitivity and workflow. The two best performing assays in this evaluation, the Oncomine and AVENIO platform, both provided good mutation detection down to 0.125% and offer comprehensive end-to-end solutions with a generic analysis workflow to support the detection of genetic alterations. The AVENIO ctDNA Targeted Assays is still able to detect 60% of the mutations at a VAF of 0.125%. The QIAact assay showed a lower performance due to lower sequencing depth, whereas QIASeq enables also satisfying detection rates (165).

A similar study by Lam et al. compared the AVENIO ctDNA Expanded (Roche) and QIAgen's QIAseq Human Comprehensive Cancer panels and showed that the AVENIO platform detected somatic mutations in over 70% of patients with common cancers, while the QIAseq platform covered nearly 90%, reporting a higher average number of variants per patient. Both panels demonstrated similar on-target rates and percentages of reads mapped. However, AVENIO exhibited more uniform sequencing coverage across regions with varying GC content, which is crucial for accurate mutation detection. Additionally, AVENIO showed higher sensitivity and concordance compared to QIAseq at the same sequencing depth. This suggests that AVENIO may be more suitable for applications requiring ultra-high depth sequencing to detect mutations in common cancer types. In contrast, QIAseq, with its broader coverage, may be better suited for applications targeting a wider spectrum of cancer types (188).

At the time of testing, no optimized analysis pipeline was available for the NEB assay, necessitating bioinformatics expertise to process raw sequencing data and generate annotated variant calls. The analysis was conducted using the MuTect2 algorithm, which is primarily intended for tumor/normal sample pairs. As a result, many mutations were not detected, despite some being clearly visible upon manual inspection of BAM files using the Integrative Genomics Viewer (IGV). These findings suggest that the recall rate of the NEB assay could be significantly improved with a tailored and fully optimized bioinformatics pipeline. (165).

Evaluating both analytical sensitivity and specificity is critical for assessing the performance of NGS-based liquid biopsy assays. In our study, variant calling accuracy showed strong specificity within the hotspot regions defined by the Seraseq® reference material. Importantly, the AVENIO and QIAseq assays did not generate any false positive (FP) reads at known variant sites in wild-type reference samples, whereas the Oncomine assay produced two FP calls at these positions. However, all assays detected additional putative false positives outside the defined hotspot regions. This finding raises the question of whether such off-target variant calls are the result of technical limitations—such as sequencing artifacts or errors in library preparation—or if they reflect true biological variability. These results highlight the

importance of further optimizing analysis pipelines and implementing robust error correction strategies to improve specificity (165).

We further demonstrated that variants with VAFs of 1% or higher could be detected with high accuracy at a LOD of 0.5%. As anticipated, the accuracy declined when identifying lower-frequency mutations or when operating at reduced LODs (165). This trend aligns with findings from Stetson et al., who reported significant variability among ctDNA assays, particularly for variants below a 1% VAF, where most discrepancies occurred (189). Deveson et al. also demonstrated high sensitivity, precision, and reproducibility for ctDNA mutations with variant allele frequencies above 0.5%. Below this threshold, detection became inconsistent and varied significantly between assays, particularly with limited input material. Missed mutations (false-negatives) were more prevalent than erroneous identifications (false-positives), highlighting the challenge of reliably sampling rare ctDNA fragments (190). These results underscore the technical challenge in accurately distinguishing low-frequency true somatic variants from

We evaluated the AVENIO assays by comparing the performance of the AVENIO ctDNA Targeted and Expanded panels using two Seraseq® reference materials. The detection rate of the AVENIO ctDNA Targeted panel with the Seraseq® ctDNA Complete™ Reference Material was similar to that with the Seraseq® ctDNA Reference Material v2. However, concordance improved slightly with the Seraseq® ctDNA Complete™ Reference Material (*pc*=0.946 vs. *pc*=0.839) (165).

Next, we compared the AVENIO ctDNA Expanded panel with the Seraseq® ctDNA Complete™ Reference Material. The Expanded assay demonstrated robust performance, offering significant depth of coverage and sensitivity, with 65% of the mutations still detectable at a VAF of 0.1%. According to vendor information, the Seraseq® ctDNA Complete™ Reference Material is produced through a gentler synthesis process which reduces the number of false positives, indicating that ongoing improvements in reference standards can enhance assay accuracy. We chose to continue with the ctDNA Expanded panel for the comprehensive mutation profiling of the NSCLC patient cohort due to its higher mutational coverage and larger panel size (192 kb) (66).

Verma et al. evaluated the performance of all AVENIO ctDNA platforms (Targeted, Expanded, and Surveillance panels) using commercial reference standards, de-identified human cfDNA samples, and contrived samples from normal and cancer cells. The kits demonstrated 100% sensitivity for detecting SNVs at >0.5% VAF and 50% sensitivity at 0.1% VAF. These results are in line with the findings of our study, confirming that AVENIO ctDNA liquid biopsy platforms are effective for clinical laboratories, particularly for detecting somatic alterations at VAFs as low as 0.5% (191).

The performance of NGS liquid biopsy tests depends critically on both analytical specificity and sensitivity. Our study highlights the importance of using well-validated reference materials and optimizing input amounts and sequencing depth to enhance accuracy. Advances in bioinformatics offer potential improvements, but careful interpretation of low-frequency variants remains crucial. Future efforts should focus on refining these assays to balance sensitivity and specificity, thereby improving clinical outcomes through precise mutation detection. However, several challenges and limitations persist. Assays analyzing smaller quantities of DNA exhibit less precision around a VAF of 1% compared to those with higher DNA input. This low DNA input can impact the analytical sensitivity and precision of tests. Laboratories must account for this variability when interpreting results and establishing detection thresholds. However, the low input of cfDNA for assays mirrors real-life clinical conditions, as patient-derived cfDNA yields are often low and large amounts of cfDNA are not typically expected.

The study also underscored the difficulty in accurately detecting low-frequency variants, despite technological advancements like unique molecular identifiers (UMIs). Discriminating between true somatic variants and technical artifacts at low allele frequencies remains a significant technical hurdle, compounded by inherent background noise in cfDNA assays (165). The synthetic nature of commercially available reference materials introduced biases, as these materials did not perfectly mimic native cfDNA, potentially affecting the accuracy of performance evaluations, as shown by Hallermayr et al. (192).

In general, the lack of standardization can lead to inconsistent results across different laboratories and assays, highlighting the need for robust and standardized analytical

workflows. These challenges illustrate the complexity of implementing liquid biopsy assays in clinical settings and the necessity for rigorous validation and standardization to ensure reliable and accurate results. Based on these findings, it is essential to establish guidelines for selecting suitable reference materials tailored to different stages of performance evaluation in liquid biopsy NGS assays. To address these challenges, the BloodPAC Consortium, in collaboration with the FDA, has developed generic protocols for the analytical validation of next-generation sequencing (NGS)-based ctDNA assays. These protocols consist of 11 guidelines designed to demonstrate and document the analytical performance of these assays, particularly for late-stage solid tumors (193). Clinical laboratories should evaluate and select panels and platforms that best meet their specific needs, considering factors such as sensitivity, specificity, coverage, and the types of mutations each assay can detect. This part of the study underscores the critical need for extensive validation of liquid biopsy tests using predefined VAFs to ensure their accuracy and reliability. Without proper validation, the clinical utility of these tests could be compromised, leading to potential misdiagnoses or inappropriate treatment plans. The variability in platform performance suggests that laboratories must carefully select and validate the appropriate assay based on their specific clinical requirements. Reliable detection of ctDNA mutations through well-validated platforms can significantly enhance personalized cancer treatment and patient outcomes. In summary, the analytical validation of ctDNA assays is a complex process that requires rigorous testing and adherence to standardized protocols to ensure the accuracy, sensitivity, and reproducibility necessary for clinical decision-making.

5.2. ctDNA as a predictor of long-term outcome in NSCLC patients treated with ICI

As lung cancer is the top cause of cancer-related deaths worldwide, responsible for around 1.8 million deaths annually (1, 2), identifying the appropriate therapy to maximize treatment outcome is of paramount importance. Plasma-based ctDNA genotyping has enhanced the delivery of targeted therapy in patients with tumors harboring *EGFR*, *BRAF*, and other targetable mutations. More recently, ctDNA has emerged as a promising biomarker for predicting response to ICI. This is of high clinical relevance as current candidate biomarkers, such as TMB and PD-L1 expression, have limited predictive value and lack specificity in distinguishing responders from non-responders (28). Given the increasing use of ICIs in NSCLC, identifying reliable biomarkers to predict patient response is crucial; however, suitable predictive biomarkers are currently lacking.

Molecular profiling of tumors typically relies on tissue biopsies, which require invasive procedures that may not always be feasible or safe - particularly for patients with advanced disease or inaccessible lesions. Moreover, tissue biopsies do not support serial sampling, limiting their use in monitoring tumor dynamics over time. To overcome these limitations, precision medicine is increasingly adopting liquid biopsy approaches. This minimally invasive method enables repeated sampling at multiple time points, making it well-suited for tracking disease progression, tumor evolution, and the development of treatment resistance (94).

Importantly, because ctDNA is shed from various regions of the tumor, it is thought to offer a more comprehensive representation of the tumor's genomic landscape, capturing both intra- and intertumoral heterogeneity (115). Numerous studies have shown that tumor genomes can be effectively reconstructed from plasma-derived DNA, indicating that ctDNA has strong potential for real-time monitoring of tumor dynamics. This capability supports its use in tracking tumor burden, clonal evolution, and emerging resistance mechanisms throughout the course of treatment. (105, 112, 130). This capability may pave the way for broader applications of biomarker-driven ICI therapies.

We assessed the potential of dynamic ctDNA levels to identify advanced NSCLC cancer patients who may benefit from immune checkpoint inhibitor therapy. Our approach incorporated several novel elements (66):

- Broad applicability of ctDNA testing: We implemented an easy-to-use ctDNA test capable of extensive NSCLC patient coverage through *de novo* mutation calling, which enhances its utility in clinical settings
- Landmark survival analysis: We conducted a landmark survival analysis, which is vital for real-time clinical decision making
- Exclusion of CH-related variants: We utilized a tumor-specific variant call set by excluding clonal hematopoiesis- related variants, improving the specificity of ctDNA.

5.2.1. High Sensitivity and Broad Coverage in ctDNA Profiling of NSCLC

Given the low levels of ctDNA in blood plasma, highly sensitive detection methods are essential for accurate molecular profiling. Techniques such as NGS, RT-PCR, and ddPCR are commonly employed in clinical diagnostics to identify clinically relevant genetic alterations ((194). In particular, RT-PCR and ddPCR are particularly useful for quantifying mutant allele frequencies in known cancer-associated genes, especially when the mutation profile is already established. In contrast, when no prior molecular information is available, a targeted NGS approach is typically utilized. This allows for the simultaneous interrogation of hotspot regions across multiple cancer-related genes, facilitating broad mutation screening and informing treatment decisions (195).

In the initial phase of this study, we aimed to identify the most effective assay for comprehensive mutation profiling in patients with advanced cancer. Based on this evaluation, we selected the AVENIO ctDNA Expanded Kit to assess molecular ctDNA response in a cohort of 167 patients with advanced NSCLC. Applying a *de novo* mutation detection approach, we were able to detect informative tumor-specific mutations in 91% of patients, with an average of 5.25 mutations per patient. This high detection rate demonstrates the clinical sensitivity of the AVENIO assay and its suitability for routine monitoring of ctDNA dynamics. The performance is comparable to other established platforms such as Guardant360 (196, 197). Real-world studies using NGS-based cfDNA assays have reported sensitivity levels between 75% and 90%, along with strong concordance with tissue-based genotyping (198-202). Consistent with known mutational patterns in NSCLC, the most commonly mutated genes in our cohort were *TP53*, *KRAS* and *KEAP1* (Figure 17B) (66).

Tissue biopsies can be challenging to obtain, especially in advanced lung cancer cases, where the tumor may be difficult to access or the patient's condition may not allow for invasive procedures. Therefore, ctDNA is a promising alternative for molecular profiling. Genetic data from tumor biopsies were available for 116 out of 167 NSCLC patients (69.5%). Among these, 61.2% had mutations in their tumor tissue, with a 75.3% concordance rate for mutations also detected in plasma (Figure 16C) (66), consistent with previous studies showing tissue-plasma concordance between 70-90% across various solid tumors (181, 203-206). Additionally, among 45 patients (38.8%) without mutations in their tumor tissue, six also had no mutations in plasma, while 39 had at least one mutation detected. This underscores AVENIO's broader coverage compared to panels focusing solely on specific hotspots. The application of *de novo* mutation calling provides a comprehensive analysis of the patient cohort, demonstrating consistency with genetic information obtained from tumor tissue examination (66).

Accurate detection of tumor-derived variants in plasma through liquid biopsy requires both high sensitivity and specificity. However, the amount of circulating tumor DNA (ctDNA) in plasma can vary greatly and is influenced by factors such as tumor burden, vascularization, and pre-analytical variables (94, 95, 207, 208). In most cancer types, ctDNA constitutes only a small fraction of the total cfDNA, typically between 0.1% and 1% (209-211). This low abundance poses a technical challenge, particularly in patients with advanced NSCLC, where nearly half of all tumor-derived mutations occur at variant allele frequencies (VAFs) below 1% (212) - a finding that was also confirmed in our study (66).

5.2.2. Predictive value of ctDNA dynamics

Since ctDNA serves as a surrogate for overall tumor burden, we evaluated whether ctDNA levels and on-treatment dynamic changes (measured before initiating ICI therapy and at first response evaluation) are associated with an immediate radiographic response. Consistent with a previous study (213), responders showed significantly higher aMM levels at t_0 compared to t_1, whereas non-responders did not show any significant difference in aMM levels between the pre- and on-treatment time points (66). Although the aMM levels at t_1 were significantly lower in responders compared to non-responders, both early and durable

responders exhibited lower pre- and on-treatment MM levels compared to non-responders. Nevertheless, molecular response was not clearly associated with radiological response. We only observed a fair agreement between molecular ctDNA response and radiographic tumor response. However, excluding CH-related variants improved this agreement without significantly affecting survival outcomes (66). This finding was also confirmed by other studies which demonstrated that NSCLC can exhibit mixed molecular responses to various therapies, including targeted therapies and immunotherapies (214). The complexity of the tumor microenvironment, tumor heterogeneity, and specific molecular markers all contribute to the potential for such heterogeneous responses in NSCLC patients treated with ICIs. Additionally, pseudoprogression, defined as an initial transient enlargement of the tumor burden or the appearance of new lesions, subsequently followed by a decrease in tumor burden, can impair molecular response assessment. This phenomenon occurs in a subset of patients treated with ICIs, with reported incidence rates ranging from 1.81% to 6% in NSCLC patients (215).

5.2.3. Prognostic impact of ctDNA dynamics

We demonstrated that patients who exhibited a ≥50% reduction in ctDNA levels after two cycles of ICI therapy showed significantly better progression-free survival (PFS) and overall survival (OS) compared to those without such a reduction (PFS: 10 vs. 2 months; OS: 18.4 vs. 5.9 months; Figure 24A). We found that patients who experienced a ≥50% reduction in ctDNA levels after two cycles of ICI therapy had significantly improved clinical outcomes compared to those without such a reduction. Specifically, these patients showed longer progression-free survival (PFS: 10 vs. 2 months) and overall survival (OS: 18.4 vs. 5.9 months) (Figure 24A). Importantly, this ≥50% decrease in ctDNA remained an independent predictor of overall survival even after adjusting for clinical variables (66).

These findings are consistent with prior studies. For instance, Goldberg et al. (2018) demonstrated in a longitudinal study of 28 advanced NSCLC patients treated with ICIs that a >50% drop in ctDNA from baseline was significantly associated with improved OS (174). Similarly, Anagnostou et al. observed that in early-stage NSCLC, tumors with a major or partial pathological response to neoadjuvant nivolumab also showed a molecular response,

characterized by the clearance of ctDNA (173). Leest and colleagues further reported that a >30% reduction in ctDNA levels within 4–6 weeks of treatment initiation strongly correlated with extended PFS and OS (216). Moreover, combining PD-L1 expression with early ctDNA dynamics provided a more robust predictor of treatment response than using either biomarker alone, highlighting the potential of integrated molecular and immunological profiling for optimizing patient stratification.

Since ctDNA dynamics can only be evaluated after the second sampling timepoint (t_1), we conducted a landmark analysis at 60 days following the initiation of ICI therapy. This time point is clinically relevant, as it allows physicians to begin discussing treatment efficacy with patients based on early molecular response data. The 2-month landmark analysis revealed a significant association between a ≥50% reduction in ctDNA levels and improved clinical outcomes. Patients with a molecular response demonstrated a HR for PFS of 0.59 (95% CI: 0.37–0.94; P = 0.0319) and an HR for OS of 0.45 (95% CI: 0.30–0.65; P = 0.001), indicating substantial risk reduction compared to non-responders (66).

In addition to higher levels of ctDNA at both time points (t_0 and t_1), the presence of *STK11* and *KEAP1* mutations has been independently predictive of poorer survival outcomes, regardless of PD-L1 expression levels (66). These mutations are not specifically associated with a response to immune checkpoint inhibitors but rather confer a poor prognosis irrespective of the treatment modality (217). Studies have demonstrated that mutations in *STK11*, *KEAP1*, and *NFE2L2* are particularly detrimental. For instance, early detection of pathogenic *PTEN* and *STK11* mutations in baseline liquid biopsy samples significantly impacted disease progression in lung cancer patients treated with ICIs (218, 219). Additionally, Zhu et al. (2021) showed that patients with *KEAP1*/*NFE2L2* mutations had lower OS under atezolizumab treatment compared to those with wild-type genes (220). The lack of prognostic effect of *NFE2L2* mutations in our study may be explained by the distinct histological distribution of these mutations. *KEAP1* mutations were predominantly observed in adenocarcinoma cases, which constitute 67.1% of our cohort, while *NFE2L2* mutations were more frequently found in squamous cell carcinoma (LSCC). This histological disparity suggests that the biological and clinical behavior associated with *NFE2L2* mutations in LSCC may differ significantly from that

of *KEAP1* mutations in adenocarcinoma, potentially leading to the observed lack of impact on overall patient stratification (221).

5.2.4. Impact of CH-related variants

Accurate interpretation of ctDNA data can be complicated not only by technical variability but also by biological confounders, including germline variants and mutations originating from PBMCs. One of the key challenges in tumor-only cfDNA sequencing workflows, which do not incorporate matched germline DNA, is differentiating somatic tumor mutations from germline alterations.

While germline variants typically appear at VAFs of ~50% (heterozygous) or ~100% (homozygous), their VAFs can be distorted by factors such as germline mosaicism or copy number alterations, making them harder to distinguish from somatic mutations (28, 222, 223). Conversely, tumor-specific mutations may occur in genomic regions affected by structural alterations such as gene amplifications or loss of heterozygosity (LOH), which can cause VAFs that resemble those of germline variants, further increasing the risk of misclassification (28).

To address these limitations, incorporating matched constitutional DNA (e.g., from PBMCs) into ctDNA analysis is strongly recommended, as it enables more reliable identification of true somatic variants and reduces the likelihood of misinterpreting germline or hematopoietic mutations as tumor-derived alterations.

These mutations derived from CH are an age-related phenomenon where hematopoietic stem cells or early blood cell progenitors create a genetically distinct blood cell fraction (99, 100, 119). This condition is often linked to previous chemotherapy or irradiation in cancer patients and is also associated with smoking and aging (122, 125, 212, 224, 225).

In our study, we included mutations calling of PBMCs to get rid of germline and CH-related variants to ensure high confidence tumor-specific mutation profile. In our cohort, CH-related variants were identified in 43% of NSCLC patients, whereas the number and presence of those were associated with higher age (66), which confirms previous reports (119, 120, 124). In contrast, in our study, CH-related variants showed no association with previous chemotherapy exposure or patient survival (66). However, recent studies have revealed that individuals with CH who have undergone chemotherapy or radiotherapy for a primary cancer are at a

heightened risk of developing secondary therapy-related myeloid malignancies (225, 226). Notably, six of the ctDNA-negative patients in our cohort had only CH-related variants, which would have resulted in an incorrect classification as ctDNA-positive if these variants had not been excluded (66). Adding to the complexity, a large number of CH-mutations are found at variant allele frequencies below 1%, similar to those derived from tumors (227).

Mutations in the genes *DNMT3A*, *TET2* and *ASXL1* (collectively referred to as the "DTA" genes) have been identified as the most prevalent driver variants in CH (119-121). However, the AVENIO Expanded Panel used in our study did not include these canonical CH-related genes, which likely resulted in an underestimation of the prevalence of CH mutation (228, 229). However, also *TP53* mutations are frequently associated with CH and consistent with previous reports, *TP53* was the most common mutated gene in our cohort in context CH. In our cohort, 30 out of 144 detected *TP53* mutations (20.8%) in 21 patients were associated with CH (66). Chabon and colleagues showed similar findings, identifying numerous *TP53* variants in cfDNA that were also detectable in PBMCs in both NSCLC patients (40.6%) and controls (100%) (179). Moreover, a wide range of additional genes - not typically associated with CH - were also found to harbor mutations (66, 120, 179, 229). The variant spectrum in cfDNA arising from CH can overlap significantly with mutations found in ctDNA, posing a risk for false-positive genotyping results in plasma-based assays. Such confounding effects have already been documented in several studies (125-127), highlighting the importance of accounting for CH-related variants during cfDNA analysis.

Understanding the genetic discrepancies between tumor and CH-related mutations is crucial for determining appropriate treatment strategies, e.g. somatic *KRAS* mutations strongly predict resistance to cetuximab, with tumors harboring *KRAS* mutations showing poor response to cetuximab therapy (230). However, *KRAS* mutations can also appear as CH-related variants, albeit in a limited number (127), posing a significant diagnostic challenge with the advent of new drugs targeting *KRAS* mutations as recently sotorasib was approved for treating NSCLC patients with *KRAS* p.G12C mutations (231).

Since CH-related variants are not associated with changes in tumor burden in patients with solid tumors, their presence in cfDNA can distort the interpretation of ctDNA dynamics.

Including these variants in the analysis may obscure the actual molecular response, potentially leading to misclassification of a patient's ctDNA response status and, consequently, inaccurate assessment of treatment efficacy. Therefore, CH-related variants can interfere with the assessment of molecular response and complicate the interpretation of ctDNA analyses. The presence CH-related variants, which remain constant or evolve independently of the tumor, can confound longitudinal measurements of ctDNA levels. This issue was observed in over 10% of our cohort. Furthermore, although not statistically significant, excluding CH-related variants enhanced the ability to distinguish survival outcomes based on molecular ctDNA response (66). Sivapalan and colleagues showed – similar to our study – that if the CH variants have not been removed, very few patients were classified as molecular responders given that CH mutations are not cleared during therapy (232).

A large-scale pan-cancer study involving more than 10,000 patients employed parallel sequencing of plasma and PBMCs, revealing that 14% of cfDNA samples contained clonal hematopoiesis-associated variants. These findings underscore the prevalence of CH-related mutations in cfDNA and the potential for misinterpretation in liquid biopsy analyses. Ongoing research is focused on developing robust analytical strategies to reliably distinguish CH-derived variants from tumor-specific alterations, aiming to improve the accuracy of ctDNA-based diagnostics and monitoring. (128). Thus, paired genotyping of a patient's PBMCs is recommended to exclude CHIP variants and prevent misdiagnosis (129).

An additional strategy for differentiating tumor-derived variants from those associated with clonal hematopoiesis (CH) is fragment size analysis. In line with previous studies, our data showed that DNA fragments carrying tumor-specific mutations tend to be slightly shorter than those harboring CH-related variants. This distinction in fragment length may serve as a complementary criterion to improve the accuracy of ctDNA interpretation and reduce false-positive classifications (Kolmogorov-Smirnov test, P, 1 × 10−10; Figure 15C) (66, 179, 233). Incorporating additional information, such as patient age and larger datasets may further enhance prediction accuracy.

Maanson and colleagues recently published work confirming that in mutation-positive cancer patients, the cfDNA fragments in mutation-positive cancer patients are shorter compared to those in mutation-negative patients. Beyond analyzing fragment lengths, they also

investigated fragment end motifs (FEMs). Their findings showed that combining cfDNA fragment length analysis with FEMs significantly enhances the detection of tumor-derived DNA. This combined approach offers a promising method for noninvasive cancer diagnostics (233).

5.2.5. Strengths and limitations

One of the primary strengths of this study is its use of a commercial ctDNA assay, which provides a broadly applicable and user-friendly approach for detecting ctDNA mutations. This method achieved high sensitivity and broad patient coverage, identifying mutations in over 90% of patients. Furthermore, we included a landmark survival analysis at a critical clinical decision point (two months post-treatment initiation), providing valuable prognostic information for clinicians. The exclusion of CH-related variants from the analysis also enhances the specificity of the ctDNA measurements, reducing biological noise and improving the accuracy of molecular response assessments (66).

A significant drawback is that ctDNA assessments were only conducted at a single on-treatment time point. Longitudinal measurements of ctDNA may better predict response to ICI compared to using just two time points. A study analyzing ctDNA across 5 time points in 466 NSCLC patients from the IMpower150 trial showed that ctDNA assessments through cycle 3 day 1 of treatment enabled effective risk stratification (234). Another limitation is the variability in the timing of on-treatment blood samples between patients. This inconsistency can affect the interpretation of the data and the accuracy of correlating ctDNA changes with clinical outcomes. On the other hand, this variability in blood collection time point and the heterogeneous treatment regimen reflects a real-world scenario, enhancing the generalizability of the results.

Overall, our data demonstrate the potential of ctDNA as a non-invasive biomarker for monitoring treatment response and prognosis in NSCLC patients undergoing ICI therapy. Further research is needed to better understand how to effectively use liquid biopsies in NSCLC patients treated with ICI. Implementing novel multiparameter strategies that combine information from multiple sources will be crucial in establishing the clinical utility of liquid biopsies.

6. CONCLUSION

This study underscores the potential of ctDNA as a non-invasive biomarker for monitoring treatment response and prognosis in patients with stage IIIB–IV NSCLC receiving immune checkpoint inhibitor (ICI) therapy.

Our findings demonstrate that ctDNA dynamics offer meaningful prognostic insight, with on-treatment changes in ctDNA levels correlating with both radiographic response and clinical outcomes. Specifically, patients who experienced a ≥50% reduction in ctDNA after two treatment cycles had significantly improved PFS and OS compared to those who did not exhibit such a decline.

Furthermore, a 2-month landmark analysis confirmed that a ≥50% molecular ctDNA response effectively stratified patients by outcome, reinforcing the clinical utility of early ctDNA monitoring in guiding treatment decisions.

This study highlights the potential of ctDNA as a non-invasive biomarker for monitoring treatment response and prognosis in stage IIIB-IV NSCLC patients undergoing ICI therapy.

The results demonstrate that ctDNA dynamics can provide valuable prognostic information, with on-treatment ctDNA changes associated with radiographic response and survival outcomes. Patients who exhibited a ≥50% decrease in ctDNA levels after two cycles of ICI therapy showed significantly better PFS and OS compared to those without such a decrease. The 2-month landmark analysis revealed also a significant stratification for a ≥ 50% molecular ctDNA response (66).

Furthermore, we incorporated mutation calling of PBMCs to eliminate germline and CH-related variants, ensuring a tumor-specific variant call set. Excluding these variants notably improved the accuracy of molecular response classification and underscored the necessity of paired genotyping of PBMCs to prevent misdiagnosis. Given that the spectrum of CH mutations often overlaps with ctDNA, parallel sequencing of PBMCs, despite the additional costs, or the use of advanced methods such as fragment size analysis and fragment end motifs, is essential to differentiate between CH and tumor-specific variants (66).

The AVENIO ctDNA Expanded Kit was particularly effective in comprehensive mutation profiling, underscoring the importance of using validated reference materials to ensure assay sensitivity and specificity. While the study faced limitations such as variability in sample collection timing and a relatively short follow-up period, the findings support the clinical utility of ctDNA in guiding personalized treatment strategies and stratifying patients for clinical trials. Future research should focus on integrating additional parameters for early tumor response prediction and implementing multiparameter strategies to enhance the clinical efficacy of liquid biopsies. Overall, this study contributes valuable insights into the optimization of NSCLC patient management, potentially leading to improved treatment outcomes (66, 165).

REFERENCES

1. Society AC. Cancer Facts & Figures 2023. Atlanta: American Cancer Society. 2023.
2. Bray F, Ferlay J, Soerjomataram I, Siegel RL, Torre LA, Jemal A. Global cancer statistics 2018: GLOBOCAN estimates of incidence and mortality worldwide for 36 cancers in 185 countries. CA Cancer J Clin. 2018;68(6):394-424.
3. Siegel RL, Miller KD, Fuchs HE, Jemal A. Cancer statistics, 2022. CA Cancer J Clin. 2022;72(1):7-33.
4. Islami F, Goding Sauer A, Miller KD, Siegel RL, Fedewa SA, Jacobs EJ, et al. Proportion and number of cancer cases and deaths attributable to potentially modifiable risk factors in the United States. CA Cancer J Clin. 2018;68(1):31-54.
5. Redfield RR, Hahn SM, Sharpless NE. Redoubling Efforts to Help Americans Quit Smoking - Federal Initiatives to Tackle the Country's Longest-Running Epidemic. N Engl J Med. 2020;383(17):1606-9.
6. United States Public Health Service Office of the Surgeon G, National Center for Chronic Disease P, Health Promotion Office on S, Health. Publications and Reports of the Surgeon General. Smoking Cessation: A Report of the Surgeon General. Washington (DC): US Department of Health and Human Services; 2020.
7. Siegel DA, Fedewa SA, Henley SJ, Pollack LA, Jemal A. Proportion of Never Smokers Among Men and Women With Lung Cancer in 7 US States. JAMA Oncol. 2021;7(2):302-4.
8. Kim AS, Ko HJ, Kwon JH, Lee JM. Exposure to Secondhand Smoke and Risk of Cancer in Never Smokers: A Meta-Analysis of Epidemiologic Studies. Int J Environ Res Public Health. 2018;15(9).
9. Kaufman EL, Jacobson JS, Hershman DL, Desai M, Neugut AI. Effect of breast cancer radiotherapy and cigarette smoking on risk of second primary lung cancer. J Clin Oncol. 2008;26(3):392-8.
10. Krewski D, Lubin JH, Zielinski JM, Alavanja M, Catalan VS, Field RW, et al. A combined analysis of North American case-control studies of residential radon and lung cancer. J Toxicol Environ Health A. 2006;69(7):533-97.
11. Lorenzo Bermejo J, Hemminki K. Familial lung cancer and aggregation of smoking habits: a simulation of the effect of shared environmental factors on the familial risk of cancer. Cancer Epidemiol Biomarkers Prev. 2005;14(7):1738-40.
12. Bailey-Wilson JE, Amos CI, Pinney SM, Petersen GM, de Andrade M, Wiest JS, et al. A major lung cancer susceptibility locus maps to chromosome 6q23-25. Am J Hum Genet. 2004;75(3):460-74.
13. Malhotra J, Malvezzi M, Negri E, La Vecchia C, Boffetta P. Risk factors for lung cancer worldwide. Eur Respir J. 2016;48(3):889-902.
14. Lewandowska A, Lewandowski T, Zych B, Papp K, Zrubcová D, Ejder Apay S, et al. Risk Factors for the Diagnosis of Lung Cancer in Poland: A Large-Scale, Population-Based Case-Control Study. Asian Pac J Cancer Prev. 2022;23(10):3299-307.
15. Meza R, Meernik C, Jeon J, Cote ML. Lung cancer incidence trends by gender, race and histology in the United States, 1973-2010. PLoS One. 2015;10(3):e0121323.
16. Chen VW, Ruiz BA, Hsieh MC, Wu XC, Ries LA, Lewis DR. Analysis of stage and clinical/prognostic factors for lung cancer from SEER registries: AJCC staging and collaborative stage data collection system. Cancer. 2014;120 Suppl 23(0 0):3781-92.
17. Howlader N NA, Krapcho M, Miller D, Brest A, Yu M, Ruhl J, Tatalovich Z, Mariotto A, Lewis DR, Chen HS, Feuer EJ, Cronin KA (eds). SEER Cancer Statistics Review, 1975-2017 Bethesda, MD: National Cancer Institute; 2020 [Available from: https://seer.cancer.gov/csr/1975_2017
18. Latimer KM, Mott TF. Lung cancer: diagnosis, treatment principles, and screening. Am Fam Physician. 2015;91(4):250-6.

19. Planchard D, Popat S, Kerr K, Novello S, Smit EF, Faivre-Finn C, et al. Metastatic non-small cell lung cancer: ESMO Clinical Practice Guidelines for diagnosis, treatment and follow-up. Ann Oncol. 2018;29(Suppl 4):iv192-iv237.
20. Travis WD, Brambilla E, Nicholson AG, Yatabe Y, Austin JHM, Beasley MB, et al. The 2015 World Health Organization Classification of Lung Tumors: Impact of Genetic, Clinical and Radiologic Advances Since the 2004 Classification. J Thorac Oncol. 2015;10(9):1243-60.
21. SEER Cancer Stat Facts: Lung and Bronchus Cancer. National Cancer Institute. Bethesda M, https://seer.cancer.gov/statfacts/html/lungb.html.
22. Lais Osmani M, Frederic Askin, MD, Edward Gabrielson, MD, Qing Kay Li, MD. Current WHO Guidelines and the Critical Role of Immunohistochemical Markers in the Subclassification of Non-Small Cell Lung Carcinoma (NSCLC). Moving from Targeted Therapy to Immunotherapy. Semin Cancer Biol. 2018;52(1):103-9.
23. Travis WD, Brambilla E, Riely GJ. New pathologic classification of lung cancer: relevance for clinical practice and clinical trials. J Clin Oncol. 2013;31(8):992-1001.
24. Wakelee HA, Chang ET, Gomez SL, Keegan TH, Feskanich D, Clarke CA, et al. Lung cancer incidence in never smokers. J Clin Oncol. 2007;25(5):472-8.
25. Luiz H. Araujo LH, Robert E. Merritt, Konstantin Shilo, Meng Xu-Welliver, David P. Carbone. Cancer of the lung: non-small cell lung cancer and small cell lung cancer. . Abeloff´s Clinical Oncology e16: ELSEVIER; 2020. p. 1108-58.
26. Jamal-Hanjani M, Wilson GA, McGranahan N, Birkbak NJ, Watkins TBK, Veeriah S, et al. Tracking the Evolution of Non-Small-Cell Lung Cancer. N Engl J Med. 2017;376(22):2109-21.
27. Rekhtman N, Travis WD. Large No More: The Journey of Pulmonary Large Cell Carcinoma from Common to Rare Entity. J Thorac Oncol. 2019;14(7):1125-7.
28. Yang SR, Schultheis AM, Yu H, Mandelker D, Ladanyi M, Büttner R. Precision medicine in non-small cell lung cancer: Current applications and future directions. Semin Cancer Biol. 2022;84:184-98.
29. Rodak O, Peris-Díaz MD, Olbromski M, Podhorska-Okołów M, Dzięgiel P. Current Landscape of Non-Small Cell Lung Cancer: Epidemiology, Histological Classification, Targeted Therapies, and Immunotherapy. Cancers (Basel). 2021;13(18).
30. PDQ® Adult Treatment Editorial Board. PDQ Non-Small Cell Lung Cancer Treatment. Bethesda MNCIUMDYAahwc.
31. Seymour L, Bogaerts J, Perrone A, Ford R, Schwartz LH, Mandrekar S, et al. iRECIST: guidelines for response criteria for use in trials testing immunotherapeutics. Lancet Oncol. 2017;18(3):e143-e52.
32. Smolle E, Leithner K, Olschewski H. Oncogene addiction and tumor mutational burden in non-small-cell lung cancer: Clinical significance and limitations. Thorac Cancer. 2020;11(2):205-15.
33. Dogan S, Shen R, Ang DC, Johnson ML, D'Angelo SP, Paik PK, et al. Molecular epidemiology of EGFR and KRAS mutations in 3,026 lung adenocarcinomas: higher susceptibility of women to smoking-related KRAS-mutant cancers. Clin Cancer Res. 2012;18(22):6169-77.
34. Lynch TJ, Bell DW, Sordella R, Gurubhagavatula S, Okimoto RA, Brannigan BW, et al. Activating mutations in the epidermal growth factor receptor underlying responsiveness of non-small-cell lung cancer to gefitinib. N Engl J Med. 2004;350(21):2129-39.
35. Paez JG, Jänne PA, Lee JC, Tracy S, Greulich H, Gabriel S, et al. EGFR mutations in lung cancer: correlation with clinical response to gefitinib therapy. Science. 2004;304(5676):1497-500.
36. Pao W, Miller V, Zakowski M, Doherty J, Politi K, Sarkaria I, et al. EGF receptor gene mutations are common in lung cancers from "never smokers" and are associated with sensitivity of tumors to gefitinib and erlotinib. Proc Natl Acad Sci U S A. 2004;101(36):13306-11.
37. Brugger W, Thomas M. EGFR-TKI resistant non-small cell lung cancer (NSCLC): new developments and implications for future treatment. Lung Cancer. 2012;77(1):2-8.
38. Bell DW, Gore I, Okimoto RA, Godin-Heymann N, Sordella R, Mulloy R, et al. Inherited susceptibility to lung cancer may be associated with the T790M drug resistance mutation in EGFR. Nat Genet. 2005;37(12):1315-6.

39. Gomatou G, Syrigos N, Kotteas E. Osimertinib Resistance: Molecular Mechanisms and Emerging Treatment Options. Cancers (Basel). 2023;15(3).
40. Camidge DR, Doebele RC, Kerr KM. Comparing and contrasting predictive biomarkers for immunotherapy and targeted therapy of NSCLC. Nat Rev Clin Oncol. 2019;16(6):341-55.
41. Gandhi L, Rodríguez-Abreu D, Gadgeel S, Esteban E, Felip E, De Angelis F, et al. Pembrolizumab plus Chemotherapy in Metastatic Non-Small-Cell Lung Cancer. N Engl J Med. 2018;378(22):2078-92.
42. Langer CJ. Emerging immunotherapies in the treatment of non-small cell lung cancer (NSCLC): the role of immune checkpoint inhibitors. Am J Clin Oncol. 2015;38(4):422-30.
43. Forde PM, Chaft JE, Smith KN, Anagnostou V, Cottrell TR, Hellmann MD, et al. Neoadjuvant PD-1 Blockade in Resectable Lung Cancer. N Engl J Med. 2018;378(21):1976-86.
44. Chapman PB, D'Angelo SP, Wolchok JD. Rapid eradication of a bulky melanoma mass with one dose of immunotherapy. N Engl J Med. 2015;372(21):2073-4.
45. Pardoll DM. The blockade of immune checkpoints in cancer immunotherapy. Nat Rev Cancer. 2012;12(4):252-64.
46. Nirschl CJ, Drake CG. Molecular pathways: coexpression of immune checkpoint molecules: signaling pathways and implications for cancer immunotherapy. Clin Cancer Res. 2013;19(18):4917-24.
47. Zhang H, Dai Z, Wu W, Wang Z, Zhang N, Zhang L, et al. Regulatory mechanisms of immune checkpoints PD-L1 and CTLA-4 in cancer. J Exp Clin Cancer Res. 2021;40(1):184.
48. Graziani G, Tentori L, Navarra P. Ipilimumab: a novel immunostimulatory monoclonal antibody for the treatment of cancer. Pharmacol Res. 2012;65(1):9-22.
49. Malhotra J, Jabbour SK, Aisner J. Current state of immunotherapy for non-small cell lung cancer. Transl Lung Cancer Res. 2017;6(2):196-211.
50. Reck M, Rodríguez-Abreu D, Robinson AG, Hui R, Csőszi T, Fülöp A, et al. Pembrolizumab versus Chemotherapy for PD-L1-Positive Non-Small-Cell Lung Cancer. N Engl J Med. 2016;375(19):1823-33.
51. Sezer A, Kilickap S, Gümüş M, Bondarenko I, Özgüroğlu M, Gogishvili M, et al. Cemiplimab monotherapy for first-line treatment of advanced non-small-cell lung cancer with PD-L1 of at least 50%: a multicentre, open-label, global, phase 3, randomised, controlled trial. Lancet. 2021;397(10274):592-604.
52. Garon EB, Hellmann MD, Rizvi NA, Carcereny E, Leighl NB, Ahn MJ, et al. Five-Year Overall Survival for Patients With Advanced Non–Small-Cell Lung Cancer Treated With Pembrolizumab: Results From the Phase I KEYNOTE-001 Study. J Clin Oncol. 2019;37(28):2518-27.
53. Raimondi A, Sepe P, Zattarin E, Mennitto A, Stellato M, Claps M, et al. Predictive Biomarkers of Response to Immunotherapy in Metastatic Renal Cell Cancer. Front Oncol. 2020;10:1644.
54. Giustini N, Bazhenova L. Recognizing Prognostic and Predictive Biomarkers in the Treatment of Non-Small Cell Lung Cancer (NSCLC) with Immune Checkpoint Inhibitors (ICIs). Lung Cancer (Auckl). 2021;12:21-34.
55. Miyake M, Hori S, Owari T, Oda Y, Tatsumi Y, Nakai Y, et al. Clinical Impact of Tumor-Infiltrating Lymphocytes and PD-L1-Positive Cells as Prognostic and Predictive Biomarkers in Urological Malignancies and Retroperitoneal Sarcoma. Cancers (Basel). 2020;12(11).
56. Naimi A, Mohammed RN, Raji A, Chupradit S, Yumashev AV, Suksatan W, et al. Tumor immunotherapies by immune checkpoint inhibitors (ICIs); the pros and cons. Cell Commun Signal. 2022;20(1):44.
57. Cha JH, Chan LC, Li CW, Hsu JL, Hung MC. Mechanisms Controlling PD-L1 Expression in Cancer. Mol Cell. 2019;76(3):359-70.
58. Sun C, Mezzadra R, Schumacher TN. Regulation and Function of the PD-L1 Checkpoint. Immunity. 2018;48(3):434-52.
59. Li X, Shao C, Shi Y, Han W. Lessons learned from the blockade of immune checkpoints in cancer immunotherapy. J Hematol Oncol. 2018;11(1):31.

60. Bardhan K, Anagnostou T, Boussiotis VA. The PD1:PD-L1/2 Pathway from Discovery to Clinical Implementation. Front Immunol. 2016;7:550.
61. Yi M, Yu S, Qin S, Liu Q, Xu H, Zhao W, et al. Gut microbiome modulates efficacy of immune checkpoint inhibitors. J Hematol Oncol. 2018;11(1):47.
62. Paz-Ares L, Luft A, Vicente D, Tafreshi A, Gümüş M, Mazières J, et al. Pembrolizumab plus Chemotherapy for Squamous Non-Small-Cell Lung Cancer. N Engl J Med. 2018;379(21):2040-51.
63. Reck M, Rodríguez-Abreu D, Robinson AG, Hui R, Csőszi T, Fülöp A, et al. Updated Analysis of KEYNOTE-024: Pembrolizumab Versus Platinum-Based Chemotherapy for Advanced Non-Small-Cell Lung Cancer With PD-L1 Tumor Proportion Score of 50% or Greater. J Clin Oncol. 2019;37(7):537-46.
64. Rizvi NA, Hellmann MD, Snyder A, Kvistborg P, Makarov V, Havel JJ, et al. Cancer immunology. Mutational landscape determines sensitivity to PD-1 blockade in non-small cell lung cancer. Science. 2015;348(6230):124-8.
65. Antonia SJ, Borghaei H, Ramalingam SS, Horn L, De Castro Carpeño J, Pluzanski A, et al. Four-year survival with nivolumab in patients with previously treated advanced non-small-cell lung cancer: a pooled analysis. Lancet Oncol. 2019;20(10):1395-408.
66. Weber S, van der Leest P, Donker HC, Schlange T, Timens W, Tamminga M, et al. Dynamic Changes of Circulating Tumor DNA Predict Clinical Outcome in Patients With Advanced Non-Small-Cell Lung Cancer Treated With Immune Checkpoint Inhibitors. JCO Precis Oncol. 2021;5:1540-53.
67. Gubin MM, Artyomov MN, Mardis ER, Schreiber RD. Tumor neoantigens: building a framework for personalized cancer immunotherapy. J Clin Invest. 2015;125(9):3413-21.
68. Schumacher TN, Schreiber RD. Neoantigens in cancer immunotherapy. Science. 2015;348(6230):69-74.
69. van Buuren MM, Calis JJ, Schumacher TN. High sensitivity of cancer exome-based CD8 T cell neo-antigen identification. Oncoimmunology. 2014;3:e28836.
70. Rizvi H, Sanchez-Vega F, La K, Chatila W, Jonsson P, Halpenny D, et al. Molecular Determinants of Response to Anti-Programmed Cell Death (PD)-1 and Anti-Programmed Death-Ligand 1 (PD-L1) Blockade in Patients With Non-Small-Cell Lung Cancer Profiled With Targeted Next-Generation Sequencing. J Clin Oncol. 2018;36(7):633-41.
71. Snyder A, Makarov V, Merghoub T, Yuan J, Zaretsky JM, Desrichard A, et al. Genetic basis for clinical response to CTLA-4 blockade in melanoma. N Engl J Med. 2014;371(23):2189-99.
72. Marcus L, Fashoyin-Aje LA, Donoghue M, Yuan M, Rodriguez L, Gallagher PS, et al. FDA Approval Summary: Pembrolizumab for the Treatment of Tumor Mutational Burden-High Solid Tumors. Clin Cancer Res. 2021;27(17):4685-9.
73. Marabelle A, Fakih M, Lopez J, Shah M, Shapira-Frommer R, Nakagawa K, et al. Association of tumour mutational burden with outcomes in patients with advanced solid tumours treated with pembrolizumab: prospective biomarker analysis of the multicohort, open-label, phase 2 KEYNOTE-158 study. Lancet Oncol. 2020;21(10):1353-65.
74. Cristescu R, Mogg R, Ayers M, Albright A, Murphy E, Yearley J, et al. Pan-tumor genomic biomarkers for PD-1 checkpoint blockade-based immunotherapy. Science. 2018;362(6411).
75. Patel SP, Kurzrock R. PD-L1 Expression as a Predictive Biomarker in Cancer Immunotherapy. Mol Cancer Ther. 2015;14(4):847-56.
76. Yarchoan M, Albacker LA, Hopkins AC, Montesion M, Murugesan K, Vithayathil TT, et al. PD-L1 expression and tumor mutational burden are independent biomarkers in most cancers. JCI Insight. 2019;4(6).
77. Fan H, Chu JY. A brief review of short tandem repeat mutation. Genomics Proteomics Bioinformatics. 2007;5(1):7-14.
78. Le DT, Durham JN, Smith KN, Wang H, Bartlett BR, Aulakh LK, et al. Mismatch repair deficiency predicts response of solid tumors to PD-1 blockade. Science. 2017;357(6349):409-13.
79. Le DT, Uram JN, Wang H, Bartlett BR, Kemberling H, Eyring AD, et al. PD-1 Blockade in Tumors with Mismatch-Repair Deficiency. N Engl J Med. 2015;372(26):2509-20.

80. Hause RJ, Pritchard CC, Shendure J, Salipante SJ. Classification and characterization of microsatellite instability across 18 cancer types. Nat Med. 2016;22(11):1342-50.
81. Hause RJ, Pritchard CC, Shendure J, Salipante SJ. Corrigendum: Classification and characterization of microsatellite instability across 18 cancer types. Nat Med. 2018;24(4):525.
82. Warth A, Körner S, Penzel R, Muley T, Dienemann H, Schirmacher P, et al. Microsatellite instability in pulmonary adenocarcinomas: a comprehensive study of 480 cases. Virchows Arch. 2016;468(3):313-9.
83. Mouw KW, Goldberg MS, Konstantinopoulos PA, D'Andrea AD. DNA Damage and Repair Biomarkers of Immunotherapy Response. Cancer Discov. 2017;7(7):675-93.
84. Hugo W, Zaretsky JM, Sun L, Song C, Moreno BH, Hu-Lieskovan S, et al. Genomic and Transcriptomic Features of Response to Anti-PD-1 Therapy in Metastatic Melanoma. Cell. 2016;165(1):35-44.
85. Pao W, Girard N. New driver mutations in non-small-cell lung cancer. Lancet Oncol. 2011;12(2):175-80.
86. Gibbons DL, Byers LA, Kurie JM. Smoking, p53 mutation, and lung cancer. Mol Cancer Res. 2014;12(1):3-13.
87. Cortez MA, Ivan C, Valdecanas D, Wang X, Peltier HJ, Ye Y, et al. PDL1 Regulation by p53 via miR-34. J Natl Cancer Inst. 2016;108(1).
88. Jeanson A, Tomasini P, Souquet-Bressand M, Brandone N, Boucekine M, Grangeon M, et al. Efficacy of Immune Checkpoint Inhibitors in KRAS-Mutant Non-Small Cell Lung Cancer (NSCLC). J Thorac Oncol. 2019;14(6):1095-101.
89. Ji M, Liu Y, Li Q, Li X, Ning Z, Zhao W, et al. PD-1/PD-L1 expression in non-small-cell lung cancer and its correlation with EGFR/KRAS mutations. Cancer Biol Ther. 2016;17(4):407-13.
90. Dong ZY, Zhong WZ, Zhang XC, Su J, Xie Z, Liu SY, et al. Potential Predictive Value of TP53 and KRAS Mutation Status for Response to PD-1 Blockade Immunotherapy in Lung Adenocarcinoma. Clin Cancer Res. 2017;23(12):3012-24.
91. Alix-Panabières C, Pantel K. Clinical Applications of Circulating Tumor Cells and Circulating Tumor DNA as Liquid Biopsy. Cancer Discov. 2016;6(5):479-91.
92. Bardelli A, Pantel K. Liquid Biopsies, What We Do Not Know (Yet). Cancer Cell. 2017;31(2):172-9.
93. Siravegna G, Marsoni S, Siena S, Bardelli A. Integrating liquid biopsies into the management of cancer. Nat Rev Clin Oncol. 2017;14(9):531-48.
94. Wan JCM, Massie C, Garcia-Corbacho J, Mouliere F, Brenton JD, Caldas C, et al. Liquid biopsies come of age: towards implementation of circulating tumour DNA. Nat Rev Cancer. 2017;17(4):223-38.
95. Heitzer E, Haque IS, Roberts CES, Speicher MR. Current and future perspectives of liquid biopsies in genomics-driven oncology. Nat Rev Genet. 2019;20(2):71-88.
96. De Rubis G, Rajeev Krishnan S, Bebawy M. Liquid Biopsies in Cancer Diagnosis, Monitoring, and Prognosis. Trends Pharmacol Sci. 2019;40(3):172-86.
97. Heitzer E, Perakis S, Geigl JB, Speicher MR. The potential of liquid biopsies for the early detection of cancer. NPJ Precis Oncol. 2017;1(1):36.
98. Hasenleithner SO, Speicher MR. A clinician's handbook for using ctDNA throughout the patient journey. Mol Cancer. 2022;21(1):81.
99. Lui YY, Chik KW, Chiu RW, Ho CY, Lam CW, Lo YM. Predominant hematopoietic origin of cell-free DNA in plasma and serum after sex-mismatched bone marrow transplantation. Clin Chem. 2002;48(3):421-7.
100. Zheng YW, Chan KC, Sun H, Jiang P, Su X, Chen EZ, et al. Nonhematopoietically derived DNA is shorter than hematopoietically derived DNA in plasma: a transplantation model. Clin Chem. 2012;58(3):549-58.
101. Snyder MW, Kircher M, Hill AJ, Daza RM, Shendure J. Cell-free DNA Comprises an In Vivo Nucleosome Footprint that Informs Its Tissues-Of-Origin. Cell. 2016;164(1-2):57-68.

102. Jahr S, Hentze H, Englisch S, Hardt D, Fackelmayer FO, Hesch RD, et al. DNA fragments in the blood plasma of cancer patients: quantitations and evidence for their origin from apoptotic and necrotic cells. Cancer Res. 2001;61(4):1659-65.
103. Stroun M, Lyautey J, Lederrey C, Olson-Sand A, Anker P. About the possible origin and mechanism of circulating DNA apoptosis and active DNA release. Clin Chim Acta. 2001;313(1-2):139-42.
104. van der Vaart M, Pretorius PJ. The origin of circulating free DNA. Clin Chem. 2007;53(12):2215.
105. Heitzer E, Auer M, Hoffmann EM, Pichler M, Gasch C, Ulz P, et al. Establishment of tumor-specific copy number alterations from plasma DNA of patients with cancer. Int J Cancer. 2013;133(2):346-56.
106. Chan KC, Zhang J, Hui AB, Wong N, Lau TK, Leung TN, et al. Size distributions of maternal and fetal DNA in maternal plasma. Clin Chem. 2004;50(1):88-92.
107. Mouliere F, Robert B, Arnau Peyrotte E, Del Rio M, Ychou M, Molina F, et al. High fragmentation characterizes tumour-derived circulating DNA. PLoS One. 2011;6(9):e23418.
108. Ulz P, Thallinger GG, Auer M, Graf R, Kashofer K, Jahn SW, et al. Inferring expressed genes by whole-genome sequencing of plasma DNA. Nat Genet. 2016;48(10):1273-8.
109. Jiang P, Chan CW, Chan KC, Cheng SH, Wong J, Wong VW, et al. Lengthening and shortening of plasma DNA in hepatocellular carcinoma patients. Proc Natl Acad Sci U S A. 2015;112(11):E1317-25.
110. Jiang P, Lo YMD. The Long and Short of Circulating Cell-Free DNA and the Ins and Outs of Molecular Diagnostics. Trends Genet. 2016;32(6):360-71.
111. Underhill HR, Kitzman JO, Hellwig S, Welker NC, Daza R, Baker DN, et al. Fragment Length of Circulating Tumor DNA. PLoS Genet. 2016;12(7):e1006162.
112. Diaz LA, Jr., Bardelli A. Liquid biopsies: genotyping circulating tumor DNA. J Clin Oncol. 2014;32(6):579-86.
113. Murtaza M, Dawson SJ, Pogrebniak K, Rueda OM, Provenzano E, Grant J, et al. Multifocal clonal evolution characterized using circulating tumour DNA in a case of metastatic breast cancer. Nat Commun. 2015;6:8760.
114. Dawson SJ, Tsui DW, Murtaza M, Biggs H, Rueda OM, Chin SF, et al. Analysis of circulating tumor DNA to monitor metastatic breast cancer. N Engl J Med. 2013;368(13):1199-209.
115. Bettegowda C, Sausen M, Leary RJ, Kinde I, Wang Y, Agrawal N, et al. Detection of circulating tumor DNA in early- and late-stage human malignancies. Sci Transl Med. 2014;6(224):224ra24.
116. Tie J, Wang Y, Tomasetti C, Li L, Springer S, Kinde I, et al. Circulating tumor DNA analysis detects minimal residual disease and predicts recurrence in patients with stage II colon cancer. Sci Transl Med. 2016;8(346):346ra92.
117. Abbosh C, Birkbak NJ, Wilson GA, Jamal-Hanjani M, Constantin T, Salari R, et al. Phylogenetic ctDNA analysis depicts early-stage lung cancer evolution. Nature. 2017;545(7655):446-51.
118. McDonald BR, Contente-Cuomo T, Sammut SJ, Odenheimer-Bergman A, Ernst B, Perdigones N, et al. Personalized circulating tumor DNA analysis to detect residual disease after neoadjuvant therapy in breast cancer. Sci Transl Med. 2019;11(504).
119. Genovese G, Kähler AK, Handsaker RE, Lindberg J, Rose SA, Bakhoum SF, et al. Clonal hematopoiesis and blood-cancer risk inferred from blood DNA sequence. N Engl J Med. 2014;371(26):2477-87.
120. Jaiswal S, Fontanillas P, Flannick J, Manning A, Grauman PV, Mar BG, et al. Age-related clonal hematopoiesis associated with adverse outcomes. N Engl J Med. 2014;371(26):2488-98.
121. Xie M, Lu C, Wang J, McLellan MD, Johnson KJ, Wendl MC, et al. Age-related mutations associated with clonal hematopoietic expansion and malignancies. Nat Med. 2014;20(12):1472-8.
122. Jaiswal S, Ebert BL. Clonal hematopoiesis in human aging and disease. Science. 2019;366(6465).
123. Thorpe J, Osei-Owusu IA, Avigdor BE, Tupler R, Pevsner J. Mosaicism in Human Health and Disease. Annu Rev Genet. 2020;54:487-510.

124. Steensma DP, Bejar R, Jaiswal S, Lindsley RC, Sekeres MA, Hasserjian RP, et al. Clonal hematopoiesis of indeterminate potential and its distinction from myelodysplastic syndromes. Blood. 2015;126(1):9-16.
125. Ptashkin RN, Mandelker DL, Coombs CC, Bolton K, Yelskaya Z, Hyman DM, et al. Prevalence of Clonal Hematopoiesis Mutations in Tumor-Only Clinical Genomic Profiling of Solid Tumors. JAMA Oncol. 2018;4(11):1589-93.
126. Coombs CC, Gillis NK, Tan X, Berg JS, Ball M, Balasis ME, et al. Identification of Clonal Hematopoiesis Mutations in Solid Tumor Patients Undergoing Unpaired Next-Generation Sequencing Assays. Clin Cancer Res. 2018;24(23):5918-24.
127. Hu Y, Ulrich BC, Supplee J, Kuang Y, Lizotte PH, Feeney NB, et al. False-Positive Plasma Genotyping Due to Clonal Hematopoiesis. Clin Cancer Res. 2018;24(18):4437-43.
128. Zhang Y, Yao Y, Xu Y, Li L, Gong Y, Zhang K, et al. Pan-cancer circulating tumor DNA detection in over 10,000 Chinese patients. Nat Commun. 2021;12(1):11.
129. Chan HT, Chin YM, Nakamura Y, Low SK. Clonal Hematopoiesis in Liquid Biopsy: From Biological Noise to Valuable Clinical Implications. Cancers (Basel). 2020;12(8).
130. Heidary M, Auer M, Ulz P, Heitzer E, Petru E, Gasch C, et al. The dynamic range of circulating tumor DNA in metastatic breast cancer. Breast Cancer Res. 2014;16(4):421.
131. Siravegna G, Mussolin B, Venesio T, Marsoni S, Seoane J, Dive C, et al. How liquid biopsies can change clinical practice in oncology. Ann Oncol. 2019;30(10):1580-90.
132. Zhou Q, Moser T, Perakis S, Heitzer E. Untargeted profiling of cell-free circulating DNA. Translational Cancer Research. 2017:S140-S52.
133. El-Heliebi A, Heitzer E. State of the Art and Future Direction for the Analysis of Cell-Free Circulating DNA. In: Filice M, Ruiz-Cabello J, editors. Nucleic Acid Nanotheranostics: Elsevier; 2019. p. 133-88.
134. Perakis S, Speicher MR. Emerging concepts in liquid biopsies. BMC Med. 2017;15(1):75.
135. Forshew T, Murtaza M, Parkinson C, Gale D, Tsui DW, Kaper F, et al. Noninvasive identification and monitoring of cancer mutations by targeted deep sequencing of plasma DNA. Sci Transl Med. 2012;4(136):136ra68.
136. Newman AM, Bratman SV, To J, Wynne JF, Eclov NC, Modlin LA, et al. An ultrasensitive method for quantitating circulating tumor DNA with broad patient coverage. Nat Med. 2014;20(5):548-54.
137. Newman AM, Lovejoy AF, Klass DM, Kurtz DM, Chabon JJ, Scherer F, et al. Integrated digital error suppression for improved detection of circulating tumor DNA. Nat Biotechnol. 2016;34(5):547-55.
138. van der Pol Y, Mouliere F. Toward the Early Detection of Cancer by Decoding the Epigenetic and Environmental Fingerprints of Cell-Free DNA. Cancer Cell. 2019;36(4):350-68.
139. Salk JJ, Schmitt MW, Loeb LA. Enhancing the accuracy of next-generation sequencing for detecting rare and subclonal mutations. Nat Rev Genet. 2018;19(5):269-85.
140. U.S. Food and Drug Administration. FDA announces approval, CMS proposes coverage of first breakthrough-designated test to detect extensive number of cancer biomarkers [press release] November 30, 2017 [Available from: https://www.fda.gov/newsevents/newsroom/pressannouncements/ucm587273.htm.
141. U.S. Food and Drug Administration. FDA unveils a streamlined path for the authorization of tumor profiling tests alongside its latest product action [press release]. November 15, 2017 [Available from: https://www.fda.gov/newsevents/newsroom/pressannouncements/ucm585347.htm. .
142. Hayes DF. Precision Medicine and Testing for Tumor Biomarkers-Are All Tests Born Equal? JAMA Oncol. 2018;4(6):773-4.
143. Sharfstein J. FDA regulation of laboratory-developed diagnostic tests: protect the public, advance the science. Jama. 2015;313(7):667-8.

144. Kim AS, Bartley AN, Bridge JA, Kamel-Reid S, Lazar AJ, Lindeman NI, et al. Comparison of Laboratory-Developed Tests and FDA-Approved Assays for BRAF, EGFR, and KRAS Testing. JAMA Oncology. 2018;4(6):838-41.
145. Herlyn D, Herlyn M, Ross AH, Ernst C, Atkinson B, Koprowski H. Efficient selection of human tumor growth-inhibiting monoclonal antibodies. J Immunol Methods. 1984;73(1):157-67.
146. Goossens-Beumer IJ, Zeestraten EC, Benard A, Christen T, Reimers MS, Keijzer R, et al. Clinical prognostic value of combined analysis of Aldh1, Survivin, and EpCAM expression in colorectal cancer. Br J Cancer. 2014;110(12):2935-44.
147. Spizzo G, Fong D, Wurm M, Ensinger C, Obrist P, Hofer C, et al. EpCAM expression in primary tumour tissues and metastases: an immunohistochemical analysis. J Clin Pathol. 2011;64(5):415-20.
148. Rao CG, Chianese D, Doyle GV, Miller MC, Russell T, Sanders RA, Jr., et al. Expression of epithelial cell adhesion molecule in carcinoma cells present in blood and primary and metastatic tumors. Int J Oncol. 2005;27(1):49-57.
149. de Wit S, van Dalum G, Lenferink AT, Tibbe AG, Hiltermann TJ, Groen HJ, et al. The detection of EpCAM(+) and EpCAM(-) circulating tumor cells. Sci Rep. 2015;5:12270.
150. Alix-Panabières C, Pantel K. Challenges in circulating tumour cell research. Nat Rev Cancer. 2014;14(9):623-31.
151. de Wit S, van Dalum G, Terstappen LW. Detection of circulating tumor cells. Scientifica (Cairo). 2014;2014:819362.
152. Cristofanilli M, Budd GT, Ellis MJ, Stopeck A, Matera J, Miller MC, et al. Circulating tumor cells, disease progression, and survival in metastatic breast cancer. N Engl J Med. 2004;351(8):781-91.
153. Krebs MG, Sloane R, Priest L, Lancashire L, Hou JM, Greystoke A, et al. Evaluation and prognostic significance of circulating tumor cells in patients with non-small-cell lung cancer. J Clin Oncol. 2011;29(12):1556-63.
154. Hiltermann TJN, Pore MM, van den Berg A, Timens W, Boezen HM, Liesker JJW, et al. Circulating tumor cells in small-cell lung cancer: a predictive and prognostic factor. Ann Oncol. 2012;23(11):2937-42.
155. Allard WJ, Matera J, Miller MC, Repollet M, Connelly MC, Rao C, et al. Tumor cells circulate in the peripheral blood of all major carcinomas but not in healthy subjects or patients with nonmalignant diseases. Clin Cancer Res. 2004;10(20):6897-904.
156. de Bono JS, Scher HI, Montgomery RB, Parker C, Miller MC, Tissing H, et al. Circulating tumor cells predict survival benefit from treatment in metastatic castration-resistant prostate cancer. Clin Cancer Res. 2008;14(19):6302-9.
157. Cohen SJ, Punt CJ, Iannotti N, Saidman BH, Sabbath KD, Gabrail NY, et al. Relationship of circulating tumor cells to tumor response, progression-free survival, and overall survival in patients with metastatic colorectal cancer. J Clin Oncol. 2008;26(19):3213-21.
158. Gervasoni A, Sandri MT, Nascimbeni R, Zorzino L, Cassatella MC, Baglioni L, et al. Comparison of three distinct methods for the detection of circulating tumor cells in colorectal cancer patients. Oncol Rep. 2011;25(6):1669-703.
159. Krebs MG, Hou JM, Sloane R, Lancashire L, Priest L, Nonaka D, et al. Analysis of circulating tumor cells in patients with non-small cell lung cancer using epithelial marker-dependent and -independent approaches. J Thorac Oncol. 2012;7(2):306-15.
160. Fehm T, Müller V, Aktas B, Janni W, Schneeweiss A, Stickeler E, et al. HER2 status of circulating tumor cells in patients with metastatic breast cancer: a prospective, multicenter trial. Breast Cancer Res Treat. 2010;124(2):403-12.
161. Antolovic D, Galindo L, Carstens A, Rahbari N, Büchler MW, Weitz J, et al. Heterogeneous detection of circulating tumor cells in patients with colorectal cancer by immunomagnetic enrichment using different EpCAM-specific antibodies. BMC Biotechnol. 2010;10:35.

162. Cortés-Hernández LE, Eslami SZ, Alix-Panabières C. Circulating tumor cell as the functional aspect of liquid biopsy to understand the metastatic cascade in solid cancer. Mol Aspects Med. 2020;72:100816.
163. Eslami-S Z, Cortés-Hernández LE, Alix-Panabières C. Circulating tumor cells: moving forward into clinical applications. Precision Cancer Medicine. 2019;3.
164. Lindsay CR, Blackhall FH, Carmel A, Fernandez-Gutierrez F, Gazzaniga P, Groen HJM, et al. EPAC-lung: pooled analysis of circulating tumour cells in advanced non-small cell lung cancer. Eur J Cancer. 2019;117:60-8.
165. Weber S, Spiegl B, Perakis SO, Ulz CM, Abuja PM, Kashofer K, et al. Technical Evaluation of Commercial Mutation Analysis Platforms and Reference Materials for Liquid Biopsy Profiling. Cancers (Basel). 2020;12(6).
166. Sidorenkov G, Nagel J, Meijer C, Duker JJ, Groen HJM, Halmos GB, et al. The OncoLifeS data-biobank for oncology: a comprehensive repository of clinical data, biological samples, and the patient's perspective. J Transl Med. 2019;17(1):374.
167. Leest PV, Boonstra PA, Elst AT, Kempen LCV, Tibbesma M, Koopmans J, et al. Comparison of Circulating Cell-Free DNA Extraction Methods for Downstream Analysis in Cancer Patients. Cancers (Basel). 2020;12(5).
168. National Comprehensive Cancer Network 2024 [Available from: https://www.nccn.org/guidelines/category_1.
169. Network NCC. NCCN clinical practice guidelines in oncology (NCCN Guidelines®). National Comprehensive Cancer Network. 2017.
170. Strom SP. Current practices and guidelines for clinical next-generation sequencing oncology testing. Cancer Biol Med. 2016;13(1):3-11.
171. Dentro SC, Leshchiner I, Haase K, Tarabichi M, Wintersinger J, Deshwar AG, et al. Characterizing genetic intra-tumor heterogeneity across 2,658 human cancer genomes. Cell. 2021;184(8):2239-54.e39.
172. Bos MK, Nasserinejad K, Jansen M, Angus L, Atmodimedjo PN, de Jonge E, et al. Comparison of variant allele frequency and number of mutant molecules as units of measurement for circulating tumor DNA. Mol Oncol. 2021;15(1):57-66.
173. Anagnostou V, Forde PM, White JR, Niknafs N, Hruban C, Naidoo J, et al. Dynamics of Tumor and Immune Responses during Immune Checkpoint Blockade in Non-Small Cell Lung Cancer. Cancer Res. 2019;79(6):1214-25.
174. Goldberg SB, Narayan A, Kole AJ, Decker RH, Teysir J, Carriero NJ, et al. Early Assessment of Lung Cancer Immunotherapy Response via Circulating Tumor DNA. Clin Cancer Res. 2018;24(8):1872-80.
175. Nabet BY, Esfahani MS, Moding EJ, Hamilton EG, Chabon JJ, Rizvi H, et al. Noninvasive Early Identification of Therapeutic Benefit from Immune Checkpoint Inhibition. Cell. 2020;183(2):363-76 e13.
176. Moding EJ, Liu YF, Nabet BY, Chabon JJ, Chaudhuri AA, Hui AB, et al. Circulating tumor DNA dynamics predict benefit from consolidation immunotherapy in locally advanced non-small-cell lung cancer. Nat Cancer. 2020;1(2):176-+.
177. Steeghs EMP, Kroeze LI, Tops BBJ, van Kempen LC, Ter Elst A, Kastner-van Raaij AWM, et al. Comprehensive routine diagnostic screening to identify predictive mutations, gene amplifications, and microsatellite instability in FFPE tumor material. BMC Cancer. 2020;20(1):291.
178. Konigshofer Y. Inventor Methods for PreparingDNAReference Material and Controls 2018 [Available from: https://patentscope.wipo.int/search/en/detail.jsf?docId=WO2018094183.
179. Chabon JJ, Hamilton EG, Kurtz DM, Esfahani MS, Moding EJ, Stehr H, et al. Integrating genomic features for non-invasive early lung cancer detection. Nature. 2020;580(7802):245-51.
180. Mouliere F, Chandrananda D, Piskorz AM, Moore EK, Morris J, Ahlborn LB, et al. Enhanced detection of circulating tumor DNA by fragment size analysis. Sci Transl Med. 2018;10(466).

181. Jiang J, Adams HP, Yao L, Yaung S, Lal P, Balasubramanyam A, et al. Concordance of Genomic Alterations by Next-Generation Sequencing in Tumor Tissue versus Cell-Free DNA in Stage I-IV Non-Small Cell Lung Cancer. J Mol Diagn. 2020;22(2):228-35.
182. Pascual J, Attard G, Bidard FC, Curigliano G, De Mattos-Arruda L, Diehn M, et al. ESMO recommendations on the use of circulating tumour DNA assays for patients with cancer: a report from the ESMO Precision Medicine Working Group. Ann Oncol. 2022;33(8):750-68.
183. Cardoso F, Paluch-Shimon S, Senkus E, Curigliano G, Aapro MS, André F, et al. 5th ESO-ESMO international consensus guidelines for advanced breast cancer (ABC 5). Ann Oncol. 2020;31(12):1623-49.
184. Mosele F, Remon J, Mateo J, Westphalen CB, Barlesi F, Lolkema MP, et al. Recommendations for the use of next-generation sequencing (NGS) for patients with metastatic cancers: a report from the ESMO Precision Medicine Working Group. Ann Oncol. 2020;31(11):1491-505.
185. Heitzer E, van den Broek D, Denis MG, Hofman P, Hubank M, Mouliere F, et al. Recommendations for a practical implementation of circulating tumor DNA mutation testing in metastatic non-small-cell lung cancer. ESMO Open. 2022;7(2):100399.
186. Deans ZC, Costa JL, Cree I, Dequeker E, Edsjö A, Henderson S, et al. Integration of next-generation sequencing in clinical diagnostic molecular pathology laboratories for analysis of solid tumours; an expert opinion on behalf of IQN Path ASBL. Virchows Arch. 2017;470(1):5-20.
187. Romero A, Serna-Blasco R, Calvo V, Provencio M. Use of Liquid Biopsy in the Care of Patients with Non-Small Cell Lung Cancer. Curr Treat Options Oncol. 2021;22(10):86.
188. Lam SN, Zhou YC, Chan YM, Foo CM, Lee PY, Mok WY, et al. Comparison of Target Enrichment Platforms for Circulating Tumor DNA Detection. Sci Rep. 2020;10(1):4124.
189. Stetson D, Ahmed A, Xu X, Nuttall BRB, Lubinski TJ, Johnson JH, et al. Orthogonal Comparison of Four Plasma NGS Tests With Tumor Suggests Technical Factors are a Major Source of Assay Discordance. JCO Precis Oncol. 2019;3:1-9.
190. Deveson IW, Gong B, Lai K, LoCoco JS, Richmond TA, Schageman J, et al. Evaluating the analytical validity of circulating tumor DNA sequencing assays for precision oncology. Nat Biotechnol. 2021;39(9):1115-28.
191. Verma S, Moore MW, Ringler R, Ghosal A, Horvath K, Naef T, et al. Analytical performance evaluation of a commercial next generation sequencing liquid biopsy platform using plasma ctDNA, reference standards, and synthetic serial dilution samples derived from normal plasma. BMC Cancer. 2020;20(1):945.
192. Hallermayr A, Keßler T, Fujera M, Liesfeld B, Bernstein S, von Ameln S, et al. Impact of cfDNA Reference Materials on Clinical Performance of Liquid Biopsy NGS Assays. Cancers (Basel). 2023;15(20).
193. Godsey JH, Silvestro A, Barrett JC, Bramlett K, Chudova D, Deras I, et al. Generic Protocols for the Analytical Validation of Next-Generation Sequencing-Based ctDNA Assays: A Joint Consensus Recommendation of the BloodPAC's Analytical Variables Working Group. Clin Chem. 2020;66(9):1156-66.
194. Rolfo C, Mack P, Scagliotti GV, Aggarwal C, Arcila ME, Barlesi F, et al. Liquid Biopsy for Advanced NSCLC: A Consensus Statement From the International Association for the Study of Lung Cancer. J Thorac Oncol. 2021;16(10):1647-62.
195. Cabel L, Riva F, Servois V, Livartowski A, Daniel C, Rampanou A, et al. Circulating tumor DNA changes for early monitoring of anti-PD1 immunotherapy: a proof-of-concept study. Ann Oncol. 2017;28(8):1996-2001.
196. FDA Recently Approved Devices. Guardant360 CDx – P200010/S008 2022 [Available from: https://www.fda.gov/medical-devices/recently-approved-devices/guardant360-cdx-p200010s008.
197. Guardant Health Inc. Guardant360® CDx Technical Information. Redwood City, CA; 2021.
198. Li BT, Janku F, Jung B, Hou C, Madwani K, Alden R, et al. Ultra-deep next-generation sequencing of plasma cell-free DNA in patients with advanced lung cancers: results from the Actionable Genome Consortium. Ann Oncol. 2019;30(4):597-603.

199. Aggarwal C, Thompson JC, Black TA, Katz SI, Fan R, Yee SS, et al. Clinical Implications of Plasma-Based Genotyping With the Delivery of Personalized Therapy in Metastatic Non-Small Cell Lung Cancer. JAMA Oncol. 2019;5(2):173-80.
200. Sabari JK, Offin M, Stephens D, Ni A, Lee A, Pavlakis N, et al. A Prospective Study of Circulating Tumor DNA to Guide Matched Targeted Therapy in Lung Cancers. J Natl Cancer Inst. 2019;111(6):575-83.
201. Leighl NB, Page RD, Raymond VM, Daniel DB, Divers SG, Reckamp KL, et al. Clinical Utility of Comprehensive Cell-free DNA Analysis to Identify Genomic Biomarkers in Patients with Newly Diagnosed Metastatic Non-small Cell Lung Cancer. Clin Cancer Res. 2019;25(15):4691-700.
202. Remon J, Lacroix L, Jovelet C, Caramella C, Howarth K, Plagnol V, et al. Real-World Utility of an Amplicon-Based Next-Generation Sequencing Liquid Biopsy for Broad Molecular Profiling in Patients With Advanced Non-Small-Cell Lung Cancer. JCO Precis Oncol. 2019;3.
203. Rothwell DG, Ayub M, Cook N, Thistlethwaite F, Carter L, Dean E, et al. Utility of ctDNA to support patient selection for early phase clinical trials: the TARGET study. Nat Med. 2019;25(5):738-43.
204. Adalsteinsson VA, Ha G, Freeman SS, Choudhury AD, Stover DG, Parsons HA, et al. Scalable whole-exome sequencing of cell-free DNA reveals high concordance with metastatic tumors. Nat Commun. 2017;8(1):1324.
205. Odegaard JI, Vincent JJ, Mortimer S, Vowles JV, Ulrich BC, Banks KC, et al. Validation of a Plasma-Based Comprehensive Cancer Genotyping Assay Utilizing Orthogonal Tissue- and Plasma-Based Methodologies. Clin Cancer Res. 2018;24(15):3539-49.
206. Park S, Olsen S, Ku BM, Lee MS, Jung HA, Sun JM, et al. High concordance of actionable genomic alterations identified between circulating tumor DNA-based and tissue-based next-generation sequencing testing in advanced non-small cell lung cancer: The Korean Lung Liquid Versus Invasive Biopsy Program. Cancer. 2021;127(16):3019-28.
207. El Messaoudi S, Rolet F, Mouliere F, Thierry AR. Circulating cell free DNA: Preanalytical considerations. Clin Chim Acta. 2013;424:222-30.
208. Merker JD, Oxnard GR, Compton C, Diehn M, Hurley P, Lazar AJ, et al. Circulating Tumor DNA Analysis in Patients With Cancer: American Society of Clinical Oncology and College of American Pathologists Joint Review. J Clin Oncol. 2018;36(16):1631-41.
209. Zhao H, Chen KZ, Hui BG, Zhang K, Yang F, Wang J. Role of circulating tumor DNA in the management of early-stage lung cancer. Thorac Cancer. 2018;9(5):509-15.
210. Molina-Vila MA, Mayo-de-Las-Casas C, Giménez-Capitán A, Jordana-Ariza N, Garzón M, Balada A, et al. Liquid Biopsy in Non-Small Cell Lung Cancer. Front Med (Lausanne). 2016;3:69.
211. Crowley E, Di Nicolantonio F, Loupakis F, Bardelli A. Liquid biopsy: monitoring cancer-genetics in the blood. Nat Rev Clin Oncol. 2013;10(8):472-84.
212. Razavi P, Li BT, Brown DN, Jung B, Hubbell E, Shen R, et al. High-intensity sequencing reveals the sources of plasma circulating cell-free DNA variants. Nat Med. 2019;25(12):1928-37.
213. Moding EJ, Liu Y, Nabet BY, Chabon JJ, Chaudhuri AA, Hui AB, et al. Circulating Tumor DNA Dynamics Predict Benefit from Consolidation Immunotherapy in Locally Advanced Non-Small Cell Lung Cancer. Nat Cancer. 2020;1(2):176-83.
214. Dong ZY, Zhai HR, Hou QY, Su J, Liu SY, Yan HH, et al. Mixed Responses to Systemic Therapy Revealed Potential Genetic Heterogeneity and Poor Survival in Patients with Non-Small Cell Lung Cancer. Oncologist. 2017;22(1):61-9.
215. Jia W, Gao Q, Han A, Zhu H, Yu J. The potential mechanism, recognition and clinical significance of tumor pseudoprogression after immunotherapy. Cancer Biol Med. 2019;16(4):655-70.
216. van der Leest P, Hiddinga B, Miedema A, Aguirre Azpurua ML, Rifaela N, Ter Elst A, et al. Circulating tumor DNA as a biomarker for monitoring early treatment responses of patients with advanced lung adenocarcinoma receiving immune checkpoint inhibitors. Mol Oncol. 2021;15(11):2910-22.

217. Papillon-Cavanagh S, Doshi P, Dobrin R, Szustakowski J, Walsh AM. STK11 and KEAP1 mutations as prognostic biomarkers in an observational real-world lung adenocarcinoma cohort. ESMO Open. 2020;5(2).
218. Guibert N, Jones G, Beeler JF, Plagnol V, Morris C, Mourlanette J, et al. Targeted sequencing of plasma cell-free DNA to predict response to PD1 inhibitors in advanced non-small cell lung cancer. Lung Cancer. 2019;137:1-6.
219. Pavan A, Bragadin AB, Calvetti L, Ferro A, Zulato E, Attili I, et al. Role of next generation sequencing-based liquid biopsy in advanced non-small cell lung cancer patients treated with immune checkpoint inhibitors: impact of STK11, KRAS and TP53 mutations and co-mutations on outcome. Transl Lung Cancer Res. 2021;10(1):202-20.
220. Zhu H, Xie D, Yu Y, Yao L, Xu B, Huang L, et al. KEAP1/NFE2L2 Mutations of Liquid Biopsy as Prognostic Biomarkers in Patients With Advanced Non-Small Cell Lung Cancer: Results From Two Multicenter, Randomized Clinical Trials. Front Oncol. 2021;11:659200.
221. Frank R, Scheffler M, Merkelbach-Bruse S, Ihle MA, Kron A, Rauer M, et al. Clinical and Pathological Characteristics of KEAP1- and NFE2L2-Mutated Non-Small Cell Lung Carcinoma (NSCLC). Clin Cancer Res. 2018;24(13):3087-96.
222. Slavin TP, Banks KC, Chudova D, Oxnard GR, Odegaard JI, Nagy RJ, et al. Identification of Incidental Germline Mutations in Patients With Advanced Solid Tumors Who Underwent Cell-Free Circulating Tumor DNA Sequencing. J Clin Oncol. 2018;36(35):Jco1800328.
223. Mandelker D, Ceyhan-Birsoy O. Evolving Significance of Tumor-Normal Sequencing in Cancer Care. Trends Cancer. 2020;6(1):31-9.
224. Pao W, Wang TY, Riely GJ, Miller VA, Pan Q, Ladanyi M, et al. KRAS mutations and primary resistance of lung adenocarcinomas to gefitinib or erlotinib. PLoS Med. 2005;2(1):e17.
225. Coombs CC, Zehir A, Devlin SM, Kishtagari A, Syed A, Jonsson P, et al. Therapy-Related Clonal Hematopoiesis in Patients with Non-hematologic Cancers Is Common and Associated with Adverse Clinical Outcomes. Cell Stem Cell. 2017;21(3):374-82.e4.
226. Takahashi K, Wang F, Kantarjian H, Doss D, Khanna K, Thompson E, et al. Preleukaemic clonal haemopoiesis and risk of therapy-related myeloid neoplasms: a case-control study. Lancet Oncol. 2017;18(1):100-11.
227. Yen J, Quinn K, Helman E, Chursov A, Nance T, Jaimovich A, et al. Abstract 2509: Analysis of clonal hematopoiesis-associated mutations in the cell-free DNA of advanced cancer patients. Cancer Research. 2019;79(13_Supplement):2509-.
228. Midic D, Rinke J, Perner F, Müller V, Hinze A, Pester F, et al. Prevalence and dynamics of clonal hematopoiesis caused by leukemia-associated mutations in elderly individuals without hematologic disorders. Leukemia. 2020;34(8):2198-205.
229. Florez MA, Tran BT, Wathan TK, DeGregori J, Pietras EM, King KY. Clonal hematopoiesis: Mutation-specific adaptation to environmental change. Cell Stem Cell. 2022;29(6):882-904.
230. Lièvre A, Bachet JB, Le Corre D, Boige V, Landi B, Emile JF, et al. KRAS mutation status is predictive of response to cetuximab therapy in colorectal cancer. Cancer Res. 2006;66(8):3992-5.
231. Liu J, Chen X, Wang J, Zhou S, Wang CL, Ye MZ, et al. Biological background of the genomic variations of cf-DNA in healthy individuals. Ann Oncol. 2019;30(3):464-70.
232. Sivapalan L, Iams WT, Belcaid Z, Scott SC, Niknafs N, Balan A, et al. Dynamics of Sequence and Structural Cell-Free DNA Landscapes in Small-Cell Lung Cancer. Clin Cancer Res. 2023;29(12):2310-23.
233. Maansson CT, Thomsen LS, Meldgaard P, Nielsen AL, Sorensen BS. Integration of Cell-Free DNA End Motifs and Fragment Lengths Can Identify Active Genes in Liquid Biopsies. Int J Mol Sci. 2024;25(2).
234. Assaf ZJF, Zou W, Fine AD, Socinski MA, Young A, Lipson D, et al. A longitudinal circulating tumor DNA-based model associated with survival in metastatic non-small-cell lung cancer. Nat Med. 2023;29(4):859-68.